



Escola de Camins
Escola Tècnica Superior d'Enginyeria de Camins, Canals i Ports
UPC BARCELONATECH

Title

Application of Local and Global Sensitivity Analysis methods to a North Sea Hydrodynamic Model – Study Case of Offshore Blue mussels and Seaweed Farms

Final Thesis developed by:

Basnayake Mudiyansele, Vindhya Basnayake

Directed by:

Pinzon, Allen Bateman

Master in:

Flood Risk Management

Barcelona, August 2021

Department of Civil Engineering

MASTER FINAL THESIS



APPLICATION OF LOCAL AND GLOBAL SENSITIVITY ANALYSIS METHODS TO A NORTH SEA HYDRODYNAMIC MODEL – STUDY CASE OF OFFSHORE SEAWEED AND BLUE MUSSEL FARMS



Master of Science Thesis

by

Vindhya Basnayake, Basnayake Mudiyansele

Supervisor

Prof. Allen Bateman Pinzon (Universitat Politècnica de Catalunya)

Mentors

Dr. Ghada EL Serafy (Deltares)

Rieke Santjer (Deltares)

Examination committee

Prof. Allen Bateman Pinzon, Chairman (UPC)

Prof. Agustín Sánchez-Arcilla (UPC)

Prof. Vicente Medina (UPC)

This research is done for the partial fulfillment of requirements for the Master of Science degree at the UNESCO-IHE Institute for Water Education, Delft, the Netherlands

August 2021

Abstract

Increasing demand for marine resources is a significant concern in today's world due to the limited availability of resources and the rapid population growth. The multi-use of offshore platforms has been introduced as a sustainable solution for resource utilization by many countries worldwide. However, the concept of multi-use is relatively new. Therefore, researches are still being carried out to check the feasibility of these offshore platforms in aquaculture activities, renewable energy generation, tourism, and many other sectors. Before designing these infrastructures, it is essential to identify the suitable marine environments for each activity based on the required conditions and characteristics of the marine environments. Thus, numerical models play a vital role in simulating these marine environments and consequently will be used as a decision-making tool in feasibility studies and operational activities. The calibration of these numerical models is essential to have more reliable model outputs. However, these numerical models have many input parameters and physical variables on which the outputs depend. Sensitivity analysis can reduce the effort to calibrate complex numerical models with many input parameters by identifying the most influential inputs to an output variable. The main objective of the current research was to select the most significant input parameters to two selected outputs of a hydrodynamic model.

DCSM is a hydrodynamic model developed for the North Sea by Deltares using the D-Flow FM model suite of Delft3D. Two selected local and global sensitivity analysis methods were applied to the above hydrodynamic model to test the sensitivities of temperature and current velocities to a selected subset of input parameters. The Morris method is used as a screening method to identify the order of the significance of input parameters. The variance-based Sobol' method was used in global sensitivity analysis for the input parameters screened by the Morris method. Finally, a comparison was made for the sensitivity indices obtained from the Morris method and variance-based Sobol' method by calculating the correlations between indices.

Temperature and current velocities were identified as critical output variables of the hydrodynamic model that will be beneficial in designing offshore Blue mussel and Seaweed farms. A subset of input parameters was selected for the analysis as the D-Flow FM model is associated with a considerable number of input parameters. The sensitivities of the temperature and current velocities to the selected set of inputs were analyzed using the two analysis techniques for few selected locations in the area of interest. Results of the Morris method show that the temperature is most sensitive to the Dalton coefficient used for calculating the evaporative heat flux, the Smagorinsky factor that is used in calculating the horizontal turbulence, and the Stanton coefficient, which is used in calculating convective heat flux. Therefore, these three factors were further analyzed by the variance-based Sobol' method. Variance-based analysis shows that, from the three inputs, the Dalton coefficient is the most sensitive parameter to the temperature. The effect of the Stanton coefficient is much smaller compared to the other two factors.

Current velocities in the three directions were separately considered in the sensitivity analyses and found out that the most significant input parameters from the selected sub-set are the air density (ρ_{air}), Smagorinsky factor, uniform vertical eddy viscosity (ν_{eddy}), and uniform vertical eddy diffusivity (D_{eddy}). Thus, the variance-based analysis was performed for these

four factors. Out of these four parameters, air density (ρ_{air}) was identified as the parameter with the highest contribution and Smagorinsky factor as the second most significant parameter to x-velocity from the results of the Sobol' method, while the V_{icoww} , and D_{icoww} has a less contributions. The sensitivity of y-velocity and z-velocity also show a similar pattern of ranking, although the percentage of contributions to output variances are different. The interaction effects of input parameters on outputs were also identified using the Sobol' indices. The rankings obtained for both temperature and currents velocities from the two methods are comparable, whereas the order of ranking is observed to be similar in both methods.

The spatial variation of the sensitivities of temperature and current velocities were observed as minimal, where the ranking order of the significant parameters remained the same for the selected six locations in the project area.

Keywords: Hydrodynamic model, sensitivity analysis, North Sea, Dutch Continental Shelf Model, One-At-a-Time method, Morris method, Sobol' variance-based method

Acknowledgment

At first, I would like to express my gratitude to Dr. Ghada El Serafy for her guidance, support, and valuable suggestions throughout my MSc research period. I am equally thankful to Rieke Santjer for always giving me her valuable time, support, and ideas throughout the research.

I would be much thankful to my academic supervisor Prof. Allen Bateman Pinzon, for his advice and support during the research and his valuable lectures during my MSc course. Also, I like to express my gratitude to all the professors, lecturers, and PhD fellows of IHE, UPC, TU- Dresden, and the University of Ljubljana for giving us the opportunity and helping throughout our Erasmus journey.

I would like to thank Deltares for giving me this valuable opportunity to complete my research and gain experience working with their staff. This work was carried out with a current EU Horizon 2020 project. The UNITED project has received funding from the European Union's Horizon 2020 Research and Innovation Programme under Grant Agreement No 862915.

Finally, I would be grateful to my family for always being there for me, believing in me, and motivating me. In addition, my warm thanks go to my husband for his understanding, dedication, and motivating me throughout my MSc life as always.

Table of Contents

Acknowledgment	iv
List of Figures	viii
List of Tables	x
Chapter 1: Introduction	1
1.1. Background	1
1.1. Problem Statement	2
1.2. Objectives.....	2
1.3. Research questions	3
1.4. Practical Value	3
1.5. Innovation.....	4
1.6. Thesis Outline	5
Chapter 2: Literature Review	6
2.1. Sensitivity Analysis techniques.....	7
2.1.1. Morris screening method	7
2.1.2. Variance-based method of Sobol’	9
2.1.3. Linear regression coefficients	10
2.1.4. Standardized regression coefficients.....	10
2.1.5. Random balance designs (RBD) method.....	11
2.2. Sampling methods for sensitivity analysis	12
2.2.1. One-Factor-At-a-Time (O-A-T) sampling.....	12
2.2.2. Fractional factorial designs	13
2.2.3. Latin Hypercube sampling	13
2.2.4. Multivariate stratified sampling.....	14
2.2.5. Monte Carlo and quasi-Monte Carlo sampling.....	14
2.3. Applications of different SA techniques	15
Chapter 3: Case Study – German Pilot	18
3.1. Key aspects of the German pilot	19
3.1.1. Blue mussel longlines	19
3.1.2. Seaweed farming.....	21
3.2. Physical characteristics of the North Sea	21
3.2.1. Bathymetry.....	21
3.2.2. Impact of atmospheric forcing	22
3.2.3. Interaction with the Atlantic Ocean	23

3.2.4.	Impact of astronomical tides	23
3.3.	Hydrodynamic model of North Sea	23
Chapter 4:	Research Methodology.....	28
4.1.	Selection of Sensitivity Analysis Methods.....	29
4.2.	Methods for analysis	30
4.2.1.	Morris method of Elementary Effects.....	30
4.2.2.	Variance based Sobol' method	33
4.3.	Comparison of the sensitivity results obtained from two methods	35
4.4.	Training on example model.....	35
4.5.	Selection of locations for the analysis.....	36
Chapter 5:	Selection of Parameters for the Analysis	38
5.1.	Selection of Output parameters for analysis	38
5.2.	Selection of Input parameters for analysis	41
Chapter 6:	Application of Python for Analysis.....	48
6.1.	Scripts for sampling & inserting samples to model	48
6.1.1.	Morris method.....	48
6.1.2.	Variance-based Sobol' method	49
6.2.	Scripts for extracting model outputs	50
6.3.	Scripts for calculating sensitivity indices.....	50
6.3.1.	Morris Method	50
6.3.2.	Variance-based Sobol' Method.....	51
6.4.	Plotting the results.....	51
6.4.1.	Time series plots	51
6.4.2.	Plots for sensitivity measures.....	51
6.4.3.	Plots for comparing the sensitivity measures of two methods.....	52
Chapter 7:	Results and Discussion.....	53
7.1.	Variation of Output parameters over time.....	53
7.1.1.	Temperature	53
7.1.2.	Current velocity	54
7.2.	Application of Morris method.....	57
7.2.1.	Temperature Sensitivity	57
7.2.2.	Sensitivity of Current velocity	62
7.2.2.1.	Current velocity - x component.....	62
7.2.2.2.	Current velocity - y component.....	66

7.2.2.3.	Current velocity - z component.....	69
7.3.	Application of Variance-based Sobol' method	73
7.3.1.	Temperature Sensitivity	73
7.3.2.	Sensitivity of Current velocity	75
7.3.3.	Sensitivity of Current velocity (x-component)	75
7.3.4.	Sensitivity of Current velocity (y-velocity)	77
7.3.5.	Sensitivity of Current velocity (z-velocity)	79
7.4.	Comparison of the results of Morris and Sobol' methods	81
7.4.1.	Temperature	81
7.4.2.	Current velocity (x-velocity component).....	82
7.4.3.	Current velocity (y-velocity component).....	84
7.4.4.	Current velocity (Z-velocity component)	85
Chapter 8:	Summary, Conclusions and Recommendations	87
8.1.	Summary and Conclusions.....	87
8.2.	Limitations and Assumptions of the study	90
8.3.	Recommendation for Future work	90
References	93
Annex I, Annex II	98
Annex III	99
Annex IV	119

List of Figures

Figure 2.2.1 Geometric representation of elementary paths for samples ($k = 3$, $p = 3$ and $s = 1$) (a) whole grid (b) One cell of the grid (Source: (Tene et al., 2018)).....	13
Figure 2.2.2 Geometric representation of stratified sampling from bisected domains of one parameter (top), 2 parameters (left), and 3 parameters (right) (Source: Saltelli A et al. (2008)).	14
Figure 2.2.3 Two-dimensional projection of (a) pseudo-random sequence and a (b) quasi-random sequence (Source:(Caflisch, 1998)).....	15
Figure 3.2.1 North Sea bathymetry (Data source: (Pätsch et al., 2017))	22
Figure 3.3.1 Model bathymetry of Dutch Continental Shelf Model (DCSM) in a logarithmic scale (water depths relative to MSL) (Source: (Zijl et al., 2021))	25
Figure 3.3.2 Variation of Mannings roughness field in DCSM-FM (Source: (Zijl et al., 2021))	27
Figure 4.2.1 Representation of a trajectory in the input space with three dimensions and five discretization levels (Source:(Saltelli A et al., 2008))	31
Figure 4.5.1 Measured data for currents at FINO3 research platform from 2010 to 2015 (Source of data: BSH (2021))	36
Figure 4.5.2 selected locations for the analysis (green color; existing wind farms of the area), (Source:(<i>Research Project: Multi-Use Offshore Platforms</i> , 2021))	37
Figure 5.1.1 Variation of measured salinity at FINO3 for the year 2016 (Source of data: (BSH, 2021)).....	39
Figure 5.2.1 Measured air pressure data at 23m height from sea level at FINO3 for January 2015 (Data source: BSH, 2021)	44
Figure 5.2.2 Air density calculations for minimum and maximum temperatures (Source:(<i>Engineers Edge</i> , n.d.)).....	44
Figure 7.1.1 Temperature variation at FINO3 over one-month period simulated with 12 trajectories ($r=12$) and using 96 samples	53
Figure 7.1.2 Variation of x velocity at FINO3 over one-month period simulated using 12 trajectories ($r=12$)	55
Figure 7.1.3 Variation of y velocity at FINO3 over one-month period simulated using 12 trajectories ($r=12$)	55
Figure 7.1.4 Variation of z velocity at FINO3 over one-month period simulated using 12 trajectories ($r=12$)	56
Figure 7.2.1 Sensitivity of temperature to each input parameter at FINO3 (a) Absolute mean(μ^*) of EE for input parameters for the three trials ($r = 10, 12$ and 20), (b) Standard deviation (σ) of EE for input parameters for the three trials ($r = 10, 12$ and 20).....	58
Figure 7.2.2 Morris results of temperature sensitivity at FINO3; ($r=12$) Scatterplot for temperature sensitivity - Variation of standard deviation with absolute mean.....	59
Figure 7.2.3 Variation of sensitivity of temperature to input parameters based on the selected location, calculated by Morris method using 12 trajectories ($r = 12$)	61
Figure 7.2.4 Sensitivity of x-velocity to each input parameter at FINO3 (a) Absolute mean(μ^*) of EE for input parameters for the three trials ($r = 10, 12$ and 20), (b) Standard deviation (σ) of EE for input parameters for the three trials ($r = 10, 12$ and 20).....	63
Figure 7.2.5 Morris results for the sensitivity of x-velocity at FINO3; ($r=12$) Scatterplot for x-velocity sensitivity - Variation of standard deviation with absolute mean.....	64

Figure 7.2.6 Variation of sensitivity of current velocity (x-velocity component) to input parameters based on the selected location, calculated by Morris method using 12 trajectories ($r = 12$).....	65
Figure 7.2.7 Sensitivity of y-velocity to each input parameter at FINO3 (a) Absolute mean(μ^*) of EE for input parameters for the three trials ($r = 10, 12$ and 20), (b) Standard deviation (σ) of EE for input parameters for the three trials ($r = 10, 12$ and 20).....	67
Figure 7.2.8 Morris results for the sensitivity of y-velocity at FINO3; ($r=12$) Scatterplot for y-velocity sensitivity - Variation of standard deviation with absolute mean.....	67
Figure 7.2.9 Variation of sensitivity of current velocity (y-velocity component) to input parameters based on the selected location, calculated by Morris method using 12 trajectories ($r = 12$).....	68
Figure 7.2.10 Sensitivity of z_velocity to each input parameter at FINO3 (a) Absolute mean(μ^*) of EE for input parameters for the three trials ($r = 10, 12$ and 20), (b) Standard deviation (σ) of EE for input parameters for the three trials ($r = 10, 12$ and 20).....	70
Figure 7.2.11 Morris results for the sensitivity of y-velocity at FINO3; ($r=12$) Scatterplot for y-velocity sensitivity - Variation of standard deviation with absolute mean.....	70
Figure 7.2.12 Variation of sensitivity of current velocity (z-velocity component) to input parameters based on the selected location, calculated by Morris method using 12 trajectories ($r = 12$).....	71
Figure 7.3.1 First-order and total-order Sobol' indices for the location FINO3.....	74
Figure 7.3.2 First-order and total-order Sobol' indices for x-velocity for location FINO3.....	76
Figure 7.4.1 Correlation of sensitivity measures of Morris method and Sobol' indices (a) Variation of Morris mean with Sobol' S_{Ti} (b) Variation of Morris standard deviation with ($S_{Ti} - S_i$).....	82
Figure 7.4.2 Correlation of sensitivity measures of Morris method and Sobol' indices (a) Variation of Morris mean (μ^*) with Sobol' S_{Ti} (b) Variation of Morris standard deviation(σ) with ($S_{Ti} - S_i$).....	83
Figure 7.4.3 Correlation of sensitivity measures of Morris method and Sobol' indices (a) Variation of Morris mean with Sobol' S_{Ti} (b) Variation of Morris standard deviation with ($S_{Ti} - S_i$).....	85
Figure 7.4.4 Correlation of Morris method and Sobol' indices (a) Variation of Morris mean with Sobol' S_{Ti} (b) Variation of Morris standard deviation with ($S_{Ti} - S_i$).....	86
Figure 8.3.1 Measured data for the temperature at FINO3 for the year 2017 (Data source: (BSH, 2021)).....	91

List of Tables

Table 2.1.1 Summary of advantages and disadvantages of different sensitivity analysis techniques	11
Table 2.2.1 Example of Latin Hypercube design for three parameters, with three levels and six simulations	13
Table 3.2.1 Freshwater discharges to the North Sea (Source: (Ducrotoy et al., 2000))	23
Table 4.5.1 Selected locations for the analysis	37
Table 5.1.1 Important parameters for Blue mussel longlines and Seaweed farming	38
Table 5.2.1 Overview of values used for Dalton and Stanton coefficients in literature (Source: (Twigt, 2006))	42
Table 5.2.2 Dalton and Stanton coefficient values obtained for the South China Sea (Source: (Twigt, 2006))	43
Table 5.2.3 Initially selected input parameters value ranges of each parameter	45
Table 7.2.1 Sensitivity of temperature to the input parameters calculated using Morris method (for $r = 10, 12,$ and 20) at location FINO3	57
Table 7.3.1 Input parameters selected by the Morris screening method for the variance-based analysis	73
Table 7.3.2 Sensitivity indices for the temperature to the input parameters calculated using the Sobol' method at FINO 3	73
Table 7.3.3 Sensitivity indices for x-velocity to the input parameters using the Sobol' method at FINO 3	76
Table 7.3.4 Sensitivity indices for y-velocity to the input parameters calculated using the Sobol' method at FINO 3	77
Table 7.3.5 Sensitivity indices for z-velocity to the input parameters calculated using the Sobol' method at FINO 3	79
Table 7.4.1 Comparison of sensitivity indices for the temperature to the input parameters calculated using the Morris and Sobol' methods at FINO3	81
Table 7.4.2 Correlation between the sensitivity measures calculated by Morris and Sobol' methods	82
Table 7.4.3 Comparison of sensitivity indices for the current velocity (x-velocity component) to the input parameters calculated using the Morris and Sobol' methods at FINO 3	82
Table 7.4.4 Correlation between the sensitivity measures calculated by Morris and Sobol' methods	83
Table 7.4.5 Comparison of sensitivity indices for the current velocity (y-velocity component) to the input parameters calculated using the Morris and Sobol' methods at FINO3	84
Table 7.4.6 Correlation between the sensitivity measures calculated by Morris and Sobol' methods	84
Table 7.4.7 Comparison of sensitivity indices for the current velocity (z-velocity component) to the input parameters calculated using the Morris and Sobol' methods at FINO 3	85
Table 7.4.8 Correlation between the sensitivity measures calculated by Morris and Sobol' methods	86

List of Abbreviations

DCSM	Dutch Continental Shelf Model
EE	Elementary Effects
FAST	Fourier Analysis Sensitivity Test
FM	Flexible Mesh
FSI	First order Sensitivity Index
GSA	Global Sensitivity Analysis
LHS	Latin Hypercube Samples
LSHD	Latin Hypercube Samples with Dependence
MDU	Master Definition Unstructured
OAT	One-At-a-Time
SA	Sensitivity Analysis
TSI	Total effect Sensitivity Index
UNITED	multi-Use platforms and co-location pilots boosting cost-effective, and Eco-friendly and sustainable production in marine environments

Chapter 1: Introduction

1.1. Background

Numerical models are being used in many fields to efficiently calculate physical systems, while these are too complicated to solve manually. These numerical models have many input parameters and physical variables on which the outputs are dependent. In many cases, these input parameters might be unknown or characterized with high uncertainties hence less precise. These unknown or partially known input parameters and physical variables will subsequently create uncertainties in the model output. The exploration of how these uncertainties of model output can be apportioned to the various sources of uncertainties in model input is the primary purpose of the sensitivity analysis (Saltelli et al., 2008). Having a measure of the importance of each input parameter on the output uncertainty will give a deep understanding of the modeled system. Also, this allows reducing the possible uncertainties in model outputs. Further, sensitivity analysis provides the idea on which inputs need a more significant concern and need to be more precise to yield a more accurate response.

Generally, these numerical models have a tremendous amount of input parameters, where some of these are correlated with each other and make it challenging to perform calibration and validation. The high amount of calculation time of these numerical models is another constraint for calibrating the models with many input parameters. As a solution, several researchers have executed many experiments to investigate the possible methods for selecting the most important and influential input parameters and screening out the less influential ones. Sensitivity analysis is one such method used to determine the significant input parameters that have the highest impact on the output of a computational model. Identifying the dependency of the output of a hydrodynamic model on its input variables is vital in simulating a model. Since these models are associated with a large number of unknowns, lots of assumptions are made in the calculation process. Moreover, if the models concern a larger area and are developed with high resolutions, they can consume a high computation time. Besides, the other characteristics of these hydrodynamic models, such as having many input parameters, including complex differential equations that take considerable time and effort for solving, need to be considered in selecting the sensitivity analysis techniques.

This research concerns the hydrodynamic model of the North Sea, which is a part of the Atlantic Ocean and borders England, Denmark, Norway, Germany, Belgium, Netherlands, and France. The North Sea is known as a site for many important shipping lines for more than 200 years. Moreover, this marine environment has been identified as a rich renewable energy source in recent times, where opportunities are considered for large-scale wind energy production, hydrogen production, and underground carbon storage. Therefore, the sea area is gaining the attention of the bounding countries and the scientific community for new developments.

For efficient and sustainable use of existing marine resources, the concept of multi-use has been introduced. The multi-use concept is defined in two aspects, including multi-use platform (MUP) and multi-use space (MUS) (Legorburu et al., 2018). This multi-use concept can be understood as the international joint use of marine resources by two or more users. In other words, it is a compatible use of infrastructure or space for combined multiple activities by different users. In the context of the design, they are introduced in two different approaches. These are Co-location and integration. Co-location is the design of separate platforms without connecting them physically but sharing the same logistic and marine space.

On the other hand, in integration, the idea is to use the same offshore platform for multiple

purposes such as renewable energy, aquaculture, and ecological restoration. Multi-use of maritime space, platforms, or synergies can create a lot more benefits than the traditional exclusive resource utilization. First, it will save the environment in space, establishing the sustainable use of the marine resource, where more space will be left for protection and future generations. Further, these will add value to the economic benefits for marine users by creating opportunities for sharing the developments, operation, and maintenance costs and risks. Besides, this will create social benefits for the users such as skill transfer, creating job opportunities, and reducing impacts. In designing these kinds of infrastructure and multi-use platforms, the designers and decision-makers need to consider the sea area's hydrodynamic conditions (water levels, velocities, waves, and currents). Therefore, simulating the hydrodynamic conditions of marine environments is of greater importance.

Sensitivity analysis can support the efficient use of hydrodynamic modeling by identifying the critical regions of input parameter space and the insignificant input parameters. Therefore, the sensitivity analysis results can help eliminate insignificant input parameters that have less influence on outputs in the modeling process. Hence it reduces the computational effort, time, and cost associated with calibration and validation processes. Therefore, sensitivity analysis has greater importance in numerical modeling, as it supports efficient calibration of models to achieve higher accuracy in model results.

1.1. Problem Statement

The motivation for the thesis was raised primarily by looking at the difficulties, such as spending a considerable time in calibration efforts when performing mathematical models, because they have a large number of input factors to be calibrated therefore require a substantial number of model runs. According to Shin et al. (2013), only a few studies (Schmid et al., 2003, Shen et al., 2008, Plecha et al., 2010, Francos et al., 2003, Kurniawan et al., 2011) have been carried out with the application of sensitivity analysis methods in ranking the parameters and identifying redundancies.

The primary users of the research will be the modelers, who perform complex numerical modeling. The results of this research will discuss the applicability of possible sensitivity analysis methods that can be used for complex numerical models with a high number of input parameters and variables. In addition to that, the researchers and students, who experiment with different sensitivity analysis techniques for numerical models, will benefit from these results for future studies of similar complex numerical models. In addition, research will benefit the UNITED project (which is further described in section 1.4) as a preliminary step for numerical modeling studies, which will be used as decision-making tools in designing and operating. Therefore, even though there is no direct impact on the public, the stakeholders of the said project will benefit indirectly from the research.

1.2. Objectives

The main objective of the research is to highlight the significant input parameters of a hydrodynamic model, which will be most influential for some selected output of the model. Furthermore, the methodology was applied to a hydrodynamic model of the North Sea. For achieving this primary objective, the following sub-objectives are defined.

- Selecting the most suitable methods of sensitivity analysis to apply to the hydrodynamic model
- Identifying the input parameters for the sensitivity analysis based on the literature, referring to the manuals and technical references of D-Flow FM, and with the support of experts from Deltares. The model typically contains a large number of parameters that would be too large for any technique. The idea here is to reduce the number of input parameters for the analysis following the literature and expert knowledge on the model parameters before applying the sensitivity analysis techniques.
- Performing sensitivity analysis for the input parameters of the hydrodynamic model using D-Flow Flexible Mesh model, which is a part of Delft 3D Flexible Mesh model suite.
- Identify the order of significance of relevant parameters according to the rating and the results of the sensitivity analysis techniques.
- Comparing the results obtained from the selected sensitivity analysis techniques.

1.3. Research questions

The main problem identified through the literature is the difficulties of calibrating complex numerical models with many input parameters. SA techniques are being used to identify important parameters of a particular model to overcome the aforementioned problems. The following research questions are specified to cover through this research, considering these facts and objectives of the study.

- What are the different techniques or methods for performing sensitivity analysis?
- Which output parameter sensitivities are going to be analyzed in the study?
- What input parameters need to be considered for the sensitivity analysis of selected output parameters of the hydrodynamic model?
- What are the possible methods that can be used and the suitability of these methods in application to the hydrodynamic model?
- What are the non-influential parameters that can be ignored or given the least priority in future calibrations?
- What are the most significant parameters that determine the accuracy of model output?

1.4. Practical Value

The research is integrated into an innovation project called UNITED (multi-Use platforms and co-location pilots boostIng cost-effecTive, and Eco-friendly and sustainable proDuction in marine environments), which is one of the current European Union Horizon 2020 projects. The UNITED project investigates the viability of the multi-use of offshore platforms in five demonstration pilots spanning the North Sea, Baltic Sea, and the Mediterranean Sea with combinations of multiple sectors such as mixed energy production, aquaculture, ecological restoration, and tourism. The project concept is defined under five pillars: environmental, technological, economic, societal, legal-policy, and safety pillars. One of the technological pillar's intentions is to support management and planning decisions for new development and improve the current design, safety, and infrastructure setups for multi-use extensions. As decision support tools, numerical models are being used for simulating these marine environments. Therefore, the numerical models for decision support systems will be developed covering these five pilot sites. The study area of research was selected considering the location

of the German pilot, which is about 80km off from the North German coast and identified as a high-energy environment.

As a part of this research, the hydrodynamic model will be used to determine the most significant input parameters that need to be highlighted in the calibration and validation and identify the non-influential parameters that can be given less attention and thereby reduce the complexity of the model to ease the calibration. Therefore, in the context of the UNITED project, this research will be beneficial, especially for the German pilot, as a preliminary study for hydrodynamic modeling. Other than that, the research outcomes can be used to calibrate hydrodynamic models for similar cases (for example, results can be used in Belgium pilot, Dutch pilot, etc.) and compare results, discuss, and find solutions to common challenges.

Hence the research will explore performing sensitivity analysis for a hydrodynamic model to determine the most significant input parameters. The knowledge of these significant input parameters will then be used to calibrate and validate the model to reduce the computational time associated with the modeling. This knowledge on critical parameters helps to save computational time and costs spent for the complex hydrodynamic models by making it easier for the modeler to concentrate on the most critical parameters and calibrate the model efficiently. Besides, the methods proposed for this application will be used not only in the field of engineering but also in other numerical model simulations.

1.5. Innovation

The admissible innovation of the study will develop a generic framework for applying sensitivity analysis methods for calibrating the hydrodynamic models, primarily focusing on a hydrodynamic model of the North Sea for the area of German pilot of UNITED project mentioned in the previous section. According to the literature, there are studies (Y. Li et al., 2015; Palermo Stefania Anna and Zischg, 2019) that have already been carried out to analyze the sensitivity of hydrodynamic models. Y. Li et al. (2015) conducted sampling-based uncertainty assessment and sensitivity analysis of a hydrodynamic model of a large shallow freshwater lake. However, the authors (Y. Li et al., 2015) have highlighted that the research only addresses the parametric uncertainty estimation, and future studies should consider sensitivities and uncertainty of boundary conditions to hydrodynamic models. A global sensitivity analysis has been applied by Palermo and Zischg (2019) to a microscale hydrodynamic model to select the most influential parameters of a stormwater management model (SWMM). However, there is still a need for methods to combine sensitivity analysis in hydrodynamic model calibration. Therefore, these research gaps have been considered in this study.

- The main contribution of this research to the scientific world will be developing a generic framework for the application of sensitivity analysis of hydrodynamic models before the calibration.
- As a tool for calculating the sensitivities of input parameters of the hydrodynamic model, an algorithm will be developed which can be used for similar model studies.
- The sensitivity analysis of a hydrodynamic model of the selected case study will support in determining the most critical regions of the input parameter space for a hydrodynamic model in calibrating to specific output variables.

1.6. Thesis Outline

Chapter 1 – Introduction.

This Chapter includes the general introduction about the research, problem statement, thesis objectives, research questions, practical value, and finally, the innovation introduced through the research.

Chapter 2 – Literature review

This chapter includes the literature research to identify the thesis problem, define the thesis objectives, develop the methodology, and interpret the results.

Chapter 3 – Case study.

The Chapter contains the details about the selected case study and physical characteristics of the study area, and software and tools used.

Chapter 4 – Research methodology

The research methodology chapter includes information on the general overview of the methodology as a flow chart, selection of sensitivity analysis techniques for the analysis, and details on selected methods and procedures of application. Further, this includes the selected analysis locations.

Chapter 5 – Selection of parameters for the analysis

Details about the selected input and output parameters and reasoning for the selection includes in this chapter.

Chapter 6 – Application of Python in the sensitivity analysis

The steps followed in applying Python programming for the sensitivity analysis are described in this chapter in detail. However, the developed scripts are not included in this chapter.

Chapter 7 – Results & discussion

Sensitivity results for the selected output parameters are included in Chapter 7, with the analysis of the results obtained from two selected analysis methods.

Chapter 8 – Conclusions and Recommendations

This chapter includes the conclusions of the research, limitations faced in the study, and finally, the recommendations for future research based on the analysis.

Annex I, Annex II – Python scripts

Python scripts developed throughout the analysis are included as Annex I and AnnexII. Annex I contain the scripts used in applying the Morris method, and Annex II contains the scripts used for analysis using the Variance-based Sobol' method.

Annex III– Sensitivity analysis results

Results plots and tables of sensitivity analysis

Chapter 2: Literature Review

Uncertainty and sensitivity analysis are used to assess the reliability and the uncertainty of particular model output. Therefore, it is essential to distinguish between uncertainty analysis and sensitivity analysis before exploring the sensitivities of input parameters. Although both uncertainty assessment and sensitivity analysis closely resemble, the former is focused on quantifying the uncertainty in model predictions without considering the source of uncertainty. According to (A Saltelli et al., 2008), sensitivity analysis can be defined as the “study of how the uncertainty in the output of a model can be apportioned to different sources of uncertainty in the model inputs.”

Sensitivity analysis can be used for different purposes. One of these will be factor prioritization, identifying which inputs contribute the most to creating model uncertainties. Secondly, it will also help quantify the fractions of contributions of the input parameters to the model uncertainty (Andrea Saltelli et al., 2019). Further, sensitivity analysis is used to fix or identify which factors have a negligible contribution to the uncertainty of model output and can be fixed in the model (Andrea Saltelli & Tarantola, 2002). Therefore, the importance of performing sensitivity analysis for numerical models is extensively acknowledged.

Different techniques have been proposed in several publications for the previously mentioned concept of sensitivity analysis. Based on the formulation and application, two different categories of methods can be identified for performing sensitivity analysis, namely local and global. The local techniques consider the partial derivatives at a single point of the input parameter space. Therefore, these local methods give only limited information about the sensitivity of input parameters on output. Typically, these methods consider the changes in model outputs when the input parameters vary about a reference value or an optimal input parameter set (Pianosi et al., 2016). Because of that, these methods will not yield an exploration of the rest of the input parameter space. The local techniques are often referred to as single point One-At-a-Time (OAT) methods. One-at-a-time sensitivity analysis is the most fundamental method with partial differentiation. Here the input parameter values are varied one at a time while keeping the other parameter values constant. However, (Andrea Saltelli & Annoni, 2010) pointed out that these single-point OAT methods are inadequate for a complete analysis of models unless the model is linear.

In contrast to the local methods, global methods do not consider an initial set of input parameter values and contemplate the entire parameter space. Instead, global methods focus on the effects on output when the inputs are varied globally. Variance-based methods are one such global technique focusing on the variance of model output and how the input variability influences the output variability. In global sensitivity analysis, the global effect of the parameters on outputs is analyzed where the parameter interactions are also considered. Therefore, global sensitivity analysis is used for a comprehensive study of sensitivity and the interactions among input parameters of a particular model, rather than concentrating on a single input at a time.

Since the local methods estimate the sensitivities by directly calculating the partial derivatives, these methods are simple to calculate. Therefore, these are best suited for the preliminary screening of complex models with high computation times. However, the local techniques only consider small perturbations around a nominal value (for example, the mean of the variables) at one reference point from the possible input parameter space. Hence the sensitivity measure will depend on the position, where the derivatives are calculated and will not represent the whole parameter space. This acts as a limitation for using local methods in sensitivity analysis in complex numerical models, which are generally non-linear.

2.1. Sensitivity Analysis techniques

As discussed in the introduction, several methods are used to perform the sensitivity analysis for a particular numerical model. Generally, sensitivity analysis techniques can be classified as local and global. The local techniques assume that all the input factors are equally important and do not consider the outputs' variance (Saltelli A et al., 2008). According to (Hall et al., 2009), the global methods have the ability to reflect the nonlinear effects and the effects due to interactions among input parameters. However, global methods require high computation demand compared to the local sensitivity analysis techniques as the required number of model evaluations increases with the number of input factors. The sensitivity analysis techniques which are used frequently are further described below.

2.1.1. Morris screening method

The Morris method named the Elementary Effects method is a 'one at a time'(OAT) design, where all the input parameters are evaluated, exploring the possible parameter range. This method aims to rank the inputs according to their significance by evaluating their average effect on output. The elementary effect method can be suggested as a feasible method for analyzing input factor sensitivities, considering the hydrodynamic models' complexity and non-linearity.

In many publications (Saltelli et al., 2008; Campolongo and Saltelli, 1997; Ruano et al., 2011, Morio, 2011), the vast applicability of the Elementary Effects method has been highlighted. The method is recommended as a preliminary screening method to eliminate non-significant parameters and rank the parameters according to the significance. The Elementary Effect method has gained attention due to its computational efficiency and adaptability. The method is a one-at-a-time method designed by (Morris, 1991) to identify the non-influential parameters and rank the parameters according to significance. Morris method is sometimes mentioned as a global method in some literature (A Saltelli et al., 2000; Shin et al., 2013), as it considers the whole input parameter space. Although it takes the elementary effects (d_j) like the partial derivatives, as in local methods, the method averages the local effects computed at different input locations. The final sensitivity measure is considered to be these averages of elementary effects.

For a given input vector with N number of input parameters, $X = (x_1, x_2, \dots, x_j, \dots, x_N)$; the elementary effect of j^{th} input parameter on the output y can be expressed as;

$$d_j = \frac{y(x_1, x_2, \dots, x_{j+\Delta}, x_{j+1}, \dots, x_N) - y(x_1, x_2, \dots, x_j, x_{j+1}, \dots, x_N)}{\Delta} \quad 2.1$$

where x_j is scaled to [0,1] and discretized to p number of levels. Δ is the Morris step and defined by

$$\Delta = \frac{s}{(p-1)}; \quad s \in \{1, 2, \dots, p-1\}$$

Here, Δ is a predetermined multiple of $1/(p-1)$.

Sensitivities of the input parameters can be identify using the following measures. The mean, absolute mean, and the standard deviation of elementary effects for j^{th} input parameter can be defined as:

$$\mu_j = \frac{1}{r} \sum_{i=1}^r d_j^{(i)}, \quad \mu_j^* = \frac{1}{r} \sum_{i=1}^r |d_j^{(i)}|, \quad \sigma_j = \sqrt{\frac{1}{r-1} * \sum_{i=1}^r (d_j^i - \mu_j)^2} \quad 2.2$$

Where r is the optimum number of repetitions.

Morris method is recommended as a reasonable approximation to variance-based sensitivity measures (Andrea Saltelli & Saisana, 2007). This method can be used to:

- Calculate the optimum repetition number for the elementary effect (EEi) calculations
The optimum number for repetition of elementary effect calculations (r) needs to be determined correctly; otherwise, it may cause Type I (i.e., identifying non-influential parameter as an influential parameter) as well as Type II (i.e., failing to identify a significant parameter as influential) errors (Ruano et al., 2011). The optimum repetition number will be determined by calculating the absolute mean (μ^*) and standard deviation (σ) for the elementary effects of each input factor, with different repetition numbers (r), until those measures for the influential parameters become stable. Considering the absolute mean values rather than mean values is essential because the elementary effects can compensate each other and yield a wrong idea. One disadvantage of this method is that many repetitions will be needed if the model is highly complex and non-linear. The computation cost of the Morris method for a model with k number of input parameters that requires an optimum repetition number of r will be $r*(k+1)$.

- Identify the non-influential input factors

The importance of the input parameters can be evaluated considering the sensitivity measures, mean (μ), absolute mean (μ^*), and the standard deviation (σ) of elementary effects. Campolongo et al. (2007) highlighted the drawbacks of using μ and σ only for deciding the significance of inputs when the model has several outputs, and the model is non-monotonic. Therefore, the authors proposed to use the absolute mean (μ^*) instead of the mean (μ), which can solve the issue of falsification of the results due to canceling out of the elementary effects with opposing signs. However, one limitation of using absolute mean values of elementary effects is losing the information about the direction or the sign of the effects.

The values of μ^* and σ will imply the significance and linearity effects of the input parameters. Input parameters with smaller values of μ^* indicate less impact of the input parameter on the output. Therefore, parameters with lesser absolute mean values can be eliminated as unimportant (Morio, 2011).

The criterion suggested by the study of Sarrazin et al. (2016) for choosing a threshold for identifying insignificant factors from a set of inputs can be applied here when deciding the unimportant input factors.

- Rank the input parameters

Parameter ranking will be based on the magnitudes of the elementary effects of each input parameter. Parameters can be interpreted into three categories (Morio, 2011), considering the above sensitivity measures,

1. Weaker values of μ^* - insignificant input parameters
2. Stronger values of μ^* and weaker values of σ - important inputs with linear effects and without interactions with other input parameters
3. Stronger values of μ^* and stronger values of σ - important inputs with non-linear effects with or without interactions with other input parameters

However, one primary assumption of the classic Morris method is the independence of the input parameters, which acts as a limitation of applying for complex numerical models.

2.1.2. Variance-based method of Sobol'

Sobol' method is a variance-based sensitivity analysis technique that can determine input variances' contributions in creating output variances and the input parameter interactions. It does not rely on the assumptions about the smoothness of input and output parameter mapping (Andrea Saltelli & Saisana, 2007). The Sobol' method is expensive for models with a high number of inputs. The number of Sobol' indices that need to be calculated will exponentially increase with the input dimensions (Morio, 2011). The Sobol' sensitivity measures are defined assuming that the total output variance can be decomposed into main effects due to individual inputs and residual effects.

The first-order sensitivity measures are used to capture the direct impact of the input factors. Then, the total effect sensitivity measures are used to capture both direct impacts and the impacts due to interactions of the input factors. Total order effects are helpful for the purpose of factor fixing. For an input factor X_i to be noninfluential for an output Y , the total order sensitivity of X_i needs to be nearly zero; $S_{Ti} \cong 0$ (Saltelli A et al., 2008). Thus, the factor can be fixed without affecting the output Y .

Before applying the variance-based analysis method, it is essential to look at its definition. We can assume a function ϕ with p number of input parameters defined in the range of $[0, 1]^p$. The input variables are also needed to be defined in the range $[0,1]$. Thus, the output Y can be decomposed to elementary functions of inputs, as shown in 2.3.

$$Y = \phi(X) = \phi_0 + \sum_{i=1}^p \phi_i(X^i) + \sum_{1 \leq i \leq j \leq p} \phi_{ij}(X^i, X^j) + \dots + \phi_{1\dots p}(X^1, \dots, X^p) \quad 2.3$$

Where; ϕ_0 is a constant, and ϕ is an integrable function of X . The inputs are random and independent, and therefore, applying the variance operator to the equation 2.3 to obtain ANOVA decomposition yields;

$$Var(Y) = Var = \sum_{i=1}^p V_i + \sum_{1 \leq i \leq j \leq p} V_{ij} + \dots + V_{1\dots p} \quad 2.4$$

Applying the Var operator, first, second and k^{th} order partial variances can be defined as;

First-order	$V_i = Var(E(Y X_i))$
Second-order	$V_{ij} = Var(E(Y X_i, X_j)) - V_i - V_j$
k^{th} order	$V_{ij..k} = Var(E(Y X_i, X_j, \dots, X_k)) - V_i - V_j \dots - V_k$

The first-order sensitivity index is defined as the partial contribution of each input parameter to the output variance, and the first-order sensitivity index (FSI) for an input variable X_i can be calculated by;

$$S_i = \frac{V_{x_i} \left(E_{x_{\sim i}}(Y|X_i) \right)}{V(Y)} \quad 2.5$$

Where X_i is the i^{th} parameter, and $X_{\sim i}$ indicates the input vector with all parameters except X_i . The inner expectation operator denotes the mean of Y , the scalar objective function values considered over all possible values of $X_{\sim i}$, where X_i is fixed. The V_{x_i} Indicates the variance over all possible X_i .

Total order sensitivity index (TSI) is defined as;

$$S_{Ti} = \frac{E_{x_{\sim i}} \left(V_{x_i}(Y|X_{\sim i}) \right)}{V(Y)} = 1 - \frac{V_{x_{\sim i}} \left(E_{x_i}(Y|X_{\sim i}) \right)}{V(Y)} \quad 2.6$$

The Sobol' index is always in the range [0 1], and the sum of all Sobol' indices should equal to 1.

$$\sum_{i=1}^k S_i + \sum_{i<j}^k S_{ij} + \dots + S_{12\dots k} = 1 \quad 2.7$$

In a review of settings and methods for global sensitivity analysis, (Andrea Saltelli & Saisana, 2007) have pointed out that the variance-based techniques give the most complete and general pattern of sensitivity analysis for the models which have a modest amount of running time (for example up to the order of one minute per run) and do not exceed about 20 input parameters.

2.1.3. Linear regression coefficients

Linear regression coefficients (r) are an adequate and straightforward method to estimate input parameter sensitivities to the output, especially for linear models. The main advantages of this method are its simplicity and having a low computational cost with respect to the previously mentioned OAT and variance-based methods. The method is applied by fitting the data and model result into a linear regression model in the form

$$y_i = b_o + \sum_{j=1}^r b_{zj} z_j^i \quad 2.8$$

The coefficients b_o and b_{zj} are determined using a least-square error of the differences of outputs calculated by the regression model and the actual output. These regression coefficients will give an indication of the sensitivities of output with respect to each input parameter. Having a larger b_z implies that the particular input factor is more sensitive to the output parameter. Nevertheless, the method can be used only for linear models. Further, linear regression coefficients cannot be used if the inputs have dependencies on each other.

2.1.4. Standardized regression coefficients

Standardized regression coefficients ($\beta_{z,j}$) are identified as a cheaper alternative for the variance-based methods. However, the method is effective only for linear or quasi-linear models, with higher regression coefficients (i.e., for example, $R^2 > 0.7$) (Saltelli and Saisana, (2007).

The standardized regression coefficients are defined as;

$$\hat{\beta}_{x_i} = \hat{b}_{x_i} \frac{\sigma_{x_i}}{\sigma_y} ; \quad (i = 1,2,3\dots r) \quad 2.8$$

Where b_{x_i} is the regression coefficient for the i^{th} parameter. Using the standardized regression coefficient method is more popular than just using the regression coefficients.

2.1.5. Random balance designs (RBD) method

The method is suitable for calculating only the first-order sensitivity indices. The advantage of the RBD method is that it has a low computational cost as it is a dimension-independent method, and the computation cost is equal to the sample size. The input points will be selected covering a sub-set of input parameter space, taking random permutations of the points' coordinate and generating a set of scrambled points over the input space. The outputs are calculated for each design point (S. Tarantola et al., 2006). Since the sensitivity analysis is based on the setting, if the purpose is to prioritize the factors, this method will be helpful in such cases (Andrea Saltelli & Saisana, 2007).

Hence, the global sensitivity analysis methods enable more details about the importance of input parameters, linearities, and interactions among input parameters than the local analysis methods. However, local methods are preferred over global methods if the model consumes a considerable computation time and has many input factors (Morio, 2011). The information about the methods discussed above is summarized in Table 2.1.1.

Table 2.1.1 Summary of advantages and disadvantages of different sensitivity analysis techniques

SA technique	Advantages	Disadvantages
Morris method	Efficient screening method Better approximation to global sensitivity analysis methods	Does not consider the parameter dependencies
Sobol' method	A quantitative analysis method for variance decomposition Input parameter interactions are considered. Model independence – method can be applied to any model (Stefano Tarantola et al., 2012)	High computational demand due to the requirement of a high number of models
Random balance design method	Dimension independent method & low computational demand	Parameter dependencies are not considered
Standardized regression coefficients	Cheap alternative for variance-based methods	Only suitable for linear or quasi-linear models
Linear regression coefficient	Dimension independent method & low computational demand	Only suitable for linear models with high regression coefficients

2.2. Sampling methods for sensitivity analysis

The first step of applying sensitivity analysis techniques is generating the input samples according to the selected analysis method. Therefore, the possible sampling techniques will be briefly discussed in this section.

There are several sampling techniques defined in the literature (Andres, 1997; Kucherenko et al., 2012b; Morris, 1991; Saltelli A et al., 2008; Andrea Saltelli et al., 2010; Sobol', 2001) for generating the input samples to apply the sensitivity analysis into the numerical models. Here we have focused on few sampling techniques commonly used in SA.

2.2.1. One-Factor-At-a-Time (O-A-T) sampling

The basic idea of this sampling method is to create samples where the input parameter values of each sample are generated by changing the value of only one parameter at a time (Saltelli A et al., 2008). This sampling scheme can be represented in the matrix form as follows.

$$\begin{bmatrix} 1 & 0 & 0 & \dots & 0 \\ 1 & 1 & 0 & \dots & 0 \\ 1 & 1 & 1 & \dots & 0 \\ \dots & \dots & \dots & \dots & \dots \\ 1 & 1 & 1 & \dots & 1 \end{bmatrix} \begin{pmatrix} b_0 \\ b_1 \\ \dots \\ b_k \end{pmatrix} = \begin{pmatrix} y_1 \\ y_2 \\ \dots \\ y_k \end{pmatrix}$$

Each parameter will have either 0 or 1 as the values, and only one parameter has changed between consecutive samples. When the above equation is simplified by applying a row operation to subtract the values from each row from the row below, it will yield

$$\begin{bmatrix} 1 & 0 & 0 & \dots & 0 \\ 0 & 1 & 0 & \dots & 0 \\ 0 & 0 & 1 & \dots & 0 \\ \dots & \dots & \dots & \dots & \dots \\ 0 & 0 & 0 & \dots & 1 \end{bmatrix} \begin{pmatrix} b_0 \\ b_1 \\ \dots \\ b_k \end{pmatrix} = \begin{pmatrix} y_1 \\ y_2 - y_1 \\ \dots \\ y_k - y_{k-1} \end{pmatrix}$$

Therefore, each value of the output matrix ($y_{i+1} - y_i$) corresponds to a change in one input parameter. The above example shows parameters only with two distinct values (0 and 1) where the parameter can change in smaller values to create more samples. The change of input parameters from one sample to the next can be done in any order. However, the order of change needs to be recorded for analyzing the effect of each perturbation on the output. If the parameter changing order is randomly chosen, the parameter change corresponds to a random walk along the surface of a hypercube from one corner to another. This concept is gematrically represented by (Tene et al., 2018), as shown in Figure 2.2.1.

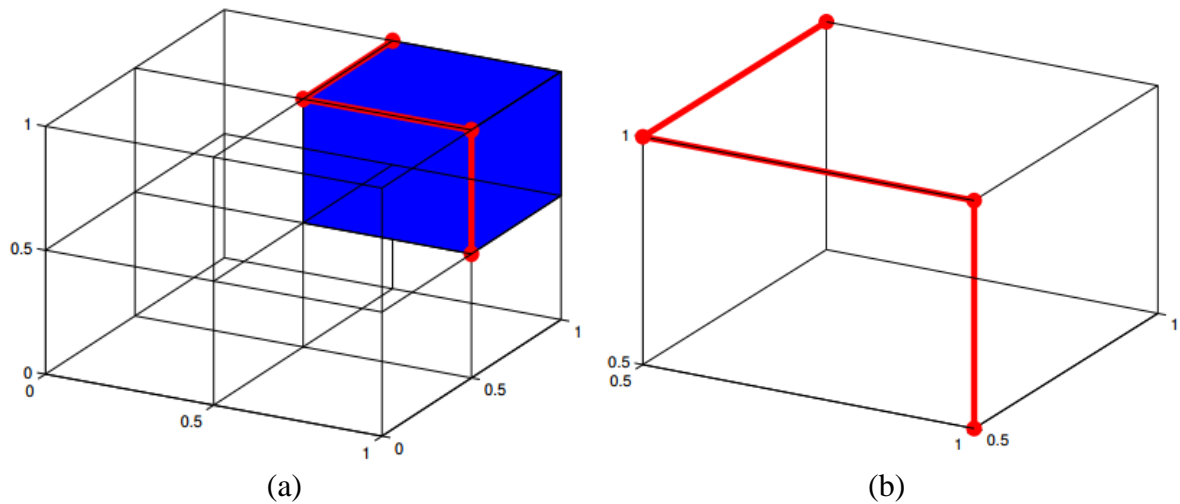


Figure 2.2.1 Geometric representation of elementary paths for samples ($k = 3$, $p = 3$ and $s = 1$)
 (a) whole grid (b) One cell of the grid (Source: (Tene et al., 2018))

2.2.2. Fractional factorial designs

Factorial designs are defined as sampling designs with two or more factors, which take only two distinct values (0 and 1). A full factorial design is where all the possible samplings are considered in the experimental design. If the experiment has k input parameters to be sampled, there should be 2^k number of samples to generate all the possible combinations. Thus, one major disadvantage of this factorial design method is the requirement of a vast number of simulations (Saltelli A et al., 2008).

However, to overcome this issue with the requirement of a large number of simulations, a fraction of the full factorial designs can be selected. This selection of a smaller fraction of the full factorial design is called the fractional factorial design.

2.2.3. Latin Hypercube sampling

In the Latin Hypercube sampling, a fraction of s -level full factorial designs is selected so that the sample represents valuable properties. The main objective of the Latin Hypercube Sampling is that each parameter is discretized into $s > 2$ levels, and each level has the same number of points. The generation of these samples is done by generating values from 0 to $s-1$ and randomizing the columns separately. For example, Table 2.2.1 shows a Latin Hypercube Sample with three input parameters, with three levels and each parameter having two samples at each level. These randomized designs are generated by storing the values from 0 to 2 (i.e., $s-1$) in each column and randomizing them separately.

Table 2.2.1 Example of Latin Hypercube design for three parameters, with three levels and six simulations

X_1	X_2	X_3
0	1	2
1	2	0
2	0	1

1	2	0
2	0	1
0	1	2

In this sampling method, it assumes the model has k number of input parameters, and the input vector is defined as $X_r = \{X_1, X_2, \dots, X_k\}$. Further, it assumes that the X_r is uniformly distributed over its domain, and all the parameters in X_r are statistically independent, where any combination of input parameters X_r is equally likely. Therefore, k sample points are defined in the k dimensional parameter space, uniformly distributed over the k -dimensional space (Saltelli A et al., 2008). The parameter space would be a k -dimensional hypercube. Suppose the number of samples (N) is much larger than the number of input parameters (k). In that case, the randomized Latin Hypercube sampling (LHS) designs will be more effective in determining the effect of each input parameter on the output (Saltelli A et al., 2008). Nonetheless, if the size of N is smaller than k , there will not be enough sampling points to compute the individual effects of the input parameter changes on the output.

2.2.4. Multivariate stratified sampling

In multivariate stratified sampling, the parameter space is divided into non-overlapping regions, and sampling points are selected from each region. The primary purpose of this sampling method is to guarantee that the sampling points represent the whole parameter space.

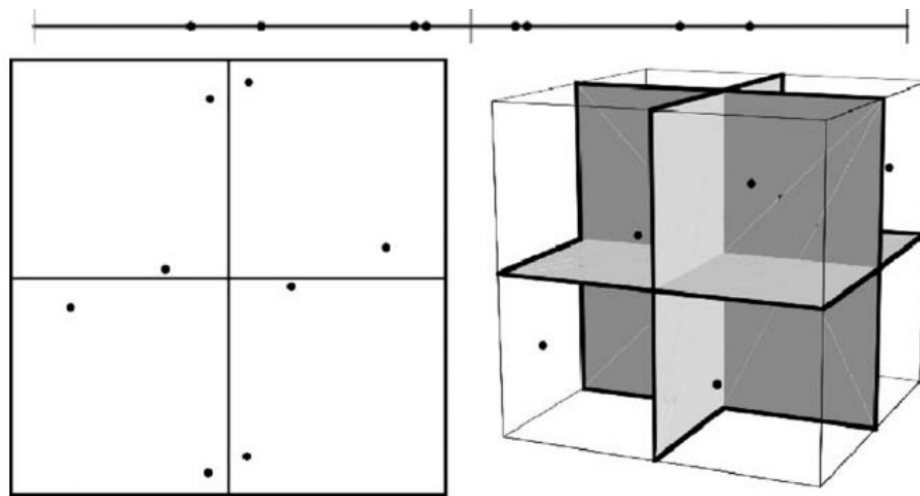


Figure 2.2.2 Geometric representation of stratified sampling from bisected domains of one parameter (top), 2 parameters (left), and 3 parameters (right) (Source: Saltelli A et al. (2008)).

Therefore, the sampling space for k number of parameters will be a k -dimensional hypercube.

2.2.5. Monte Carlo and quasi-Monte Carlo sampling

The Monte Carlo sampling is used to generate random samples from a probability distribution in such a way that the samples will approximate the actual distribution. This Monte Carlo method uses a pseudo-random sequence (Saltelli A et al., 2008). The limitation of pseudo-random sequences is the clumping of points and having spaces with no sampling points. In simple terms: the uniformity of the distribution of sample points is less in the pseudo-random

sampling method. This clumping happens due to the independence of the generation of sampling points, as all the points are randomly generated without considering the other points.

In the quasi-Monte Carlo approach, the sampling is done with quasi-random sequences where the correlations between the points are considered to eliminate the clumping of the generated random points (Caflisch, 1998). The method is designed considering the uniformity of the sample points. Therefore, it estimates the uniformity measure for the sample in terms of the discrepancy of the sequence of points. The difference in the samples generated by these two approaches are shown in Figure 2.2.3 (a) and (b).

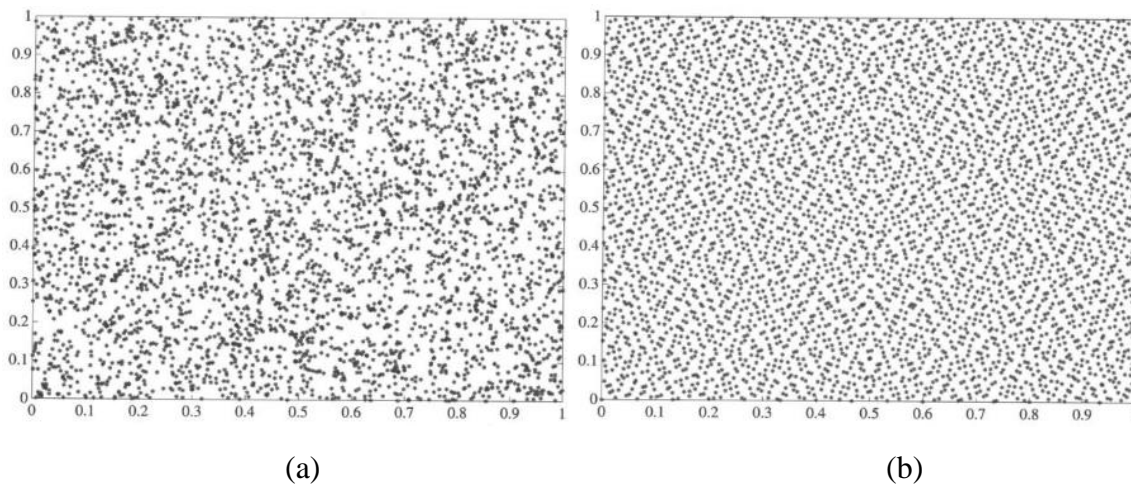


Figure 2.2.3 Two-dimensional projection of (a) pseudo-random sequence and a (b) quasi-random sequence (Source:(Caflisch, 1998)).

2.3. Applications of different SA techniques

These sensitivity analysis techniques are being used for evaluating the input-output interactions in models in many fields such as engineering, economic and environmental. (Ruano et al., 2011) experimented on the application of Morris method, which is mentioned in section 2.1.1, for screening the influential parameters of fuzzy controllers applied to a wastewater treatment plant. Although the technique has some drawbacks, such as high computational cost and inability to measure input parameters' dependencies, Morris method is considered a good approximation of a global sensitivity measure. It has overcome local methods whose results are valid only locally.

To overcome the limitation of the inability to measure the dependency information in Morris method, (Tene et al., 2018) introduced a copula-based sensitivity analysis method to incorporate the dependency information among input parameters into the sampling strategy. The number of model runs was then decided using the algorithm Latin Hypercube Samples with Dependence (LHSD), proposed by Packham and Schmidt (2008). Finally, Tene et al. (2018) performed a sensitivity analysis for a computationally expensive Delft3D WAQ sediment transport model to test the applicability of the proposed copula-based Morris method. A copula is understood as a joint distribution defined on the n -dimensional unit hypercube, with uniform marginal distribution (Nelson, 2007). Thus, this extended method can separate the influence of marginal distributions and parameter dependencies (Tene et al., 2018).

To identify the sensitive parameters in surface water quality models, Huang & Liu (2008) introduced a hybrid approach that integrates the parameter perturbation method and Morris method. A total of 96 input parameters were considered for the analysis. Initially, the parameter perturbation method, a local sensitivity analysis technique, was applied to eliminate the insignificant parameters from the total parameter pool. The required number of model evaluations in the parameter perturbation method is lesser than those needed in the Morris method. Hence, the method is simple to implement and computationally more economical than the Morris method (Huang & Liu, 2008). Then the Morris method was used in ranking the remaining 51 sensitive parameters, which were screened using the parameter perturbation method according to their sensitivities and relative importance. Although the introduced method can determine the order of significance of the input parameters, it lacks the quantitative measure of input parameter interactions.

The variance-based sensitivity analysis method briefly discussed in section 2.1.2 (will be discussed in more detail in Chapter 4) is a global sensitivity analysis technique where the sensitivities of input parameters are considered over the whole parameter range rather than considering the local effect of one parameter. These variance-based methods are being used (Archer et al., 1997; Chen et al., 2018; da Veiga, 2015; G. Li et al., 2010) for obtaining a more detailed analysis of the sensitivities of the model outputs. These methods are designed to decompose the variance of a particular model's outputs and attribute those to the input variances. (Chen et al., 2018) applied variance decomposition method for sensitivity analysis of 1D and 2D hydraulic models developed to simulate branched urban flood flows. The authors have quantified the sensitivities of two selected outputs, including simulated water height and the discharge repartition in a branched network, to some selected input parameters of the 1D and 2D shallow-water models.

Further, the study illustrates the pattern of spatial variation of the input parameter sensitivities. The research has presented a quantification of non-linearities of the complex flow patterns and dependencies of the input parameters using Sobol' indices. They have recommended using the results and findings of this study in future work related to the uncertainty propagation of hydrological models.

Although the variance-based sensitivity analysis methods can determine the effect of input parameters on output variance, it has limitations in providing a complete picture of the output distributions. Veiga (2015) introduced a new class of sensitivity indices that considers the dependence measures and extended those indices using the other dependence measures such as distance correlation and Hilbert-Schmidt independence criterion. Further, da Veiga, (2015) pointed out that those dependence measures will be an alternative to the screening methods, especially for models with high dimensions, as the indices are robust to dimensionality and have low computational costs. Therefore, the method is a powerful tool for global sensitivity analysis. Cosenza et al. (2013) applied three global sensitivity analysis methods to select significant input factors and eliminate non-influential factors of a complex integrated membrane bioreactor (MBR) model in a wastewater treatment system. The performance of three methods (standard regression coefficients, Morris screening, and extended-Fourier analysis Sensitivity Test (FAST) method) was analyzed by taking the most reliable method (extended-FAST) as a reference. The comparison of methods was carried out by considering the similarity of sensitivity indices compared to a reference method, the similarity of ranking, identification of the non-influential inputs, the ability of the method to determine the interaction among input factors, and the method's ability to provide the result within a reasonable time (Cosenza et al., 2013).

Glen & Isaacs (2012) discussed a new notation for Sobol' indices regarding Pearson correlation

of outputs and introduced a simple correlation-based numerical approach to include a correction term for removing spurious correlations. Additionally, different estimation techniques were compared for accuracy and precision. The advantages of this method are providing a reasonable estimate for first-order and total effect indices, easiness of implementation, and suitability for complicated stochastic models (Glen & Isaacs, 2012).

Kucherenko et al. (2012) suggested a novel approach for estimating variance-based sensitivity indices for models with dependent variables. In the study, a copula-based sampling technique was used for sampling probability distributions. Subsequently, the formulas and Monte Carlo estimates were derived for analyzing the relative importance and correlations of inputs. For comparison and testing of the derived formulas, three test functions were used. Analytical solutions were obtained for two of them and observed a good agreement with the numerical results. Furthermore, the authors Kucherenko et al. (2012) concluded that the convergence rate of the proposed approach is much higher than the brute force method. They concluded that the technique is efficient and general to use in numerical models to estimate variance-based sensitivities

Considering the lack of guidance to assist the users of sensitivity analysis in choosing the sample size and threshold for identifying insignificant factors from a set of inputs, Sarrazin et al. (2016) proposed a criterion to select the sample size and screening threshold based on a bootstrap approach. The methodology was applied to three hydrological models with different complexities, utilizing three global sensitivity analysis methods (Regional Sensitivity Analysis, Morris method, and Sobol' method). Moreover, the screening thresholds were validated using a quantitative validation procedure. As a result, the method is highlighted as a suitable approach for a wide range of Global Sensitivity Analysis methods and cases (Sarrazin et al., 2016).

Bellos et al. (2020) applied SA using the Morris method to determine the significant parameters of a 2D hydrodynamic model to reconstruct a flash flood event. Sensitivity analysis was used before analyzing the uncertainties of model output created due to uncertainties of two estimated input parameters identified through the SA. To reduce the calibration efforts of hydrodynamic models, Y. Li et al. (2015) studied the parametric uncertainties of hydrodynamic processes of shallow lakes and recommended that the uncertainties of boundary conditions (wind fields, flow boundaries) should be considered in future studies.

Campolongo & Saltelli (1997) have compared sensitivity tests on an environmental model (GMSK) using different analysis techniques, including the Morris method, variance-based Sobol' method, and standardized regression coefficients. Further, in this study, authors have highlighted the importance of using bootstrapping to estimate the empirical confidence bounds of the sensitivity indices calculated in the Morris method. Considering the physical meaning of these indices calculated by the Morris and Sobol' methods, Campolongo & Saltelli (1997) have suggested possible correlations between Morris mean (μ^*) and the total-order index (S_{Ti}) calculated by the Sobol' method.

Chapter 3: Case Study – German Pilot

UNITED is one of the current Horizon 2020 projects of the European Union, designed to demonstrate the feasibility of the multi-use of offshore platforms and marine space. The project concerns different sectors, including renewable energy, aquaculture, ecology, and tourism. UNITED project is designed under five pillars to check the viability of these multi-use solutions. These five pillars are technological, environmental, economic, societal, and legal-policy-safety pillars. The German pilot of the UNITED project was selected as the study area in this research. This pilot project is designed to check the viability of offshore cultivation of Seaweed and Blue mussels, combined with existing offshore wind farms. In this pilot project, the design conditions and challenges in the operations are going to be studied, simulating the marine environment of the North Sea. Therefore, a North Sea hydrodynamic model will be used as a tool for decision-making in the design and operation of these aquaculture activities.

The pilot project will be installed in the FINO 3 research platform, which is located 80km west of Sylt island near the North German coast. The location is shown in Figure 3.1.1.

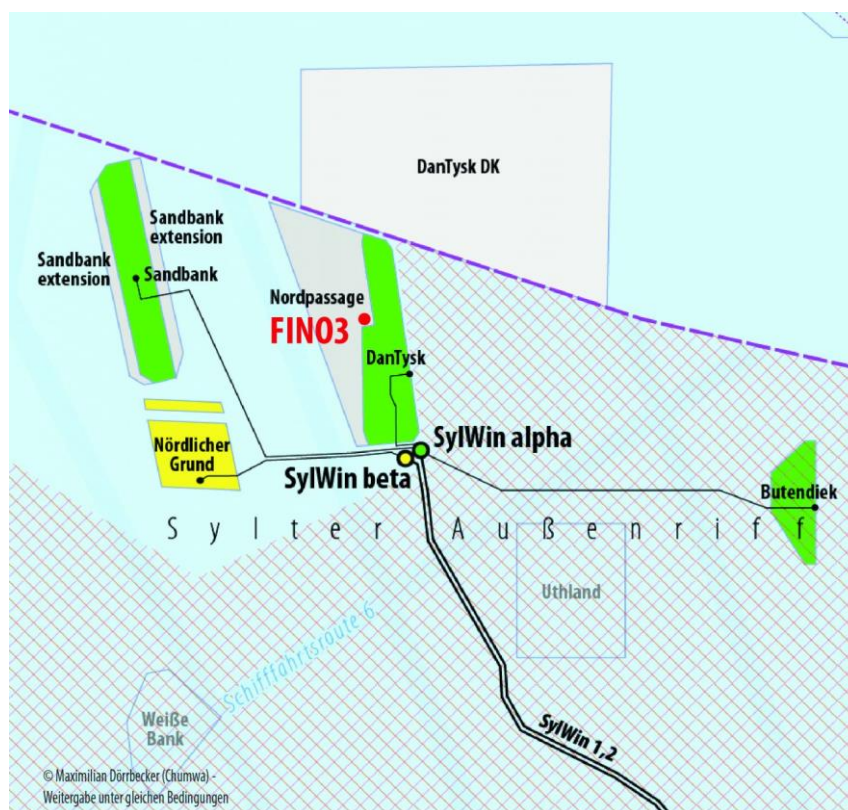


Figure 3.1. 1 Location of German pilot - FINO3 Research platform (Source: *Research Project: Multi-Use Offshore Platforms*, 2021)

3.1. Key aspects of the German pilot

The key aspect of the German pilot is to demonstrate the technological, environmental, and financial feasibility of offshore cultivation of Seaweed and Blue mussel longlines. Currently, in most cases, these Blue mussel and Seaweed farms are established nearshore or inshore environments due to the technological requirements for offshore sites. Nevertheless, there are several drawbacks and problems faced by the marine environment because of these nearshore farms. The main problem is the navigation difficulties for the marine vessels. The nutrient depletion on account of the Blue mussel and Seaweed farms can harm the other marine species in those areas. Other than that, the pseudofaeces and the marine litter generated by the mussels will alter the benthic environment under these mussel farms. As a consequence of these factors, mussel farming and Seaweed cultivation strive for offshore cultivation (Landmann et al., 2019).

Therefore, it is crucial to identify the favorable conditions for those aspects and the significant environmental variables that will affect Seaweed and Blue mussel cultivation effectiveness. For example, in the offshore environments, these Blue mussel and Seaweeds have to bear the high energy acting on them as high currents and waves. Therefore, after identifying the parameters which affect the Blue mussel and Seaweed farming, the sensitivity analysis was focused on the identified output parameters. The purpose here was to calibrate the hydrodynamic model for these parameters to predict those outputs from the model with minimum uncertainties. Thus, this specific project will benefit as a decision-making tool for planning and operating the Blue mussel and Seaweed cultivation.

Output parameters were selected by considering which parameters will mainly affect the offshore cultivation of

- Blue mussel (*Mytilus edulis*) using longlines and
- Seaweed (*Saccharina Latissima*) using longlines

3.1.1. Blue mussel longlines

The longline technique will be used in the cultivation of Blue mussel and Seaweeds in the offshore platform. In offshore Blue mussel farming, these lines are submerged to a few meters depth and moored to the sea bed. The purpose of submerging the longlines to a certain depth from the sea surface is to avoid the disturbances caused by the waves, rough weather conditions of the sea surface. The mooring system supports the submergence of these longlines. As shown in figure 3.1.2, these mussels are attached to the ropes until harvest time. However, in the early growth stages of the mussels, these ropes are housed in ‘protection socks,’ which will disintegrate within a short period of growth (Mizuta & Wikfors, 2019).

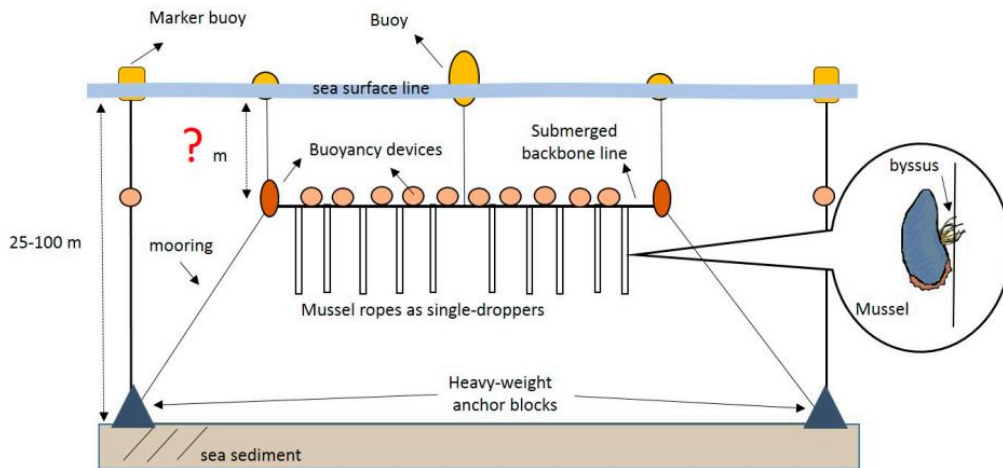


Figure 3.1.2 Schematic of an offshore mussel longline (Source: Mizuta & Wikfors, 2019)

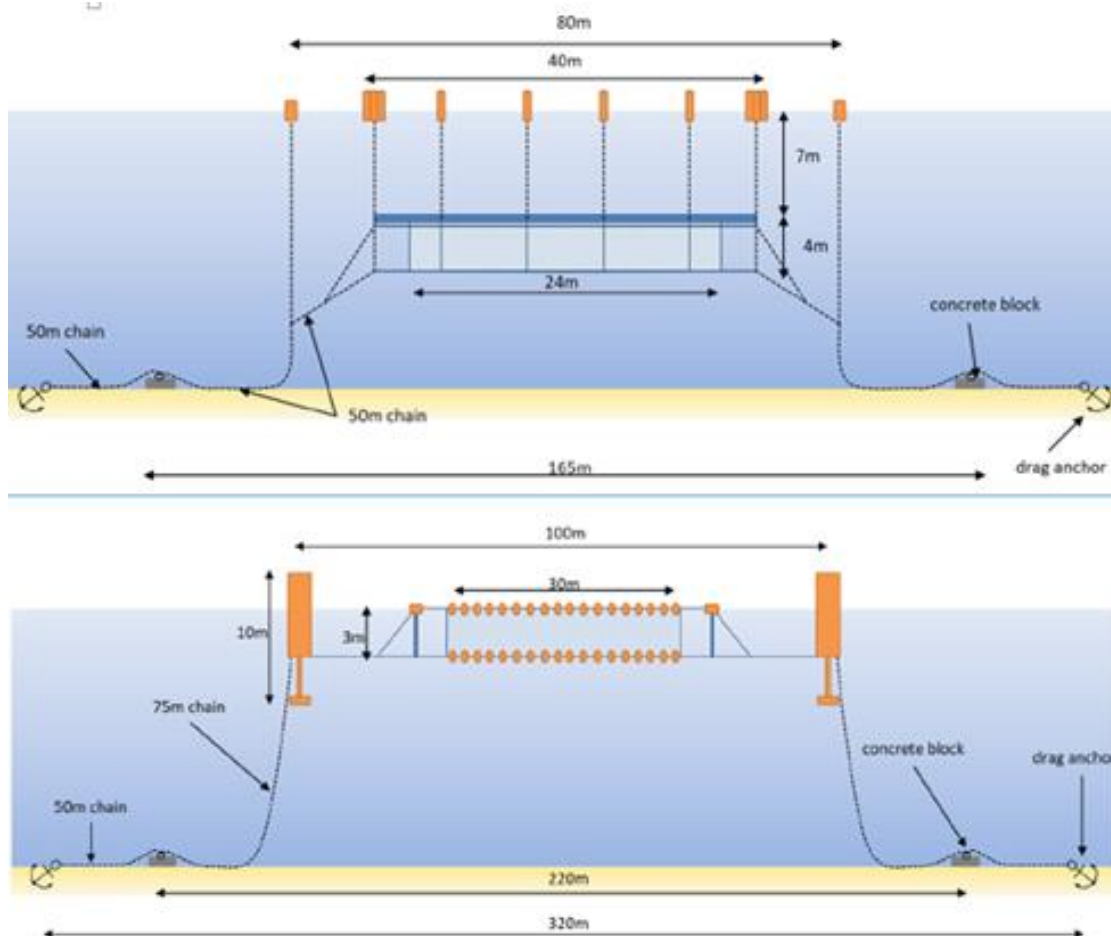


Figure 3.1.3 A design of an offshore longline structure (Source: Forschungs- und Entwicklungszentrum Kiel. (2021))

In deciding the suitability of an offshore mussel farm, different factors in the marine environment need to be considered. According to the literature (Lachance-Bernard et al., 2010; Mizuta & Wikfors, 2019; Waldeck & Larsson, 2013; Westerbom et al., 2002), the most important factors are temperature, chlorophyll concentration, salinity, and current speed. The

selected factors for the analysis and the reasons for choosing each one will be described in Chapter 5.

3.1.2. Seaweed farming

The considered Seaweed species *Saccharina Latissima*, commonly known as sugar kelp, belongs to the brown microalgae. This species prefers low light intensities and cold temperatures (Bikker et al., 2016). Further, in designing the Seaweed farms, it needs to pay attention to the flow conditions of the area, primarily to provide sufficient nutrients to the algae. In this project, the cultivation of Seaweed will be done using longlines. Figure 3.1.4 shows an example of longline structures used to cultivate sugar kelp (*Saccharina Latissima*) in an offshore environment.

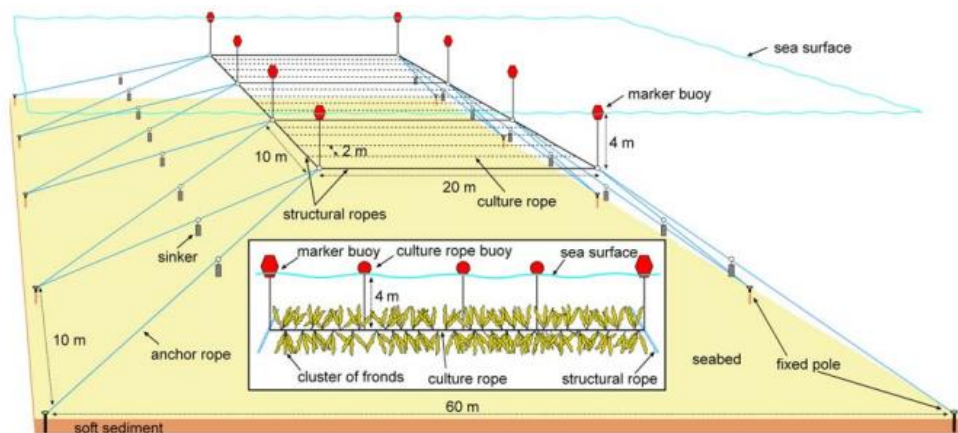


Figure 3.1.4 Longline rope culture for open sea cultivation of *Saccharina Latissima* (Source: Peteiro et al., 2014)

3.2. Physical characteristics of the North Sea

The North Sea can be identified as one of the most utilized and investigated seas globally with long records in maritime history. Densely populated and developed industrial countries surround it. The North Sea is connected to the North Atlantic Ocean from North and through the English Channel and to the Baltic Sea from East.

3.2.1. Bathymetry

The North Sea is considered a shallow shelf sea where the average depth is about 80m. The maximum depth of the North Sea is observed in the Norwegian trench with a depth of around 800m (Sündermann & Pohlmann, 2011).

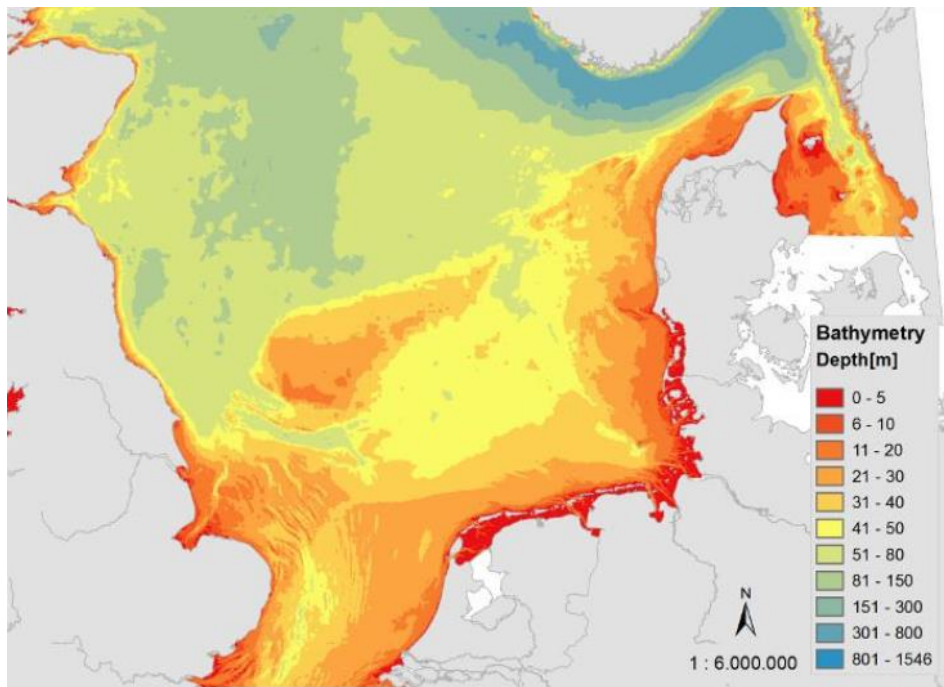


Figure 3.2.1 North Sea bathymetry (Data source: (Pätsch et al., 2017))

When looking at the North Sea bathymetry, it is observable that water depth increases from South to the North and from East to West.

3.2.2. Impact of atmospheric forcing

The atmospheric forces play an essential role in the general circulation patterns of the North Sea. The wind forcing drives the sea waves, and the storms can create the storm surge with dangerous effects. Other than that, the atmosphere affects the heat budget of the North Sea. Generally, the thermal stratification is primarily observed in the Northern and Central parts of the North Sea from early summer until the early autumn (Sündermann & Pohlmann, 2011). However, the Southern North Sea experiences strong tidal mixing, which avoids the thermal stratification in the Southern coastal areas.

Further, the salinity levels of the North Sea are affected by the continental discharges, which brings the precipitation received by the Northwest European shelf. The North Sea has a total catchment area of around 840,000 km², contributing about 300 – 350 km³ of discharge annually (Ducrotoy et al., 2000). The primary freshwater discharge to the North Sea is from the Rhine river and meltwater from the Scandinavian countries. These freshwater inflows mainly drive the salinity variations.

Consequently, these salinity variations cause density differences in seawater. Therefore, the vertical density distributions are observed near these river mouths with very high outflows and with shallow water depths. The annual discharges experienced by the North Sea are shown in Table 3.2.1.

Table 3.2.1 Freshwater discharges to the North Sea (Source: (Ducrottoy et al., 2000))

Freshwater inputs to the North Sea (modified from OSPAR, in press).

Coastal areas	Run-off (km ³ yr ⁻¹)	Catchment area (km ²)
Scotland (including Forth)	16	41 000
Norway	58–70	45 500
Skagerrak and Kattegat	58–70	102 200
East coast of England (including Tyne, Tees, Humber and Thames)	32	74 500
Denmark and Germany (including Wadden Sea)	32	219 900
The Netherlands and Belgium (including Wadden Sea, Rhine, Meuse and Scheldt)	91–97	221 400
English Channel (including Seine)	9–37	137 000
Total North Sea	296–354	841 500

3.2.3. Interaction with the Atlantic Ocean

The North Sea has a broad opening to the Atlantic Ocean from the North and a narrow opening through the English Channel. Therefore, the mass, energy, and momentum exchange between the two oceans are observed. The waves generated by the atmospheric and tidal forces enter the North Sea from these boundaries and support the mass and momentum transport from the Atlantic Ocean.

3.2.4. Impact of astronomical tides

Astronomical tides have a significant effect on the dynamics of the North Sea. However, according to the literature (Sündermann & Pohlmann, 2011), the North Sea is not large enough to experience the direct tidal impact and is influenced by the co-oscillations with the tidal waves of the Atlantic Ocean. The tidal currents can reach up to a few dm/s, and it is mentioned that the tidal currents are dominant than the other flows in this region. The spring and neap tides are caused due to the superposition of semi-diurnal lunar and solar tides.

3.3. Hydrodynamic model of North Sea

Delft 3D flexible mesh model suite was used for modeling the North Sea. Dutch Continental shelf model (DCSM) is a 3D hydrodynamic model developed for the Northwest European continental shelf and was used in this research to simulate North Sea hydrodynamics. The details of this model given in the following sections are mainly obtained referring to the model setup of DCSM and the technical report of Development of 3D DCSM-FM by (Zijl et al., 2021).

The extent of the Dutch Continental Shelf Model is from 15°W to 13°E in the West-East direction and 43°N to 64°N in the North-South direction. The DCSM model has been validated against measured sea surface temperature, sea surface salinity, and seasonal temperature stratification in the central North Sea. Further, simulated residual transport through the English Channel has also been validated and confirmed to be in the realistic range (Zijl et al., 2021). However, the purpose of this study is to identify the significant input parameters for calibrating this model for the area of interest (i.e., the FINO3 research platform).

- **Grid size**

The horizontal grid size of the model used in this study has a resolution of 4 Nautical miles (4nm). The DCSM model has been developed with two grid resolutions where the coarser grid is with 4nm resolution, and a 0.5nm resolution has been used in the finer grid. The intention of using a coarser grid is to reduce the computation time of the model by reducing the restrictions on the computation time step, where coarser grids will allow a larger time step and subsequently reduce the computation time.

Vertical grid schematization is done by dividing the total water depth into several layers with the same height. This method is called the z-layer approach. Although the layer thickness is independent of the water depth at a specific location, the number of z-layers depends on the bathymetry. Altogether, 20 z-layers have been used for vertical schematization in the model. Using z-layers will allow the opportunity to extract the model results at the same depth by selecting a specific z-layer at any location.

An image of the grid used in DCSM is shown in Annex IV of this report.
- **Numerical time step**

The maximum time step is 120s, and the minimum computation time step is limited based on Courant criteria. The initial time step has been set to 60s. A maximum Courant number is given as 0.7. The model automatically adjusts the time step concerning the Courant criteria, depending on the grid size and velocity. Therefore, when the network has small flow links and high velocities, the model changes the computation time step to a smaller value to satisfy the Courant criteria.
- **Bathymetry**

Model bathymetry has been generated using the gridded bathymetric data set (October 2016 version) of the European Marine Observation and Data Network (EMODnet). The gridded data of EMODnet has a resolution of $1/8^{\circ} \times 1/8^{\circ}$ which is approximately 160m \times 230m. The reference level for the EMODnet bathymetric data is the Lowest Astronomical Tide (LAT). Therefore, the data has been converted to the Mean Sea Level (MSL) reference plane before inputting into the model. The bathymetry data are provided on the nodes of the grid network, and the interpolation options are specified in the model setup. The bathymetry for the model domain is shown in Figure 3.1.2.

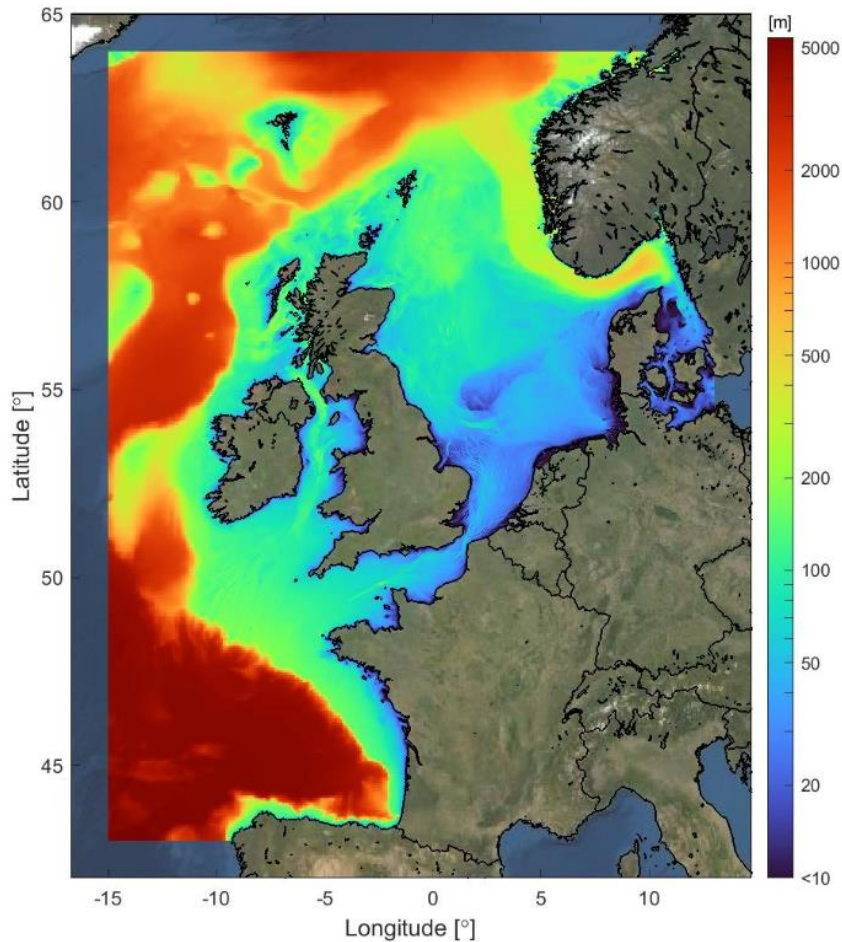


Figure 3.3.1 Model bathymetry of Dutch Continental Shelf Model (DCSM) in a logarithmic scale (water depths relative to MSL) (Source: (Zijl et al., 2021))

- Boundary conditions

Water level

Northern, western, eastern, and southern open boundaries of the model were given as water level boundaries. The Eastern boundary is connected to the Baltic Sea, an essential source of fresh water supply to the North Sea through the Norwegian trench. These water levels have been imposed using astronomical tides.

Temperature and Salinity

For the lateral boundaries, temperature and salinity boundaries have been given in the DCSM. The data for temperature and salinity were obtained from the World Ocean Atlas 2013 (WOA 2013). This data has a resolution of 0.25° and 107 depth levels. These have been interpolated to obtain the temperature and salinities at the required boundary locations and the depth levels.

- Meteorological Forcing

Meteorological forcing is given to the DCSM by coupling to the ECWMF's ERA5 reanalysis data set. These data are with a 0.25° spatial resolution and hourly temporal resolution.

Momentum flux

Wind speed and air pressure are applied to the model to introduce the momentum flux between air and sea surfaces. The wind speed is given at 10m height, and the air pressure at the surface (at the mean sea level).

Heat flux

Temperature variations in the seawater can create density differences that can generate the horizontal flow of the water mass. This will eventually affect the thermal stratification and reduce the vertical mixing.

The transport of temperature is modeled in the DCSM by introducing a heat flux model. Here the main components of the heat budget are included as

- Solar (shortwave) radiation,
- atmospheric (longwave) radiation
- heat loss – due to back radiation, evaporation, and convection

The heat exchange between the air-water interface due to the evaporation and convection is calculated using dew point temperature, the local temperature at 2m height, and the wind speed from ERA5 data. Net shortwave radiation and longwave radiation have been imposed into the model, and the back radiation is being calculated based on the sea surface temperature from the model. The solar radiation received to this is distributed over the whole domain based on the transparency of the water column. To introduce this into the model, a Secchi depth is applied as a constant value of 4m, except at the Wadden Sea, where the Secchi depth has been given as 1m.

Mass flux

Exchange of mass flux between atmosphere and sea is introduced by including the inflows due to precipitation and the losses due to evaporation processes.

- **Bed roughness**
Sea bed roughness was specified in the model as a spatially varying Manning roughness coefficient. These values have been adjusted by calibrating the model to obtain optimal water levels. The calibration has been performed using measured data from more than 200 tide gauge stations.

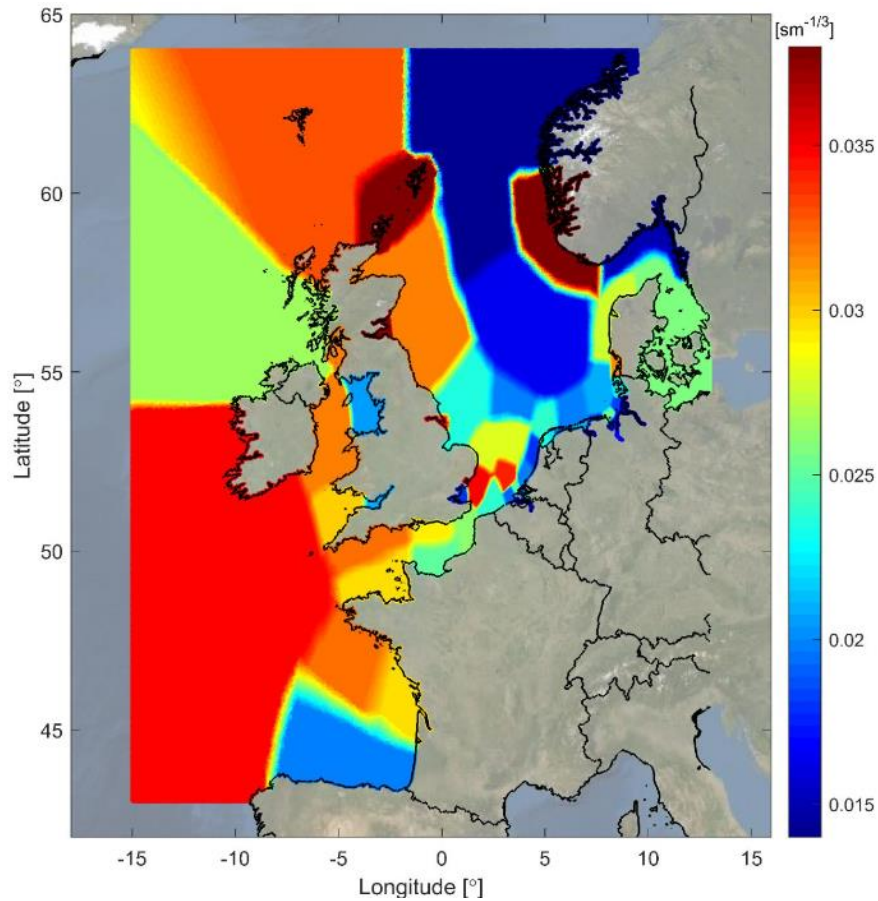


Figure 3.3.2 Variation of Mannings roughness field in DCSM-FM (Source: (Zijl et al., 2021))

- Observation points
The selected locations can be specified in the model setup by giving the coordinates of those locations as a .xyn file. In this research, six locations were given to the model as observation points.

Chapter 4: Research Methodology

The methodology is developed to attain the research objectives by reviewing the literature to explore the work already completed for the identified problem associated with the complex numerical models. Before selecting the SA method for the hydrodynamic model, the different approaches for sensitivity analysis, their applicability for the complex numerical models will be discussed. The overview of the research methodology is presented below as a flowchart.

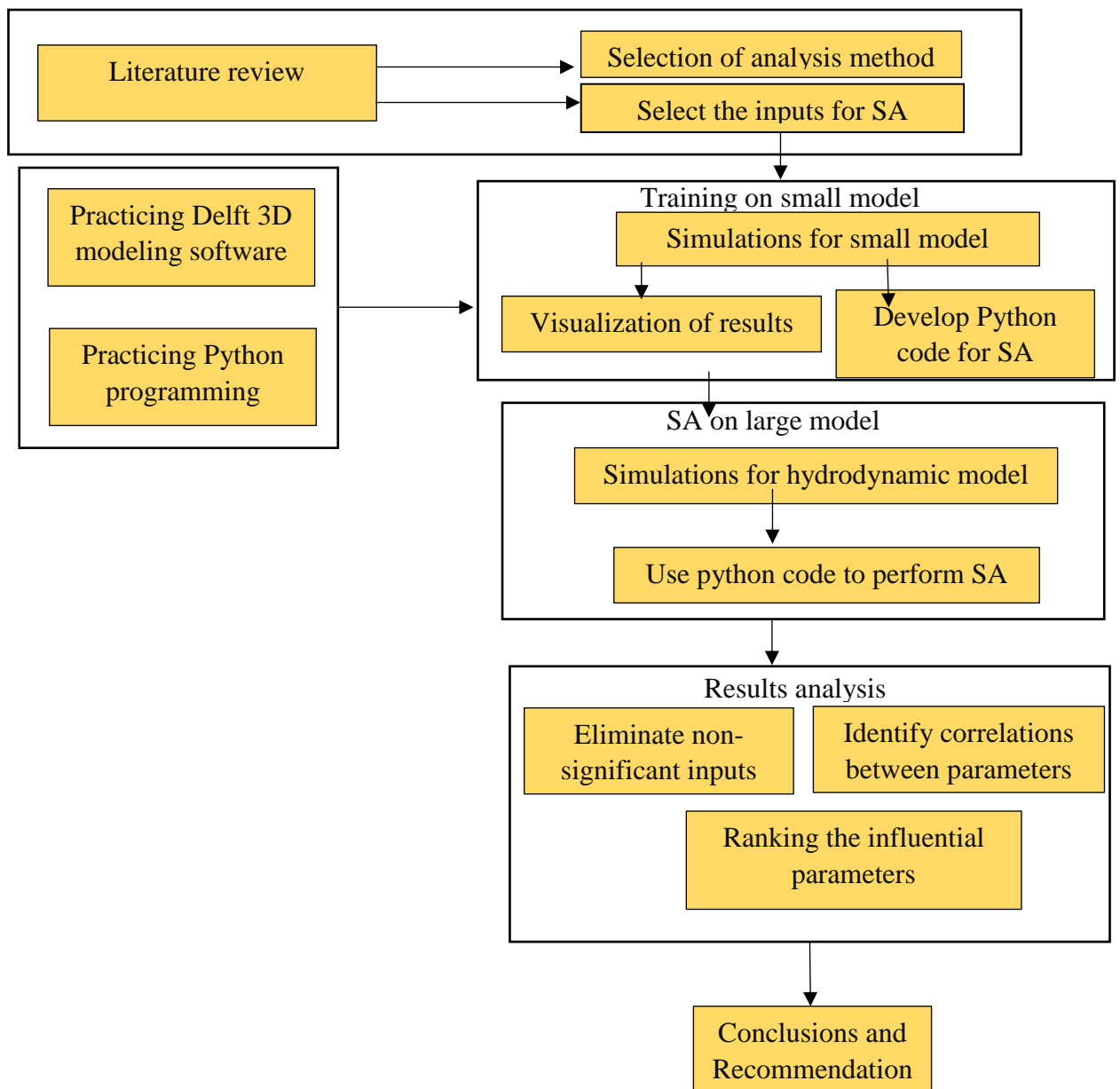


Figure 4.1. 1 Flowchart of the research methodology

4.1. Selection of Sensitivity Analysis Methods

Considering the required number of model evaluations and the complexity of the models, (Iooss et al., n.d.) distinguished between the screening methods and the more precise variance-based quantitative methods. The screening methods are used to coarsely sort the influential input parameters from a more significant number of inputs. The variance decomposition methods are used for a more precise quantitative exploration which measures the effect of input variations on the output variance over the whole range of input variation (Iooss et al., n.d.). Since the required number of model runs for most methods depends on the dimensions or number of input factors, an additional class of methods is defined as dimension-independent methods. The classification of different sensitivity analysis techniques to their complexities and the required number of model runs are shown in Figure 4.1.1

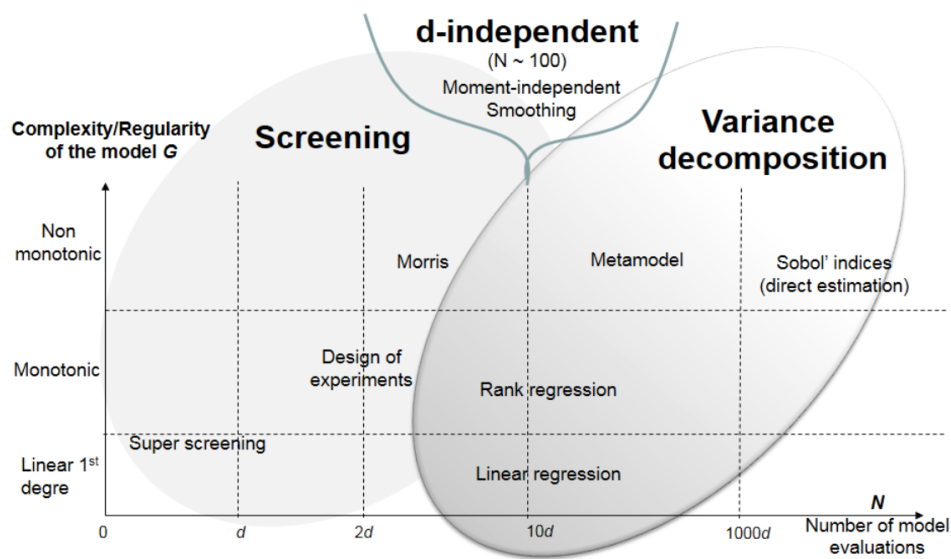


Figure 4.1.2 Coarse classification of main global SA methods in terms of the required number of model evaluations and model complexity (Iooss et al., n.d.)

Selection of a method for performing the sensitivity analysis for the developed model is carried out considering the applicability of each method's hydrodynamic model and limitations. The method of analysis can be selected mainly based on the (a) computational cost of running the models in each method, (b) the number of input parameters, (c) features of the hydrodynamic model, (d) input parameter dependency and the interactions of the inputs among each other and (e) setting for the analysis (Andrea Saltelli & Saisana, 2007). Following methods can be proposed for calculating the sensitivities of the hydrodynamic model, considering the literature and the above factors. In this methodology section, possible methods have been put forward, first to screen the influential parameters and then determine the ranking of significant input parameters and check the correlations of these parameters.

As described by (Andres, 1997) input parameters often have comparatively very little influence from most of the parameters. Apart from that, since the complex hydrodynamic models demand significant computation resources, the screening process has high importance for minimizing the required number of model executions. Therefore, as a preliminary step, a subset of input parameters that govern the hydrodynamic processes was selected with the help of expert knowledge.

4.2. Methods for analysis

This section describes the selected two methods and the process of application of each method.

4.2.1. Morris method of Elementary Effects

Steps followed in implementing the classic Morris method for calculating the sensitivities in the North Sea hydrodynamic model are listed below.

1. Selection of the output and input parameters for analysis & plausible ranges for input parameters
The selection was carried out considering the project objectives, referring to the literature and expert judgment. The procedure will be discussed in more detail in Chapter 5.
2. Choosing the discretization levels (p), Morris step (Δ) and optimum number of trajectories (r)
3. Generating the samples for r number of trajectories
4. Generate outputs using DCSM model developed with Delft3D FM
5. Extracting the outputs from the results files, which are in the netCDF4 format
6. Calculating the elementary effects (EE) for each sample
7. Calculating sensitivity measures (absolute mean of EE and standard deviation of EE)
8. Ranking of input parameters based on sensitivity measures
9. Analysis of sensitivities for the two variables (Temperature and current speed)

In Morris method (Morris, 1991) sampling strategy is selected considering r number of trajectories over the input space. As the Morris method is an OAT method, each sample is generated by changing one input parameter at a time. The distribution of parameters is assumed to be uniform over the parameter space. All the input parameters are first considered in the range [0,1] and then transformed to the actual ranges (Campolongo et al., 2007).

- *Selection of number of trajectories, discretization levels, and Morris step*

According to the literature (Tene et al., 2018), increasing the number of discretization levels (p) alone does not subsequently increase the accuracy of sensitivity indices unless it is done together with an increase in the trajectories (r). Further, having a higher number of discretization levels can yield more paths to remain undiscovered. (Campolongo et al., 2007) has recommended that using $r = 10$ and $p = 4$ levels produces good results in many experiments. Further, they demonstrated a convenient choice for the discretization levels (p) and Δ is such that p is even and $\Delta = p/[2 \cdot (p - 1)]$. Therefore, as the initial values for discretization levels, Morris step and the number of trajectories were selected as;

- $p = 4$,
- $\Delta = 3/2$ and
- $r = 10$

Further, the optimum number of trajectories was found by increasing the r -value and checking the stability of sensitivity measures (mean, absolute mean, and standard deviation) of each parameter.

- *Sampling strategy*

In one-factor-at-a-time (OAT) designs, there should be two sample points to calculate one Elementary Effect (EE). If the sensitivities are computed for k input factors, and this will be

done for r times, it needs to have $2rk$ samples in the simplest form. However, Morris (1991) suggested an efficient method for sampling designs with fewer samples. In this sampling strategy, for a model with k number of selected input parameters, $(k+1)$ model evaluations are needed for calculating one elementary effect for each input. To calculate r number of elementary effects for each parameter, this must be repeated r times. This will yield a total computation cost of $r*(k+1)$ model evaluations. Therefore, $r*(k+1)$ input samples need to be generated, each consisting of k input parameters.

The method considers a hypercube with k dimensions where k equals the number of input factors selected for the analysis. Each dimension represents one input factor where the parameters are normalized to lie between 0 and 1. This hypercube is then discretized to p number of levels with equal intervals. For example, Figure 4.2.1 represents a unit hypercube with three dimensions and with four discretization levels.

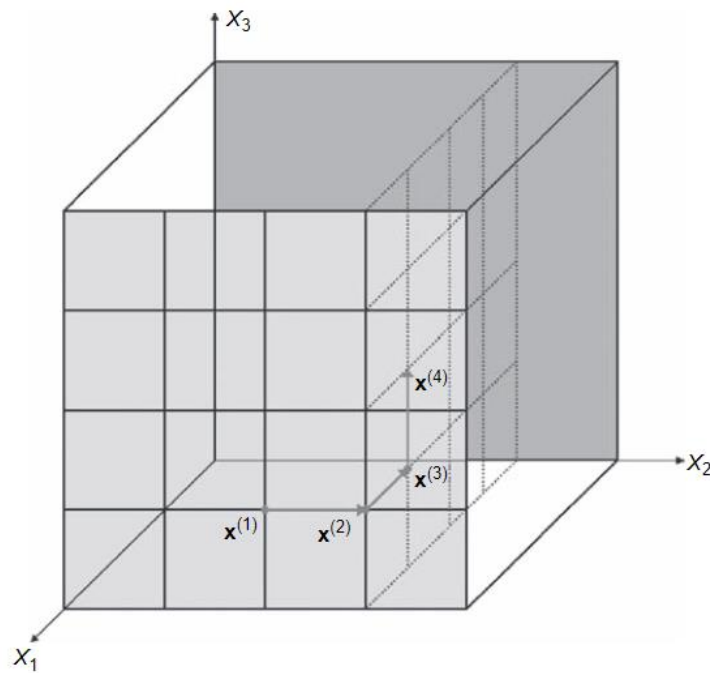


Figure 4.2.1 Representation of a trajectory in the input space with three dimensions and five discretization levels (Source:(Saltelli A et al., 2008))

A total number of possible trajectories for the unit hypercube can be calculated as follows.

$$N_{paths} = N_{cells} * N_{corners} * N_{orders}/2 \quad 4.1$$

Where;

$$N_{cells} = (p - s)^k, N_{corners} = 2^n, N_{orders} = 2!$$

Here; k = number of input factors

p = discretization levels

s = number of grid cells chosen for variation ($s \in \{1, 2, \dots, (p - 1)\}$)

The first step of generating the samples is to generate the trajectories as described below.

- A trajectory will be a matrix(B^*) with dimensions $(k+1) \times k$ where the rows of the matrix are the vectors $X^1, X^2, \dots, X^{(k+1)}$
- To define B^* , a lower triangular matrix (B) of 1's should be defined first, such that;

$$B = \begin{bmatrix} 0 & 0 & 0 & \dots & 0 \\ 1 & 0 & 0 & \dots & 0 \\ 1 & 1 & 0 & \dots & 0 \\ 1 & 1 & 1 & \dots & \dots \\ 1 & 1 & 1 & \dots & 1 \end{bmatrix}$$

- The matrix B' is defined by

$$B' = J_{(k+1),k}x^* + \Delta B \quad 4.2$$

where; $J_{(k+1),k}$ is a $(k+1) \times k$ dimension matrix with 1s and x^* is a randomly chosen base value vector of X. Δ is equal to the Morris step size

- The orientation matrix B* is given by the equation,

$$B^* = (J_{(k+1),k}x^* + (\Delta/2)[(2B - J_{(k+1),k})D^* + J_{(k+1),k}])P^* \quad 4.3$$

Here, D^* is a k dimensional diagonal matrix where each element in the diagonal is either +1 or -1 and has equal probability. P^* is called the random permutation matrix, which means the matrix is obtained by randomly permutating the columns of a $k \times k$ identity matrix.

- Since r number of trajectories is selected, there should be r number of orientation matrices, B^* .
- Therefore, the final sampling matrix is derived by repeating this r times

These parameter samples explained above are generated in the range [0,1]. To convert them to the original interval, upper and lower boundaries of the parameter ranges as to be specified. Therefore, samples were scaled to their actual ranges before inserting into the hydrodynamic model. Input samples generation and inserting those samples into the model were performed using Python programming language. This application has been further explained in Chapter 6.

Simulating the outputs

The hydrodynamic model outputs for the North Sea were simulated with Dutch Continental Shelf Model (DCSM) using the Delft3D Flexible Mesh model suite. The Models were run using the Linux cluster utilizing 2 nodes and 4 cores each (model takes 3.07 hours run time on a coarser grid). Parallel running was performed to reduce the running time.

Extraction of model results

Two types of output files, spatial outputs, and the time series outputs are created in the D-Flow FM model, both in the netCDF format. As the purpose of the research is to investigate mainly the variation of values of the outputs from one model run to another, the time series output files (his.nc) were selected to extract the output values of each model at few selected locations. Extracting the model results was done with the use of Python programming language.

Calculating EE and sensitivity measures

Elementary effects for each parameter were calculated using equation 2.1 for each trajectory separately. This yields a $k \times r$ number of elementary effects (EE). As described in Chapter 2, the sensitivity measures were defined as the mean, absolute mean, and standard deviation of elementary effects.

Ranking of the input parameters based on the significance

The input parameters were ranked according to their contribution to the output parameter sensitivity based on the calculated sensitivity measure. The absolute mean of EE was used as the sensitivity measure in ranking. Finally, the most influential inputs were screened by this

method.

This analysis was performed for both temperature and current velocities. Finally, to check the spatial variation of the sensitivities, these rankings were obtained for all the selected six locations.

4.2.2. Variance based Sobol' method

As explained earlier, the purpose of using the variance-based method in this research is to prioritize the factors by identifying the input factors which cause the highest fractions of the variance in output. Therefore, the Sobol' method was used to determine the ranks of significance and the fraction of total variance caused by each parameter individually or as a combination of input parameters.

As mentioned earlier, one key concern of this Sobol' method is its high computational cost. The computation time for one month of simulation of DCSM with 4nm resolution is approximately 3.5 hours using 4cores of computation facilities. The variance-based method requires input samples (N) for one parameter in the range of 100 – 10,000. Hence, it is challenging to analyze all the selected parameters due to the high computation demand. Therefore, it was decided to test the sensitivities of temperature and current velocities for a limited number of input factors, screened by the Morris method.

The variance-based analysis was performed for the two outputs separately after selecting three input parameters for temperature and another three parameters for current velocities, contributing the most in changing temperature and current velocities in the hydrodynamic model. Thus, Sobol' indices were calculated mainly to determine input variances on the output variance and analyze input parameter interactions.

The steps followed in implementing the variance-based Sobol' method are listed below.

1. Selecting the input parameters and their ranges for sensitivity analysis.
Three input parameters were chosen for temperature, and three inputs were selected for current velocities, considering the results of the Morris screening. Input parameter ranges were the same as the ones used for Morris method
2. Choosing a distribution for each of the parameters. In this case, parameter distributions are assumed as uniform distributions for all three parameters.
3. Create the input samples
According to (Saltelli A et al., 2008), the best way to compute a complete set of sensitivity indices using only the model evaluations is to follow Monte Carlo-based simulations. Therefore, the method suggested by (Saltelli A et al., 2008) is adopted in this research. The process of sample generation is listed below
 - The first step of creating the samples is to define two matrices containing the random values within the parameter range of each input parameter, with dimensions (N, k) . Here k is the number of input parameters, and N is the selected sample size.

$$A = \begin{bmatrix} x_1^1 & x_2^1 & \dots & x_i^1 & \dots & x_k^1 \\ x_1^2 & x_2^2 & \dots & x_i^2 & \dots & x_k^2 \\ x_1^3 & x_2^3 & \dots & x_i^3 & \dots & x_k^3 \\ \dots & \dots & \dots & \dots & \dots & \dots \\ x_1^N & x_2^N & \dots & x_i^N & \dots & x_k^N \end{bmatrix}$$

$$B = \begin{bmatrix} x_{(k+1)}^1 & x_{(k+2)}^1 & \dots & x_{(k+i)}^1 & \dots & x_{2k}^1 \\ x_{(k+1)}^2 & x_{(k+2)}^2 & \dots & x_{(k+i)}^2 & \dots & x_{2k}^2 \\ x_{(k+1)}^3 & x_{(k+2)}^3 & \dots & x_{(k+i)}^3 & \dots & x_{2k}^3 \\ \dots & \dots & \dots & \dots & \dots & \dots \\ x_{(k+1)}^N & x_{(k+2)}^N & \dots & x_{(k+i)}^N & \dots & x_{2k}^N \end{bmatrix}$$

- Then a 3rd matrix C is defined using the same columns from B except for the ith column where the ith column of matrix A replaces this.

$$C_i = \begin{bmatrix} x_{(k+1)}^1 & x_{(k+2)}^1 & \dots & x_i^1 & \dots & x_{2k}^1 \\ x_{(k+1)}^2 & x_{(k+2)}^2 & \dots & x_i^2 & \dots & x_{2k}^2 \\ x_{(k+1)}^3 & x_{(k+2)}^3 & \dots & x_i^3 & \dots & x_{2k}^3 \\ \dots & \dots & \dots & \dots & \dots & \dots \\ x_{(k+1)}^N & x_{(k+2)}^N & \dots & x_i^N & \dots & x_{2k}^N \end{bmatrix}$$

- Then the model outputs were computed for all the samples. Since we considered k input parameters, the C matrix should be created k times to account for all the input factors. Thus, the numbers of model runs required are;
Corresponding to A – N model runs
Corresponding to B – N model runs
Corresponding to C – N×k model runs
Therefore, N*(k+2) model runs are required for estimating the first order and total order sensitivity indices for the model.
- Considering the computation demand, sample size N was chosen as 100 and input parameters as k=3. Therefore, 100*(3+2)= 500 input samples were generated using the above method.
- As in the previous method, these inputs were generated and inserted into the hydrodynamic model using Python programming language.

4. Calculate the outputs for input samples

The hydrodynamic model outputs for the North Sea were simulated with Dutch Continental Shelf Model (DCSM) using the Delft3D Flexible Mesh model suite. Models were run using the Linux cluster utilizing 2nodes and 4cores. Parallel running was performed to reduce the running time.

The outputs for each sampling matrix can be denoted as;

$$Y(A) = f(A), Y(B) = f(A), Y(C_i) = f(C_i)$$

5. Calculate the first-order sensitivity indices for each parameter

According to the definition of first-order sensitivity explained in Chapter 2, for ith input parameter,

$$S_i = \frac{V_{x_i}[E_{\sim x_i}(Y|X_i)]}{V(Y)} = \frac{Y(A) \cdot Y(C_i) - f_0^2}{Y(A) \cdot Y(A) - f_0^2} = \frac{(\frac{1}{N}) \sum_{j=1}^N Y(A)^j Y(C_i)^j - f_0^2}{(\frac{1}{N}) \sum_{j=1}^N (Y(A)^j)^2 - f_0^2} \quad 4.4$$

Where f_0 is the mean which is calculated by $f_0^2 = (\frac{1}{N} \sum_{j=1}^N Y(A)^j)^2$

This calculation will be repeated for $i = [1,3]$ for obtaining the indices for three parameters.

A high value of first-order sensitivity indicates that the input factor is a significant factor in changing the output.

6. Compute total sensitivity effects for the three parameters

The total order sensitivity index for i^{th} input parameter can be estimated as described below;

$$S_{Ti} = 1 - \frac{V_{\sim x_i}[E_{x_i}(Y|X_{\sim i})]}{V(Y)} = 1 - \frac{Y(B) \cdot Y(C_i) - f_0^2}{Y(A) \cdot Y(A) - f_0^2} = 1 - \frac{(\frac{1}{N}) \sum_{j=1}^N Y(B)^j Y(C_i)^j - f_0^2}{(\frac{1}{N}) \sum_{j=1}^N (Y(A)^j)^2 - f_0^2} \quad 4.5$$

Similarly, this calculation will also be repeated for $i=[1,3]$ for obtaining the indices for three parameters.

7. Analysis of the sensitivities

Rank the input parameter based on the sensitivity indices. As the variance-based method gives a quantitative measure on the importance of the input factors, it can be used to determine how much interactions an input X_i has with other input factors. For estimating this, the difference of the two sensitivity indices ($S_{Ti} - S_i$) was used in the analysis.

4.3. Comparison of the sensitivity results obtained from two methods

Ultimately the results obtained using the two analysis techniques were compared to distinguish between the resulting ranks of significance calculated by two methods and to determine the correlations between sensitivity indices given by Morris and Sobol' methods.

4.4. Training on example model

Before applying the sensitivity analysis methods into the hydrodynamic model (DCSM), an example model was used to practice the Delft 3D software and understand the methods for application of selected analysis techniques to a hydrodynamic model. Further, this example model was used to develop the Python scripts for the sample generation, input the sample to the model, and analysis.

The ‘Western Scheldt’ model is one of the tutorial examples included with the D-Flow FM model suite, and this was used to practice the software and to start developing the Python scripts.

4.5. Selection of locations for the analysis

Analysis locations were selected in the FINO3 research platform and surrounding area to have a complete analysis of the spatial variation of sensitivities of temperature and currents. These locations were chosen after considering the existing wind farm locations and the current direction in the FINO3 to cover the possible effects due to the waves and currents. The measured currents for the FINO3 research platform are available through The Federal Maritime and Hydrographic Agency in Germany. Therefore, the current data were plotted for the period from 2010 to 2015. The direction of currents in the FINO 3 research platform area was observed mainly from the North to East direction at 2m depth and Northwest and Southeast directions at higher depths. Therefore, it was decided to choose the points for analysis considering the existing wind farm locations and covering the possible current directions to study the spatial variations of the output parameters and the variation of sensitivities based on the location.

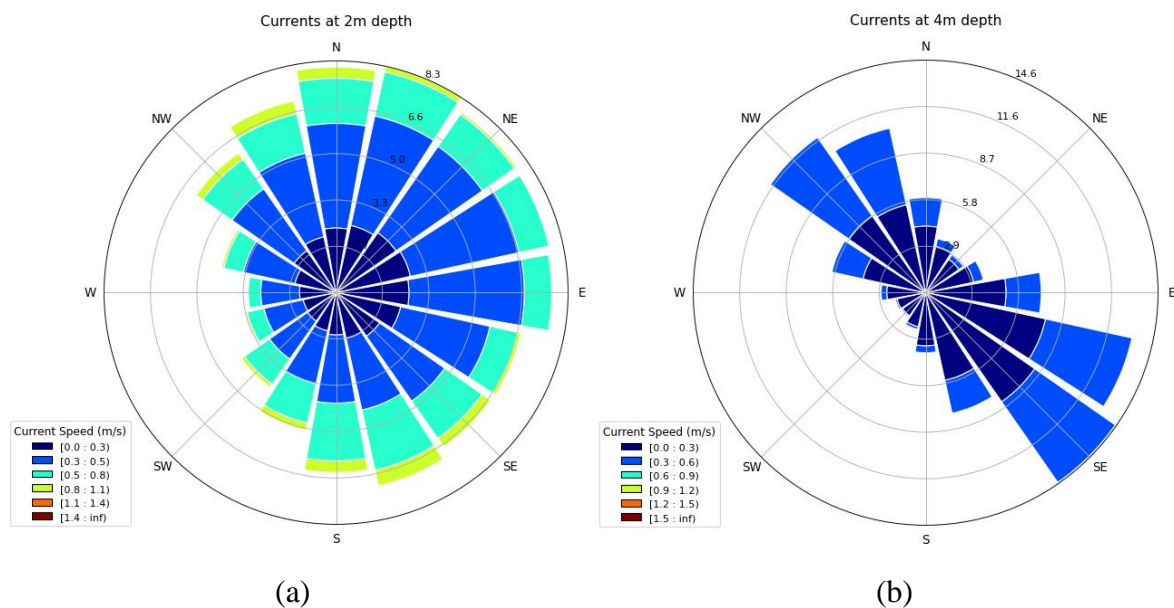


Figure 4.5.1 Measured data for currents at FINO3 research platform from 2010 to 2015 (Source of data: BSH (2021))

Six points were chosen such that one point is located in the FINO3 platform, and the remaining points surround the FINO3 to capture all possible effects of waves and currents coming from different directions.

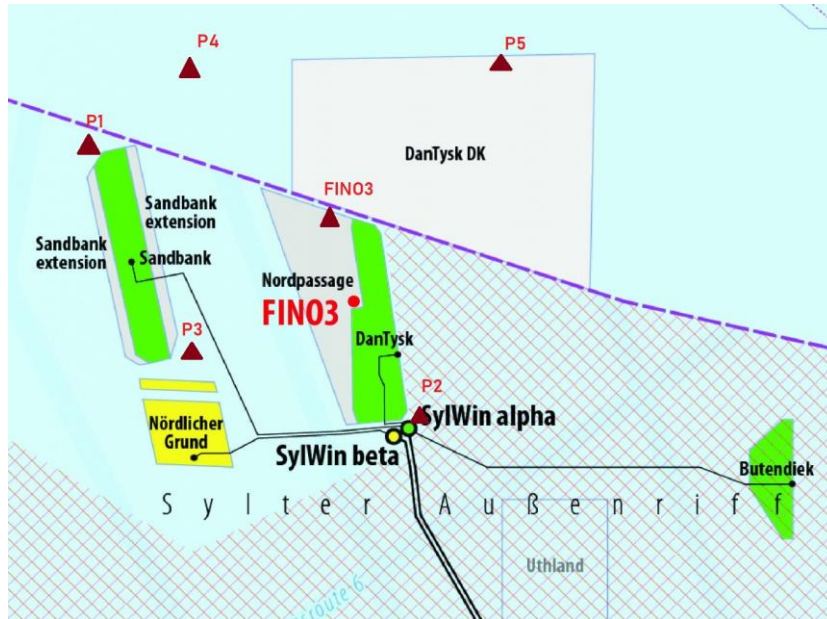


Figure 4.5.2 selected locations for the analysis (green color; existing wind farms of the area),
 (Source:(*Research Project: Multi-Use Offshore Platforms*, 2021))

The coordinates of selected locations are listed in Table 4.4.1. These locations were input to the model set up by inserting them in the observation points file (.obs).

Table 4.5.1 Selected locations for the analysis

Observation point	Latitude	Longitude
FINO3	54.193037 N	7.162783 E
P1	53.980188 N	7.255316 E
P2	54.243168 N	6.824124 E
P3	54.060740 N	6.890461 E
P4	54.383571 N	6.917645 E
P5	54.374132 N	7.372081 E

Chapter 5: Selection of Parameters for the Analysis

As explained in previous chapters, before applying the analysis techniques, a sub-set of input parameters was identified referring to the literature and guidance from experts at Deltares. Prior to the selection of input parameters, output parameters to focus on were identified considering the requirements of the selected case study.

5.1. Selection of Output parameters for analysis

Table 5.1.1 includes the critical parameters that need to be considered in designing the offshore Blue mussel and Seaweed farms using longline structures.

Table 5.1.1 Important parameters for Blue mussel longlines and Seaweed farming

Purpose	Important Parameters	Description	Reference
Blue mussel	Temperature	In a study done on offshore mussel aquaculture in North East United States (Mizuta & Wikfors, 2019) stated that temperature is the most affecting factor in filtration and clearance rates of mussels. Also, in longline mussel farming, the ability of the byssus to adhere to the rope depends on the temperature. Temperature affects the body mass loss of Blue mussel (for example, the body mass of the Baltic Blue mussels was smaller in mild winters than the cold winters).	(Mizuta & Wikfors, 2019) (Waldeck & Larsson, 2013)
	Salinity	Salinity gradient affects the size and biomass of Blue mussels. A decline in mean size, biomass, and growth rate was observed from the saline areas to the less saline regions in a study done in the Northern Baltic sea.	(Westerbom et al., 2002)
	Chlorophyll concentration	An important factor as it provides an estimation of food availability for the mussels growing.	(Mizuta & Wikfors, 2019)
	Current velocity	In the offshore cultivation of mussels, the mussels will be exposed to more motion than in the nearshore sites. Therefore, the current speed is another significant factor to be considered.	(Mizuta & Wikfors, 2019)
Seaweed	Temperature	Water temperature is one of the factors that determines the success of Seaweed farming. Biomass of <i>Saccharina Latissima</i> was found to be positively correlated with elevated sea temperatures. Specific growth of the Seaweeds is negatively correlated to the temperature.	(Matsson et al., 2019)

	Salinity	Biomass of <i>Saccharina Latissima</i> was found to be positively correlated with the high salinity levels.	(Matsson et al., 2019)
	Nitrate and Phosphate concentration	Specific growth of Seaweed is found to be positively correlated to the nitrate concentration and the current velocities.	(Nursidi et al., 2017)
	Current velocity		
	Light intensity	Light intensity is considered one of the most important abiotic factors for kelp growth, as it is a significant factor that decides the photosynthesis rates.	(Bikker et al., 2016)

Salinity levels of the sea are mainly controlled by the freshwater budget received by the sea. The freshwater budget in the North Sea depends on the exchanges between the Atlantic Ocean, Baltic Sea, and the freshwater discharges from rivers. However, in an article on the analysis of North Sea physics, (Sündermann & Pohlmann, 2011) mentioned that the inflows from the Atlantic Ocean exceed the total inflows of freshwaters to the North Sea. Therefore, comparatively high salinity levels are observed in the North Sea. Significant variations in the salinity are mainly observed near the coastal areas where there are freshwater inflows to the North Sea. According to the literature ((Sündermann & Pohlmann, 2011); (Zijl et al., 2021)), it has been demonstrated that the average salinity levels of the North Sea are in the range of 32-35 ppb, which is optimum for Blue mussel and Seaweed farming. Therefore, the salinity does not affect as a critical parameter in this specific area.

Further, to understand the average salinity levels and seasonal variations of the salinity at the interested area, measured salinity data at FINO3 were obtained from the Federal Maritime and Hydrographic Agency website in Germany (BSH).



Figure 5.1.1 Variation of measured salinity at FINO3 for the year 2016 (Source of data: (BSH, 2021))

Available measured salinity data at FINO3 illustrates that the maximum salinity variation over one year is about 3 – 4 mg/l in the selected area, which will not significantly affect the cultivation of Blue mussel and Seaweed. Although salinity is an essential factor in Seaweed and Blue mussel farming, salinity in the study area (FINO 3 research platform) does not show a significant spatial variation over the considered region. Therefore, salinity was not selected as a critical parameter for the sensitivity analysis in this research.

Several factors affect the cultivation of Blue mussels and Seaweed. However, since the focus of our study is only on the hydrodynamic model, the temperature and environmental variables can be selected, referring to the literature as the critical outputs for the sensitivity analysis.

- Temperature

The seawater temperature was simulated using the 3D hydrodynamic model developed for Northwest European Shelf, using the D-Flow Flexible Mesh model suite. The temperature computation method is given to the model by the ‘temperaturemodel’ parameter in the .mdu file. In this study, the ‘temperaturemodel’ was given as the ‘composite ocean model,’ which is the most complex heat flux model according to the D-Flow FM User Manual. The model calculates the heat budget by accounting for the incoming solar radiation from atmospheric radiation and heat losses due to the back radiation, evaporative heat flux, and convective heat flux.

- Current velocity

Different current types are considered in the hydrodynamic model, including tidal, wind-driven currents, stratified currents, and residual currents. The definition of residual currents can be found in literature from different points of view. Mathematically, the residual currents are defined as the steady flow patterns, where there is no change with time. These currents are obtained with the fundamental equations and assuming independence in time. According to the hydrodynamicists, the residual currents are the resulting mean velocity over a sufficiently large period to cancel the transitory wind and tidal currents (Nihoul & Roday, 1975). The definition which is given to the residual currents by the experimentalists is “the residuary flow after subtracting the tidal current contribution from the actual flow computed.” (Otto, 1983).

The wind-driven currents are generated due to the turbulence effects that occur with the interactions between the air-water surface. Stratified currents are observed where the stratification exists due to the density differences of seawater. This stratification process is commonly observed in places where there are freshwater discharges into the sea and where there are thermal discharges. Hence, the stratified currents are expected to be minimal in this offshore region as there are no such discharges near this selected location.

5.2. Selection of Input parameters for analysis

Sensitivities of the two selected outputs were assessed to a selected set of input parameters. As explained in the previous chapters, the Delft 3D Flow model requires many input factors to set up a simulation. However, each of these input factors will not significantly affect the sensitivity of the output parameters. On the other hand, applying sensitivity analysis for many input factors will be difficult due to the extremely high computation demand of the Delft 3D hydrodynamic model. Therefore, selecting a subset of the input parameters which could affect the output variation is an essential preliminary step for the study. Selection of this subset of input parameters was carried out referring to the literature ((Maulik & San, 2016) (Otto, 1983; Sündermann & Pohlmann, 2011)), the manuals of Delft3D Flow and with the help of experts at Deltares. The spatially uniform input factors were considered for analysis, considering the complexity of the model and the analysis time required to apply selected sensitivity analysis methods.

The input factors were tested in plausible ranges around their baseline values of the DCSM model. The baseline values of DCSM have been obtained after validating the model against measured sea surface temperature, sea surface salinity, and measurements of seasonal temperature stratification in the central North Sea. Further, simulated residual transport through the English Channel has also been validated and confirmed to be in the realistic range (Zijl et al., 2021).

Therefore, the following input parameters were selected as the possible influential factors to seawater temperature and current velocity.

- Smagorinsky coefficient

In large-eddy simulations, the eddies can be larger than one grid cell, hence too large to break down with the molecular viscosity. Therefore, an additional stress term is introduced to the Navier-Stokes equation which can filter those large eddies from the grid. This stress is called sub-grid stress and modeled using the eddy viscosity approach, where the sub-grid kinematic viscosity of the model is calculated using Elder's formula or the Smagorinsky model (Deltares, 2021). In the DCSM, Smagorinsky sub-grid model is used in calculating the sub-grid scale eddy viscosity, which is given by the equation

$$v_j = (C_s \sqrt{\Delta x_j w_{uj}})^2 \sqrt{2 \frac{\partial u_n}{\partial n}^2 + \left(\frac{\partial u_n}{\partial n} + \frac{\partial u_t}{\partial n}\right)^2 + 2 \frac{\partial u_t}{\partial n}^2}$$

Where C_s is a user-defined coefficient for describing the average size of the eddies within a grid cell. The length scale l_0 is defined as

$$l_0 = C_s \Delta$$

Where Δ is the size of grid cells. For l_0 to be always less than the grid size, the Smagorinsky coefficient should be between 0 and 1.

Since the Smagorinsky coefficient is used to calculate horizontal turbulence of the model, this factor was used as a possible important input parameter for the sensitivity analyses of temperature and current velocity. The coefficient has been set to 0.2 in the original DCSM.

Based on the literature, technical reference manual of D-Flow FM, and the comments from the experts of Deltares, initially it was decided to use the range from 0 to 0.3 as summarized in Table 5.2.1.

- Dalton

In calculating seawater temperature in the model, heat losses due to processes like evaporation and convection are considered. Dalton is the coefficient given to the model to calculate the heat loss due to evaporation. Therefore, the temperature is supposed to decrease with the increase of the coefficient as the heat loss is increased.

- Stanton

Stanton coefficient is used to calculate the convective heat loss of the model and was selected as an essential input for analyzing the temperature sensitivity. The temperature is supposed to decrease with the increase of the coefficient as the heat loss due to the convection is increased. Therefore, Dalton and Stanton coefficients were selected as another two critical factors possibly affecting the temperature calculation of the model.

Possible values for the Dalton and Stanton coefficients were found in some literature, and an overview of these values is listed in the below Figure 5.2.1. The values given in the first six sources are related to the researches done in the Northern hemisphere (the North Sea and North American region), while the last one is related to the temperature modeling carried out for Lake Malawi in the Southern African region.

Table 5.2.1 Overview of values used for Dalton and Stanton coefficients in literature (Source: (Twigt, 2006))

Source	Stanton number	Dalton number
Gill, 1982	0.83×10^{-3} (stable), 1.1×10^{-3} (unstable)	1.5×10^{-3}
Millar et al., 1999	0.79×10^{-3}	1.5×10^{-3}
Smith et al., 1996	1.1×10^{-3}	1.32×10^{-3}
Simon et al., 1999	1.0×10^{-3}	1.2×10^{-3}
Emery et al., 2006	1.0×10^{-3}	1.2×10^{-3}
Lane, 1989	N.A	1.33×10^{-3}
De Goede et al., 2000	1.45×10^{-3}	1.2×10^{-3}
Kernkamp & Smits, 2000	2.255×10^{-3}	1.885×10^{-3}

Besides, (Twigt, 2006) obtained optimum coefficient values for Dalton and Stanton coefficient for the South China Sea using two methods, optimizing the coefficients using a comparison of heat exchange and optimizing the two coefficients using a test basin.

Table 5.2.2 Dalton and Stanton coefficient values obtained for the South China Sea (Source: (Twigt, 2006))

Source	Stanton number	Dalton number
	[-]	[-]
Literature	0.9×10^{-3}	1.5×10^{-3}
$\frac{\partial T}{\partial t}$ comparison	0.9×10^{-3}	2.4×10^{-3}
Test basin	2.1×10^{-3}	2.1×10^{-3}

- Vicouv and Vicoww

The Reynold stresses in the momentum equation, which can affect the modeled current velocities and temperature in the D-Flow FM model, are calculated using the eddy viscosity concept.

According to the technical reference manual of D-Flow FM, the horizontal viscosity is calculated as the combination of three parts.

$$v_H = v_{SGS} + v_V + v_H^{back}$$

Where v_{SGS} is termed as the sub-grid-scale horizontal eddy viscosity, v_H^{back} is the background horizontal eddy viscosity which is a user-defined background value and v_V is termed as the three-dimensional turbulence computed by a 3D turbulence closure model.

In the turbulence closure model, the vertical eddy viscosity coefficient is defined as,

$$v_V = v_{mol} + \max(v_V^{back}, v_V)$$

Here v_{mol} is the kinematic viscosity of water and v_V^{back} is the user-defined background vertical eddy viscosity.

Besides, according to the user manual (Deltares, 2021), both the coefficients are considered as calibration parameters and need to be optimized through the calibration process. Thus, these two background values for horizontal and vertical eddy viscosities were selected as two other possible input factors to simulate the current velocities and temperatures.

- Dicouv and Dicoww

The eddy diffusivities are derived from the eddy viscosities in the $k-\varepsilon$ turbulence model. Therefore, the uniform eddy diffusivities were also selected for the sensitivity analysis. The value ranges were selected based on the manual of D-Flow FM, Dutch continental Self Model (DCSM) settings, and experts' help.

- Rhoair

The current velocities depend on the wind force acting on the sea surface. Wind velocities are affected by the air densities, and therefore consequently, the currents are indirectly affected by the air density. To analyze the effect of Rhoair on current velocities, the Rhoair parameter given in the .mdu file is select for the analysis.

Possible values for the air density were decided after considering the average temperature and air pressure variations at the FINO3 location with the help of measured data for the area available through the Federal Maritime and Hydrographic Agency website in Germany (BSH).

According to the measured temperatures, the temperature values vary from -15°C to 30°C over one year. The range of air pressure variation is observed as 970 – 1030 hPa. Therefore, maximum and minimum possible air densities were calculated using an average pressure of 1000hPa and two extreme temperatures. These calculations were done using an online calculator for air density and specific weight calculations.

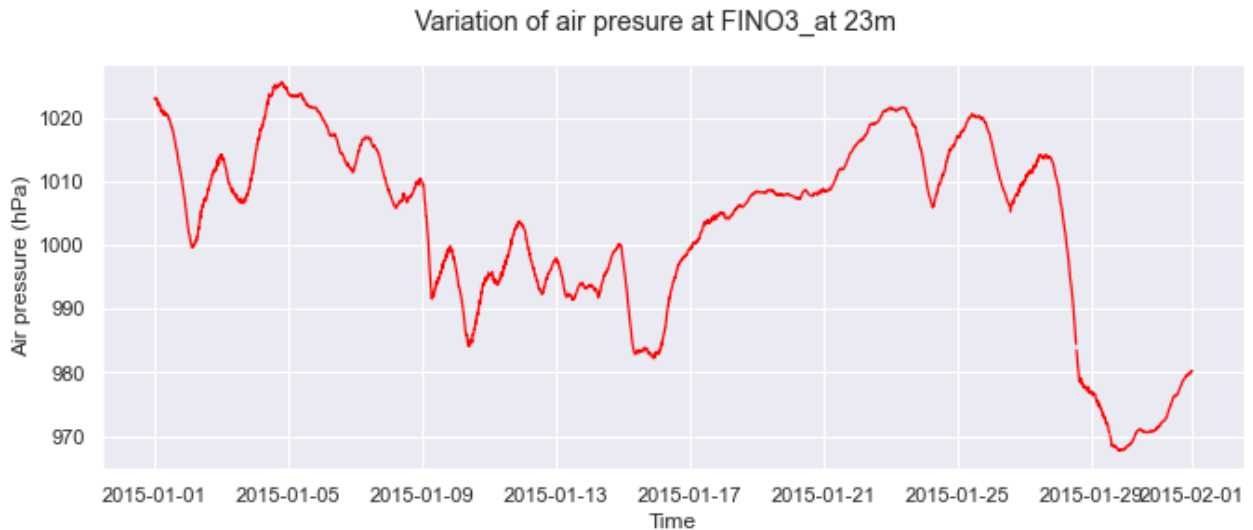


Figure 5.2.1 Measured air pressure data at 23m height from sea level at FINO3 for January 2015 (Data source: BSH, 2021)

Variables		Variables		
Temperature F =	5.0000	Temperature F =	86.0000	
Relative Humidity % RH =	70.0000	Relative Humidity % RH =	70.0000	
Barometer B (in) =	29.9200	Barometer B (in) =	29.9200	
Altitude (ft Above Sea Level) A =	10.0000	Altitude (ft Above Sea Level) A =	10.0000	
Results		Results		Equation
Altitude (meters) Alt=	3.0480	Altitude (meters) Alt=	3.0480	$A*12*2.54/100$
Temperature Degrees C =	-15.0000	Temperature Degrees C =	30.0000	$((F-32)*5/9)$
Temperature kelvin K =	258.0000	Temperature kelvin K =	303.0000	$C+273$
Barometer (mbar) =	1013.0000	Barometer (mbar) =	1013.0000	$B/(29.92/1013)$
Barometer (sea-level) (mb) =	1012.5590	Barometer (sea-level) (mb) =	1012.5590	$1013*EXP(-B/7000)$
Barometer (sea-level) (in) =	29.9070	Barometer (sea-level) (in) =	29.9070	$mb*(29.92/1013)$
Ms (g/kg) =	1897265032.0	Ms (g/kg) =	1197537619.0	$3.884266*10^{((7.5*K)/(237.7+C))}$
M (g/kg) =	1328085522.4	M (g/kg) =	838276333.3	$Ms*RH/100$
Tvc =	415.1220	Tvc =	487.5270	$((1+1.609*M)/(1+M))*K$
Es (saturation pressure mb) =	3.6232	Es (saturation pressure mb) =	15.9283	$6.11*10^{(7.5*C/(237.7+K))}$
E (Vapor Ressure mb) =	2.5362	E (Vapor Ressure mb) =	11.1498	$(RH*Es)/100$
Tdc =	-11.5155	Tdc =	8.5775	$(-430.22+237.7*LN(E))/(-LN(E)+19.08)$
Tdf =	11.2721	Tdf =	47.4395	$Tdc*9/5+32$
Equation: D=P/(T*R) =	1.22556	Equation: D=P/(T*R) =	1.22556	Std Density (100)
Temp, Altitude, Pressure, and Humidity		Temp, Altitude, Pressure, and Humidity		
Barometer (alt-station) as =	1012.1182	Barometer (alt-station) as =	1012.1182	$mb*EXP(-Alt/7000)$
D (air density) (kg/m3) ad =	1.3669	D (air density) (kg/m3) ad =	1.1639	$(as*100)/(K*287)$
Corrected Density =	111.531	Corrected Density =	94.967	
D (virt air density) (kg/m3) vad =	0.5125	D (virt air density) (kg/m3) vad =	0.4637	$(as*100)/((Tvc+273)*287)$
Corrected Density =	41.817	Corrected Density =	37.836	

Figure 5.2.2 Air density calculations for minimum and maximum temperatures (Source:(Engineers Edge, n.d.))

At first, the parameter values were selected, including the minimum values as zero for the factors, Smagorinsky, uniform viscosities in horizontal and vertical directions (i.e., Vicouv, Vicoww), and uniform diffusivities in horizontal and vertical directions (i.e., Dicouv, Dicoww). These possible ranges are shown in Table 5.2.1.

Table 5.2.3 Initially selected input parameters value ranges of each parameter

Parameter	Description	Parameter range			Unit	Influence on	
		Baseline	Min	Max		Temperature	Current velocity
Smagorinsky	Smagorinsky factor in horizontal turbulence	0.2	0	0.3	-	✓	✓
Dalton	Coefficient for evaporative heat flux	0.0013	0.001	0.0016	-	✓	-
Stanton	Coefficient for convective heat flux	0.0013	0.001	0.0016	-	✓	-
Vicouv	Uniform horizontal eddy viscosity	0.1	0	2	m ² /s	✓	✓
Vicoww	Uniform vertical eddy viscosity	0.00005	0	0.0001	m ² /s	✓	✓
Dicouv	Uniform horizontal eddy diffusivity	0.1	0	2	m ² /s	✓	✓
Dicoww	Uniform vertical eddy diffusivity	0.00002	0	0.0001	m ² /s	✓	✓
Rhoair	Air density	1.2265	1.1639	1.3669	Kg/m ³	-	✓

However, model runs performed using some of these input samples crashed due to instabilities. As explained in the previous Chapter, three trials were carried out for Morris method, with $r = 10, 12,$ and 20 . For the 1st trial with 10 trajectories, 80 models were run for checking temperature sensitivity. In this trial, 10 out of the 80 models gave errors and crashed due to the instabilities. The input sample values for these crashed models are shown in Figure 5.2.5.

Table 5.2.2 Input samples of the crashed models

Smagorinsky	Dalton	Stanton	Vicouv (m ² /s)	Vicoww (m ² /s)	Dicouv (m ² /s)	Dicoww (m ² /s)
0	0.001	0.001	1.333333	0	1.333333	0
0	0.0014	0.001	1.333333	0	1.333333	0
0	0.0014	0.001	1.333333	0	0	0
0	0.0012	0.0016	2	0	0.666667	3.33E-05
0	0.0016	0.001	2	0	2	3.33E-05
0.2	0.0014	0.0014	0	0	1.333333	3.33E-05
0	0.0014	0.0014	0	0	1.333333	3.33E-05
0	0.001	0.0014	0	0	1.333333	3.33E-05
0	0.001	0.0014	0	0	0	3.33E-05
0	0.001	0.0014	0	0	0	0.0001

Therefore, it can be assumed that these instabilities in the model are due to single parameter values of these samples or combinations of input parameter values given to the model, which cannot exist practically. One significant observation was, all these model runs have the input parameters Vicoww and Smagorinsky factor as zero. Therefore, it was decided to change the minimum boundary for the parameters Smagorinsky, uniform viscosities, and diffusivities in the horizontal and vertical directions. Thus, the minimum values for these parameters were changed to small non-zero values.

Table 5.2.3 Selected input parameter value ranges of each parameter after adjustments

Parameter	Description	Parameter range			Unit	Influence on	
		Baseline	Min	Max		Temperature	Current velocity
Smagorinsky	Smagorinsky factor in horizontal turbulence Coefficient	0.2	0.05	0.3	-	✓	✓
Dalton	for evaporative heat flux Coefficient	0.0013	0.001	0.0016	-	✓	-
Stanton	for convective heat flux	0.0013	0.001	0.0016	-	✓	-
Vicouv	Uniform horizontal eddy viscosity	0.1	0.1	2	m ² /s	✓	✓

Vicoww	Uniform vertical eddy viscosity	0.00005	0.000001	0.0001	m ² /s	✓	✓
Dicouv	Uniform horizontal eddy diffusivity	0.1	0.1	2	m ² /s	✓	✓
Dicoww	Uniform vertical eddy diffusivity	0.00002	0.000001	0.0001	m ² /s	✓	✓
Rhoair	Air density	1.2265	1.1639	1.3669	Kg/m ³	-	✓

Chapter 6: Application of Python for Analysis

Python programming language was applied to efficiently carry out the sensitivity test on the North Sea Hydrodynamic model. All the scripts developed for the analysis are attached to this report as Annex I and Annex II. The steps followed in the application of Python in the analysis are shown below as a flowchart.

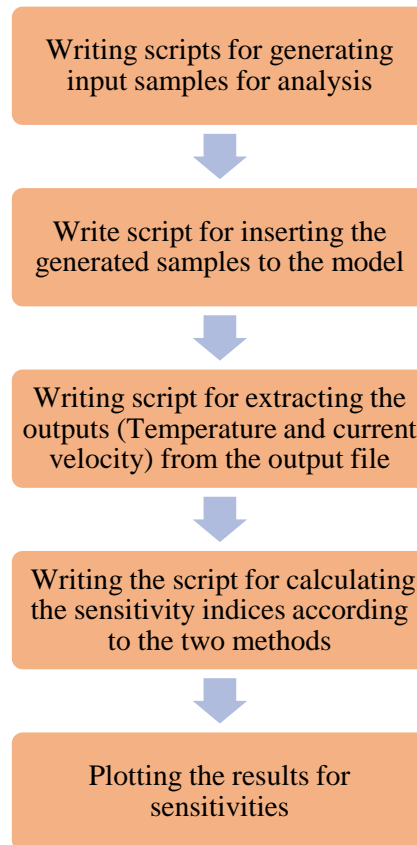


Figure 6. 1.1 Flow chart for application of Python in the sensitivity analysis

6.1. Scripts for sampling & inserting samples to model

6.1.1. Morris method

As described in the previous chapter, an individually randomized one-at-a-time (OAT) sampling method was adopted in generating the input samples for the Morris method. Hoey S. (2012) developed a python script to create the Morris samples, and this code was adjusted accordingly for this case study.

The script contains a function defined for returning a sampling matrix with input parameter values and a code to create model setup files with the generated new samples. Therefore, the script returns a csv file with all the generated samples and subfolders containing three files required for running the model. These three files will be,

1. Master definition Unstructured file (.mdu) for the model

2. dimr.xml file
3. A shell script (run_dimr-h6-c7.sh) needs to run the model in the cluster

The script is written for the two selected output variables. Therefore, six input variables need to be given by the user for running the script to generate the Morris sample for a specific sensitivity test on an output of the model. These are;

- p - number of discretization levels
- r - number of trajectories
- varName - the name of the output variable
- k - number of input parameters
- LB - lower boundary for the input parameters
- UB - upper boundaries for the input parameters

These generated parameter values were then inserted into the model by replacing the original values in the Master Definition Unstructured file (.mdu file). The source code for generating the samples and the code developed to create the new .mdu files are attached to this report as Annex I. All these setup files were saved inside separate folders.

As mentioned in Chapter 4, three trials were performed for sensitivity analysis using the Morris method for different r values. Therefore, the script for Morris sampling and creating .mdu files was executed three times separately to create the model setups for Morris samples for each trial.

6.1.2. Variance-based Sobol' method

An open-source Python package called SALib, developed by (Herman & Usher, 2017) was applied to generate the samples for the variance-based method. This Python package has the module SALib.sample.saltelli, which generates a Monte Carlo sampling matrix. The total number of samples depends on which sensitivity indices are going to be calculated. The total cost for calculating first and total order sensitivity indices is $(k+1)*N$. The second-order sensitivity indices are calculated with an extra cost of N , where N represents the selected sample size. In this study, the sample size was taken as 100 samples, and the most significant input parameters screened by the Morris method were used for variance-based sensitivity analysis.

Here, it was decided to calculate only the First-order and Total-order sensitivities for the selected input factors. Therefore, the sampling matrix has $(k+1)*N$ rows and k number of columns, where k is the number of input parameters and N is the resample size. Similar to the Morris method, these generated samples were then inserted to the model by replacing the default values in the .mdu file. This part of the code is similar to the one written for Morris method.

The script requires few inputs to be specified as fixed variables before executing the script.

- N - sample size
- varName - the name of the output variable
- num_vars - number of input parameters
- names - names of the selected input parameters for the analysis
- bounds - parameter range for each input

The source code used in the sample generation and the script wrote for inserting the generated samples into the model setup is attached to this report as Annex II.

6.2. Scripts for extracting model outputs

The outputs of the D-Flow-FM model are in the format of netCDF4 (.nc), and they are either map outputs(_map.nc) or time series outputs (_his.nc). Here the time series output (_his.nc) file was used for extracting results for temperature and current velocities in three dimensions; for x, y, and z components. The 'netCDF4' python library was imported to the script for reading the netCDF4 files as the first step. As the model results contained 50 vertical layers (z-layers) in total, the layer number for extracting the results needs to be given as an input, additional to the observation location and the output parameter name. Then, the scripts were created to extract the output values from all ensembles at a specific time and calculated the sensitivities of outputs to each input parameter for a timestep.

6.3. Scripts for calculating sensitivity indices

6.3.1. Morris Method

Using the basic concept of the Morris method, the Python script was developed first to calculate the elementary effects for each trajectory for each input factor. Elementary effects were defined as the ratio between the change of output values (either temperature or current velocity) between two adjacent model runs and the input change scaled to [0,1]. These scaled values of input parameter changes were taken to avoid the effect of the parameter range on the calculation of elementary effects. Therefore, it enables the comparison of sensitivities between parameters independent of their parameter ranges.

The sensitivity measures were calculated for each input by averaging the Elementary Effects of all the trajectories. Mean (μ), absolute mean (μ^*), and standard deviations (σ) of Elementary Effects were calculated for each time step for the whole time series covering one month. These sensitivity measures of each time step were then averaged over the entire month to have the overall results for sensitivity measures over the entire month. These average results are shown in Chapter 7.

The script needs the following variables to be assigned and files to be given for the calculations.

- p - number of discretization levels
- r - number of trajectories
- varName - the name of the output variable
- k - number of input parameters
- timesteps – number of time steps in the model results
- a set of "DCSM-FM_4nm_0000_his.mdu" – model results files (time series output of the model)
- "input_samples.csv" – a csv file contains the input samples created at the sampling step.

6.3.2. Variance-based Sobol' Method

First-order and total order Sobol' indices were calculated referring to an existing Python library, SALib.analyze.saltelli developed by (Herman & Usher, 2017) for variance-based sensitivity analysis. The sensitivities of temperature and current velocities to the input factors were calculated based on the selected period, based on the equations (4.4 and 4.5) mentioned in Chapter 4 for calculating First-order and Total-order Sobol' indices. These sensitivity indices for the selected time steps were then averaged to get the results for sensitivity indices for the month.

The following input variables need to be assigned before running the script for calculating the Sobol' indices

- N - sample size
- varName - the name of the output variable
- timesteps – number of time steps in the model
- k - number of input parameters
- names - names of the selected input parameters for the analysis

The script returns a csv file with the averages of first-order sensitivities (S1) and total-order sensitivities (ST) for the selected time period, for each input parameter.

6.4. Plotting the results

The existing Python library, 'matplotlib' was used in creating the plots for the analysis.

6.4.1. Time series plots

The time series plots containing all the model runs were generated for both Morris and Sobol' methods for temperature and current velocities in x, y, and z directions at the selected six locations. These were generated to estimate the general pattern of variation of temperature and current velocities at each location.

6.4.2. Plots for sensitivity measures

The sensitivity of the two outputs was represented based on the absolute mean and standard deviation of elementary effects in the application of Morris method. Therefore, three types of plots were created for the first method, using the average results for the whole month.

1. Scatterplots representing the sensitivity measures (absolute mean (μ^*) and standard deviation (σ) of EE) for the three trails with different r .
2. A scatterplot representing the variation of standard deviation (σ) vs. absolute mean (μ^*) of EE for selected input parameters
3. Bar plot representing the sensitivity results of all six locations

In the Sobol' method, sensitivities of the parameters were represented using the first and total order Sobol' indices. Therefore, the two types of plots were created for the output variables (temperature and current velocities) to visualize the results obtained from the variance-based method.

1. Scatterplots representing the two sensitivity indices at each location for selected input parameters
2. Scatterplots representing the variation of sensitivity measures (first-order sensitivity index (S_i) and total-order sensitivity index (S_{Ti})) for the selected input parameters at selected six locations.

6.4.3. Plots for comparing the sensitivity measures of two methods

To compare the indices obtained by the Morris and Sobol' methods, the correlation between the sensitivity measures were analyzed by plotting the variations of,

1. Absolute mean (μ^*) of EE obtained from Morris analysis with total-order Sobol' index (S_{Ti}) from Sobol' method
2. Standard deviation (σ) of EE obtained from Morris analysis with the difference of total-order Sobol' index and first-order Sobol' index ($S_{Ti} - S_i$) from Sobol' method

Chapter 7: Results and Discussion

Analyses were carried out for the Morris method and the variance-based Sobol' method separately. The number of simulations was selected based on the technique and selected sample sizes/ number of trajectories.

7.1. Variation of Output parameters over time

This sub-section contains results of the hydrodynamic model runs performed for calculating the sensitivities of temperature and current velocities in 3 dimensions. The DCSM model takes 1.67 days for simulating one year using a coarse grid. Therefore, it was challenging to perform a vast number of model runs for a very long period. Moreover, the analysis can take a considerable time for the whole year. Besides, since the study's primary goal was to analyze the sensitivities of selected output parameters to the input parameters, a specific period of the year was selected for analyzing the sensitivities. Therefore, the simulation period was taken as one month of the year, starting from 25-12-2004 up to 26-01-2005. The output temperature and current velocities were extracted at the selected six locations, including the FINO3 research platform. The average water depth of this area was observed as 23m. The output values for both variables were extracted from the surface layer of the 3D hydrodynamic model.

7.1.1. Temperature

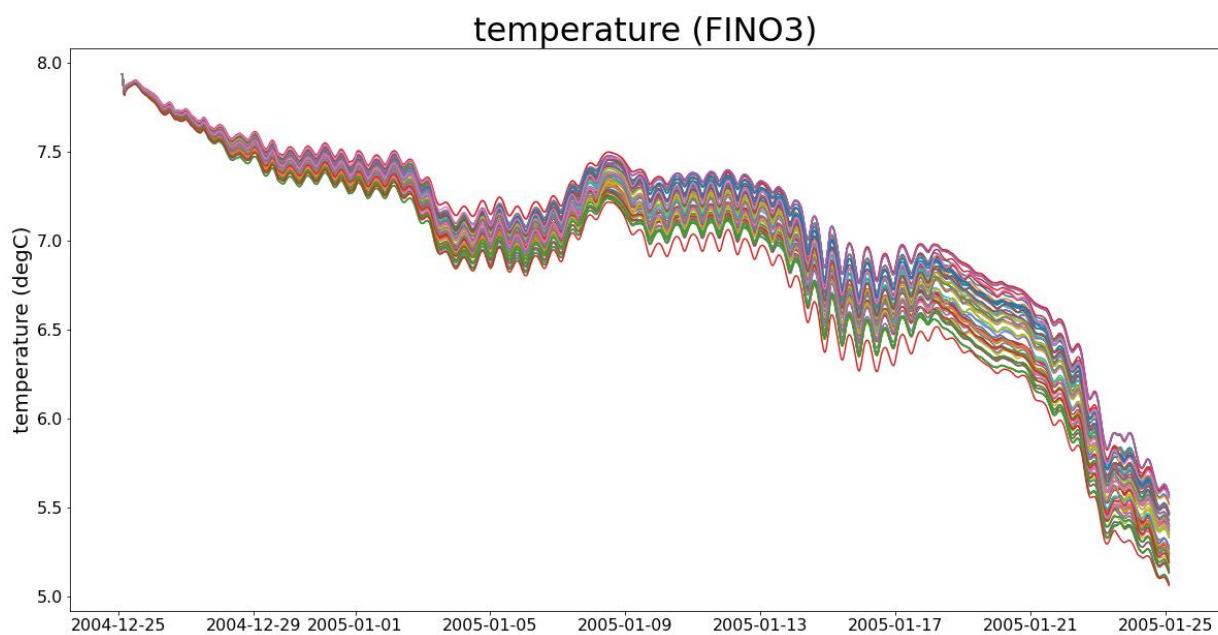


Figure 7.1.1 Temperature variation at FINO3 over one-month period simulated with 12 trajectories ($r=12$) and using 96 samples

The temperature variation of the FINO3 shows a decreasing trend over the whole month. The minor periodic variations can be explained by the temperature change in the daytime and nighttime. These modeled temperatures were compared with the available temperature data at FINO3. However, measured data at FINO 3 was not available for the selected year. Therefore,

data for January 2010 was used to compare the model results with measured temperature data at the FINO3 research platform, which is illustrated in Figure 7.2.1.

Variation of measured temperature at FINO3

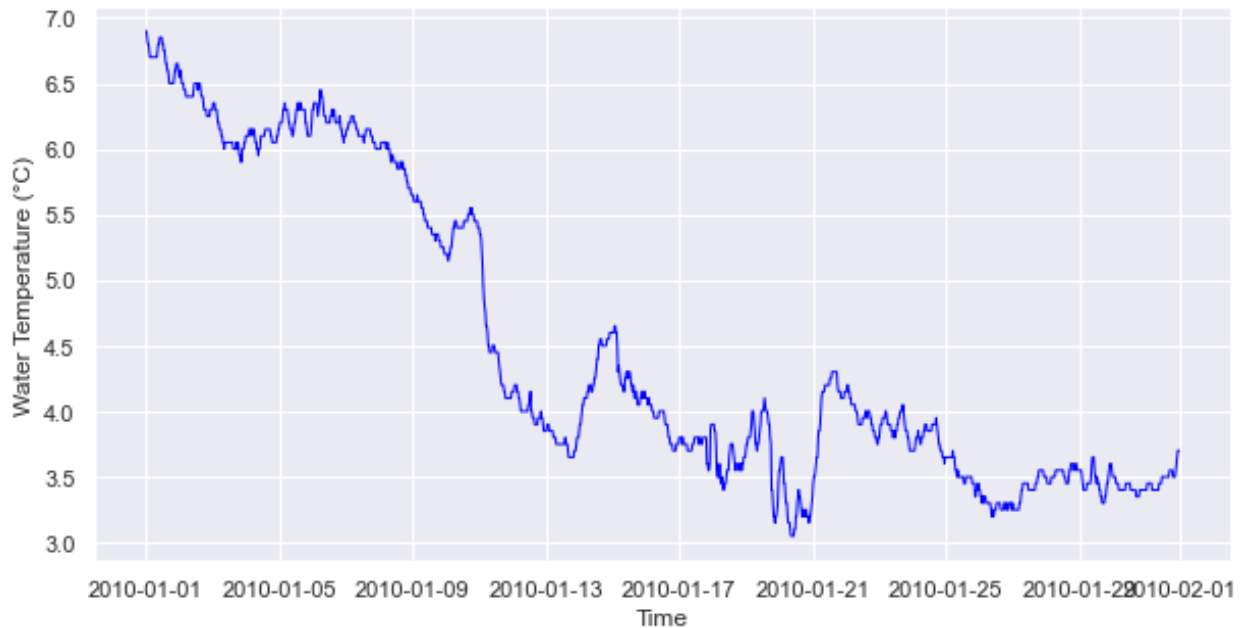


Figure 7.1.2 Measured data from buoy for surface water temperature at FINO3 for January 2010 (Data Source: BSH, 2021)

The temperature variations are similar in the simulated temperature and measured data, although the averages are not the same in two years, which can be expected.

7.1.2. Current velocity

The simulated current velocities at FINO3 for the three directions (x, y, and z directions) are shown below for the generated samples using 12 trajectories (84 model runs). Similar to the temperature result extraction, current velocities were also extracted from the surface layer at a depth of 0.5m from the mean sea level at FINO3.

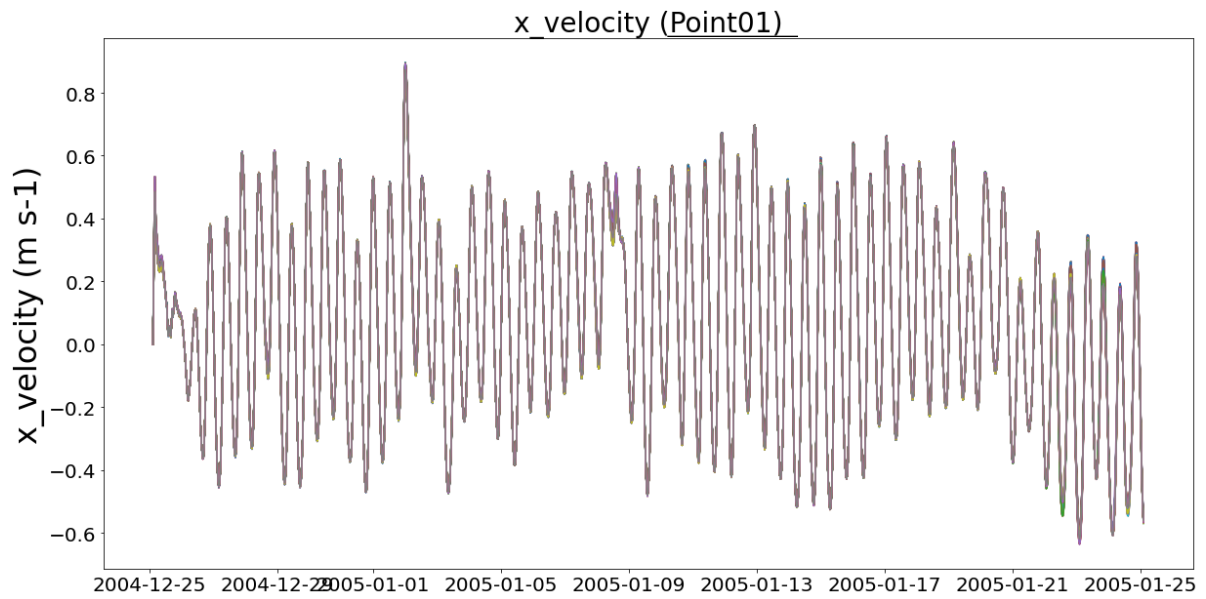


Figure 7.1.2 Variation of x velocity at FINO3 over one-month period simulated using 12 trajectories ($r=12$)

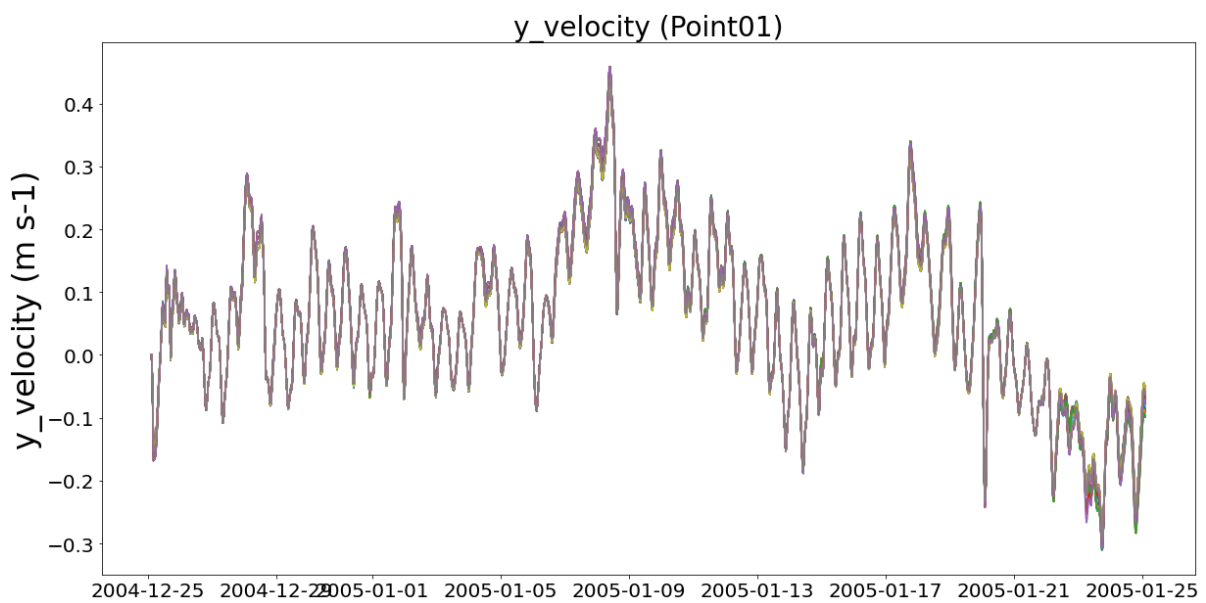


Figure 7.1.3 Variation of y velocity at FINO3 over one-month period simulated using 12 trajectories ($r=12$)

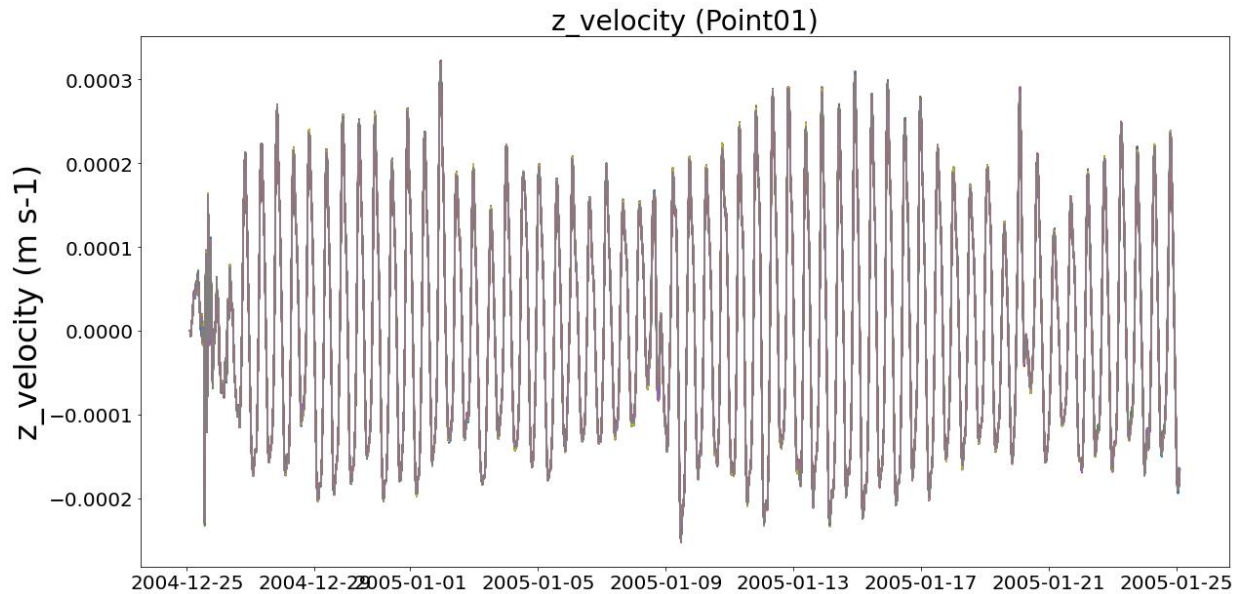


Figure 7.1.4 Variation of z velocity at FINO3 over one-month period simulated using 12 trajectories ($r=12$)

When compared the three components of the current velocities, the highest variation was observed in the x-direction. The magnitude of current velocity values is in the range of 0 – 0.8m/s for x-direction and 0 – 0.4m/s for the y-direction. However, the velocities in the vertical direction show minimal values compared to the other two. These small velocities can be explained as the stratified currents generated by the stratification occur due to temperature and density variations expected over the depth. However, it shows that the selected location experiences negligible currents in the vertical direction, which agrees with the initial assumptions on stratified currents.

As mentioned in Chapter 3, according to the literature (Sündermann & Pohlmann, 2011), the tidal currents are observed to be the dominant current type in the North Sea. The simulated current patterns in x-direction show a periodic variation. However, the current variation in the y-direction does not show a regular pattern as in the x-velocity. As the current results are extracted from the surface layer of the model vertical schematization, the reason might be the effect of wind and waves.

7.2. Application of Morris method

The Morris method was applied, selecting different numbers of trajectories or repetition numbers. As a starting point, 10 trajectories ($r = 10$) were used to calculate the sensitivity measures using the simulated results. Afterward, the number of trajectories was increased to 12 and 20, respectively, and analyses were done for the three cases. This repetition was done mainly to investigate the effect of the number of selected trajectories on the order of ranking.

Since the simulations were performed for one month, the results for sensitivity measures (mean, absolute mean, and standard deviation of Elementary Effects) were averaged in time after removing the spin-up time of 2 days for the model to be stable. The analyses were performed separately for each location. The following subsections include the sensitivity measures calculated at the FINO3 location for three trials with $r = 10, 12,$ and 20 . The results for the other locations are attached to the Annex III of this report. Moreover, a summary of the sensitivity ranking of each input parameter at selected six locations is presented at the end of each subsection.

7.2.1. Temperature Sensitivity

The Morris method results for sensitivity measures calculated for the location FINO3, using three different numbers of trajectories (r), are shown in Table 7.2.1 and Figure 7.2.1.

Table 7.2.1 Sensitivity of temperature to the input parameters calculated using Morris method (for $r = 10, 12,$ and 20) at location FINO3

Parameter	Trial 1 ($r = 10$)				Trial 2 ($r = 12$)				Trial 3 ($r = 20$)			
	$\mu(^{\circ}\text{C})$	$\mu^{*}(^{\circ}\text{C})$	$\sigma(^{\circ}\text{C})$	Ra nk	$\mu(^{\circ}\text{C})$	$\mu^{*}(^{\circ}\text{C})$	$\sigma(^{\circ}\text{C})$	Ra nk	$\mu(^{\circ}\text{C})$	$\mu^{*}(^{\circ}\text{C})$	$\sigma(^{\circ}\text{C})$	Ra nk
Smagorinsky	- 0.0215	0.0628	0.0617	2	- 0.0406	0.0560	0.0433	2	- 0.0209	0.0627	0.0626	2
Dalton	- 0.0392	0.2156	0.2082	1	- 0.0697	0.2039	0.2003	1	- 0.0610	0.1991	0.2032	1
Stanton	- 0.0007	0.0303	0.0278	3	0.0015	0.0271	0.0288	3	- 0.0018	0.0286	0.0270	3
Vicouv	0.0000	0.0000	0.0000	7	0.0000	0.0000	0.0000	7	0.0000	0.0000	0.0000	7
Vicoww	0.0002	0.0027	0.0021	4	0.0000	0.0016	0.0021	4	- 0.0001	0.0023	0.0018	4
Dicouv	0.0000	0.0000	0.0000	6	0.0000	0.0000	0.0000	6	0.0000	0.0000	0.0000	6
Dicoww	0.0002	0.0008	0.0007	5	0.0000	0.0006	0.0008	5	0.0002	0.0008	0.0007	5

The two Morris sensitivity measures, absolute mean (μ^{*}) and standard deviation (σ) of EE for the three trials, are shown in Figure 7.2.1

Morris results for sensitivity of Temperature at FINO3

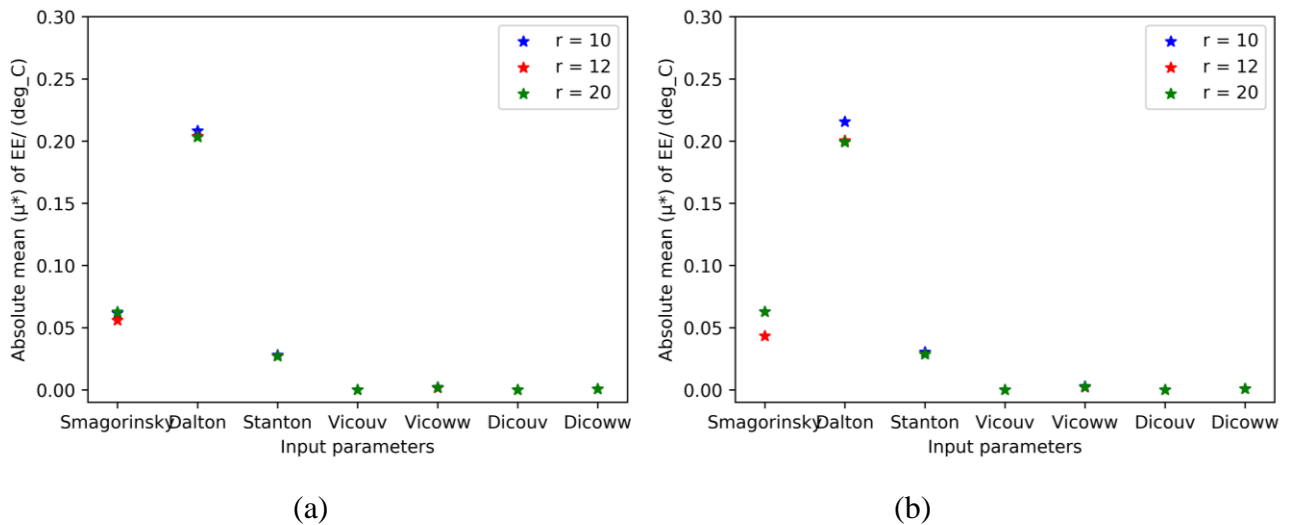


Figure 7.2.1 Sensitivity of temperature to each input parameter at FINO3 (a) Absolute mean (μ^*) of EE for input parameters for the three trials ($r=10, 12$ and 20), (b) Standard deviation (σ) of EE for input parameters for the three trials ($r=10, 12$ and 20)

- The results for the three trials corroborate that although the numerical values for mean, absolute mean, and standard deviation are slightly changed with the selected number of trajectories, the order of significance has not changed with the increased r .
- When considering the sensitivity measures μ and μ^* for some parameters, there is smaller mean (μ) values and higher absolute mean (μ^*) values. This indicates that the parameters have effects with opposing signs.
- Therefore, to capture both positive and negative values of the Elementary Effects, the absolute mean (μ^*) of EE was used in deciding the importance of input factors to the model.

Figure 7.2.2 shows the relation between the absolute mean and the standard deviation of EE for each input parameter. Since it is proven that there is no significant difference in the values obtained by the three trials ($r=10, 12, 20$), the results of trial 2 with 12 trajectories has been used here for the analysis. One primary observation of the Figure 7.2.2 is that all the points lie in the diagonal. This indicates that all the parameters that affect the simulated temperature have non-linear effects on the temperature.

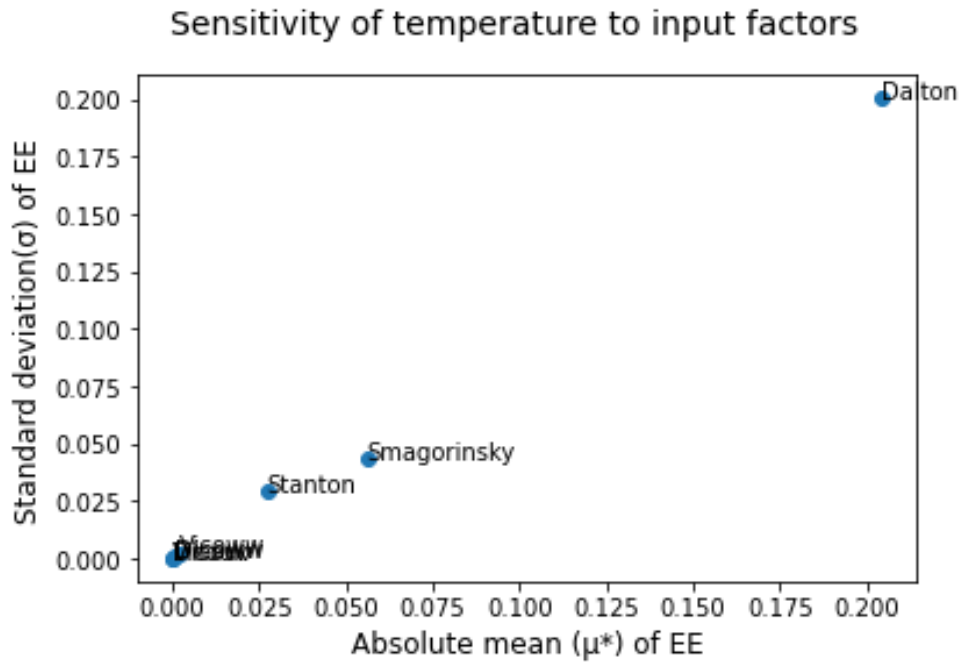


Figure 7.2.2 Morris results of temperature sensitivity at FINO3; (r=12) Scatterplot for temperature sensitivity - Variation of standard deviation with absolute mean

The Morris analysis can only be used as a qualitative method to screen the significant input factors, as discussed in Chapter 2. The absolute mean of EE values indicates the importance of each input parameter. The standard deviation is a qualitative measure of the non-linearities of the input-output relationship. Further, this is an indication of the possible interactions with other parameters. According to the tabulated values of these sensitivity measures, the most influential parameter is the Dalton coefficient, which is the coefficient of evaporative heat flux. Therefore, it can be claimed that the process of evaporative heat loss contributes the most in defining the modeled temperature values out of these selected input parameters.

When considering the physical meaning of these two coefficients used in the D-Flow FM model, as described in sections 5.1 and 5.2, the temperature is modeled considering the net radiation and heat losses due to convective and evaporative heat fluxes. Evaporative heat loss is dependent on meteorological factors (i.e., wind-driven convection) and vapour pressures. According to the technical reference manual of D-Flow FM (Deltares, 2021), there are two processes considered to calculate the latent heat flux, free and forced convection. The equation below gives the latent heat flux of forced convection

$$Q_{ev,forced} = L_v \rho_a f(U_{10}) \{q_s(T_s) - q_a(T_a)\} \quad 7.1$$

The wind function in this equation ($f(U_{10})$) is calculated as a function of wind velocity (U_{10}) and Dalton coefficient (c_e) using the equation

$$f(U_{10}) = c_e U_{10} \quad 7.2$$

The Stanton coefficient was identified as the third most important factor from the above results. Like in the Dalton coefficient, the Stanton coefficient is also used in the calculation of the heat budget of the model. The sensible heat flux or the convective heat flux is calculated with two

processes, free convection and forced convection. The forced convective heat flux is calculated with the equation

$$Q_{CO,forced} = c_p \rho_a g(U_{10}) \{T_s - T_a\} \quad 7.3$$

The wind function in the above equation is calculated as a function of wind speed and the Stanton coefficient (c_H).

$$g(U_{10}) = c_H U_{10} \quad 7.4$$

The above equations indicate that both, Dalton and Stanton coefficients, affect the simulated temperature in the model. Therefore, the results substantiate these physical definitions.

The second most important parameter was identified to be the Smagorinsky factor in horizontal turbulence. As discussed in section 5.2, the Smagorinsky factor is used in calculating the horizontal eddy viscosity of the model as an input to calculate the sub-grid scale eddy viscosity. Thus, it can be assumed that the Smagorinsky factor affects the horizontal turbulence of the water mass and indirectly contributes to calculating the temperature in the model to a considerable extent.

One significant observation from the above results is that the Elementary Effects for uniform eddy viscosity and eddy diffusivity (Vicouv, Dicouv) show no effect on temperature sensitivity. This means that these values are not considered when calculating the temperature in the model for this period. It is essential to look at the physical meaning of these results with respect to applying these inputs to the model. As mentioned in section 5.2, uniform viscosities and diffusivities are applied to the model as uniform background values, where the final values of viscosities and diffusivities are calculated as a combined function of the applied uniform values and those from the sub-grid model, vertical eddy viscosities, and kinematic viscosity of water. However, the horizontal eddy viscosity and horizontal eddy diffusivity are specified in the external forcing file (.ext file) in the model as well. Thus, the final values are taken as the maximum of these uniform background values and the spatially varying values given in the external forcing file.

Therefore, it can be assumed that for the selected period, the Vicouv and Dicouv values given in the .mdu file have always been less than the values given in the external forcing (.ext) file. Thus, the model always considers the viscosities from the external forcing file for the calculations. Therefore, the sensitivity analysis shows that these inputs are insignificant for temperature calculation in the model. Nonetheless, there is still a possibility that these two parameters affect the temperature sensitivity if the models were run for a different period of the year or considered different locations.

The tables and graphs for sensitivity measures of the temperature for the other five locations are attached to Annex III. The summary of the sensitivity measures at each location is presented in Figure 7.2.4. The results for the other five locations are comparable with the results obtained for FINO3 although the numerical values change slightly from one location to another .

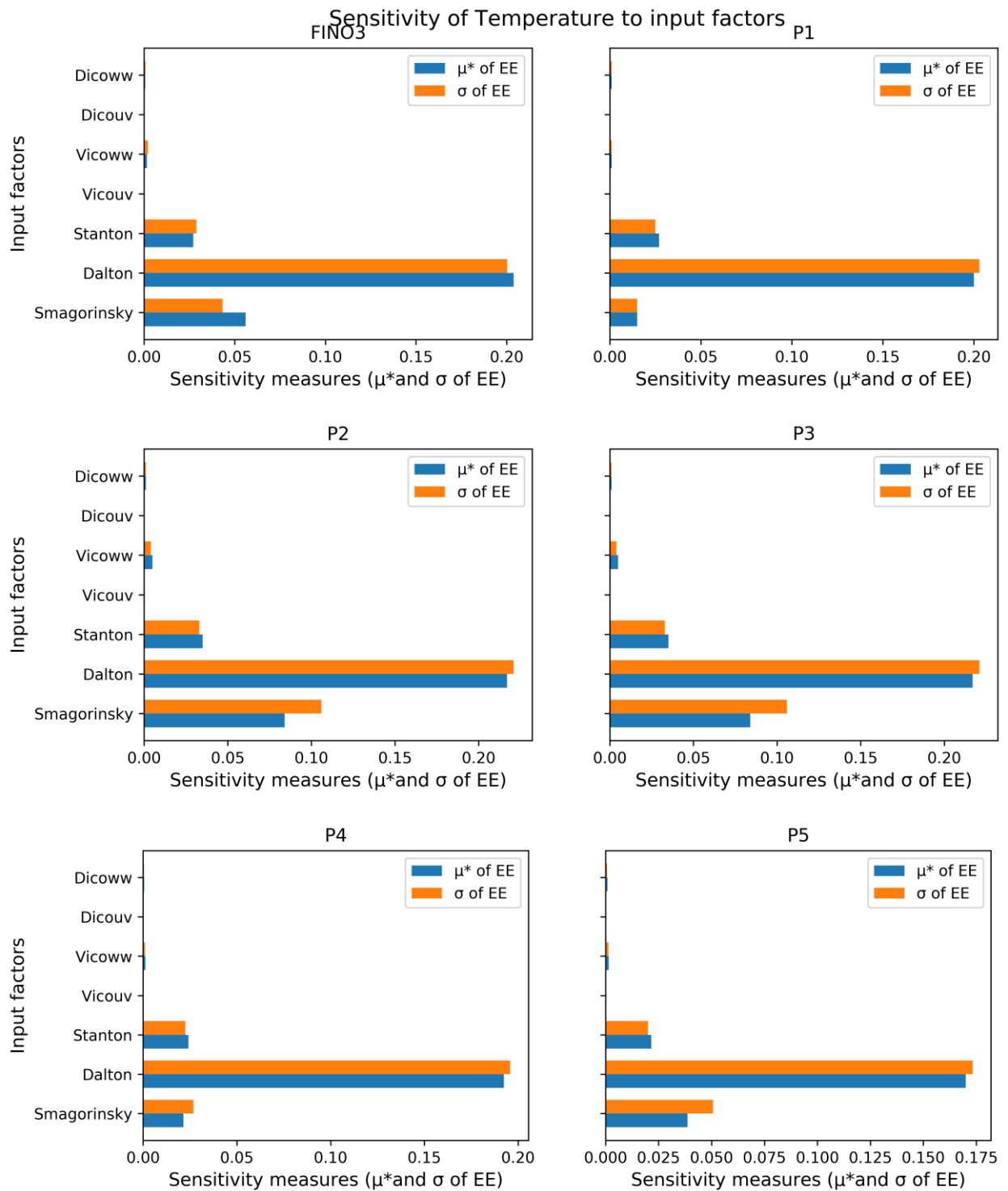


Figure 7.2.3 Variation of sensitivity of temperature to input parameters based on the selected location, calculated by Morris method using 12 trajectories ($r = 12$)

A summary of the ranking obtained through the Morris analysis for selected six locations is given in Table 7.2.2.

Table 7.2.2 Ranking of Significance of input parameters on temperature (r=12) based on location

Parameter	Ranking of input parameter at Location					
	FINO 3	P1	P2	P3	P4	P5
Smagorinsky	2	3	2	2	2	2
Dalton	1	1	1	1	1	1
Stanton	3	2	3	3	3	3
Vicouv	7	7	7	7	7	7
Vicoww	4	4	4	4	4	4
Dicouv	6	6	6	6	6	6
Dicoww	5	5	5	5	5	5

The resulting ranks for all the selected locations except point 1 (P1) show the same order. Out of the selected set of inputs, the temperature was most sensitive to the input Dalton coefficient. The second most important factor is identified as the Smagorinsky factor and, thirdly, the Stanton coefficient.

7.2.2. Sensitivity of Current velocity

The D-Flow FM model calculates the currents in all three directions x, y, and z. These were analyzed separately as three components of the currents. Similar to the temperature analysis, three trials were done to check the effect of the selected number of repetitions (r) on the calculated sensitivity measures.

7.2.2.1. Current velocity - x component

The following table contains the sensitivity measures calculated (mean, absolute mean, and standard deviation of Elementary Effects (EE)) for the x-velocity component of currents.

Table 7.2.3: Sensitivity measures of current velocity (x-component) to the input parameters calculated using Morris method (for r = 10, 12 and 20) at location FINO3

Parameter	r = 10				r = 12				r = 20			
	μ (m/s)	μ^* (m/s)	σ (m/s)	Ra nk	μ (m/s)	μ^* (m/s)	σ (m/s)	Ra nk	μ (m/s)	μ^* (m/s)	σ (m/s)	Ra nk
Vicouv	0.00E+00	0.00E+00	0.00E+00	6	0.00E+00	0.00E+00	0.00E+00	6	0.00E+00	0.00E+00	0.00E+00	6
Vicoww	-6.88E-06	1.74E-03	1.44E-03	3	6.61E-05	1.30E-03	1.12E-03	3	4.44E-06	1.23E-03	1.48E-03	3
Dicouv	0.00E+00	0.00E+00	0.00E+00	5	0.00E+00	0.00E+00	0.00E+00	5	0.00E+00	0.00E+00	0.00E+00	5
Dicoww	1.24E-04	6.10E-04	5.17E-04	4	4.98E-06	5.92E-04	4.58E-04	4	8.65E-05	5.14E-04	6.47E-04	4
Rhoair	2.95E-03	1.13E-02	1.31E-02	1	2.87E-04	1.40E-02	1.34E-02	1	2.07E-04	1.33E-02	1.38E-02	1
Smagorinsky	-8.72E-04	4.42E-03	4.30E-03	2	1.01E-03	3.62E-03	4.18E-03	2	6.66E-04	4.33E-03	4.51E-03	2

Out of the selected input parameters, the most significant inputs for defining the x-velocity component in the model were air density (Rhoair) and the Smagorinsky coefficient. Other than that, uniform viscosity and uniform diffusivity in the vertical direction affect the sensitivity of the x-velocity component on a minor scale.

Air density is used in calculating wind stress in the model. However, a spatially varying air density is provided (as a parameter in ERA5 data) to the model. The constant air density value used here (Rhoair) is generally used to adjust the wind speed in the model such that the right wind stress is achieved. The wind stress acting on the sea surface affects the computation of current velocities. Thus, Rhoair can be expected to affect the current velocity calculation indirectly.

Smagorinsky coefficient is used in the Smagorinsky sub-grid model to calculate horizontal viscosity, which defines horizontal turbulence. Therefore, the coefficient is expected to contribute to calculating eddy viscosities and indirectly affect the current velocity calculation.

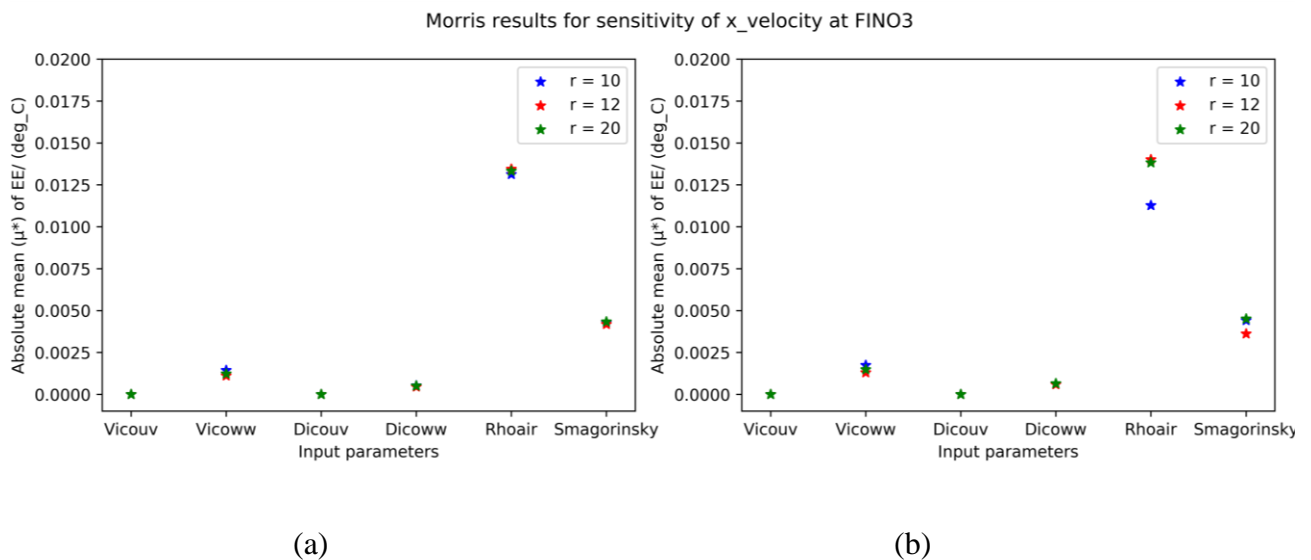


Figure 7.2.4 Sensitivity of x-velocity to each input parameter at FINO3 (a) Absolute mean (μ^*) of EE for input parameters for the three trials ($r=10, 12$ and 20), (b) Standard deviation (σ) of EE for input parameters for the three trials ($r=10, 12$ and 20)

The results for three trials with different numbers of trajectories show that the ranking order has not changed with the number of trajectories. Therefore, we can conclude that using $r=10$ with four discretization levels ($p=4$) is sufficient in deciding the order of sensitivities.

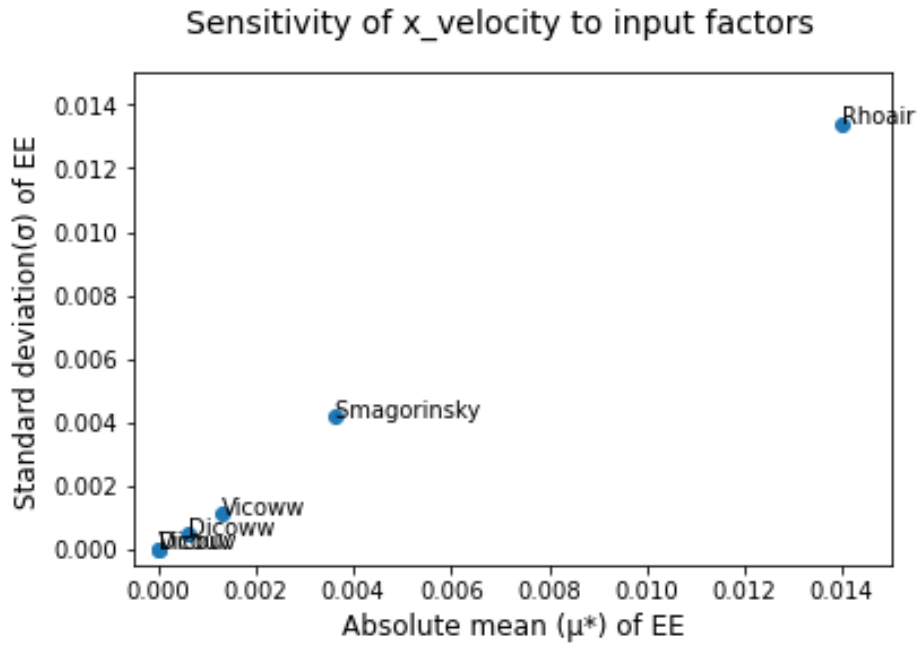


Figure 7.2.5 Morris results for the sensitivity of x-velocity at FINO3; (r=12) Scatterplot for x-velocity sensitivity - Variation of standard deviation with absolute mean

According to the above figure, all the input factors lie in the diagonal, indicating that the input factors which are influential to the simulated current velocity in x-direction have non-linear effects on the output.

The tabulated values of sensitivity measures for the x-velocity component of currents for the other locations are attached to Annex III. The sensitivity measures for the x-velocity component at each location are given in Figure 7.2.6.

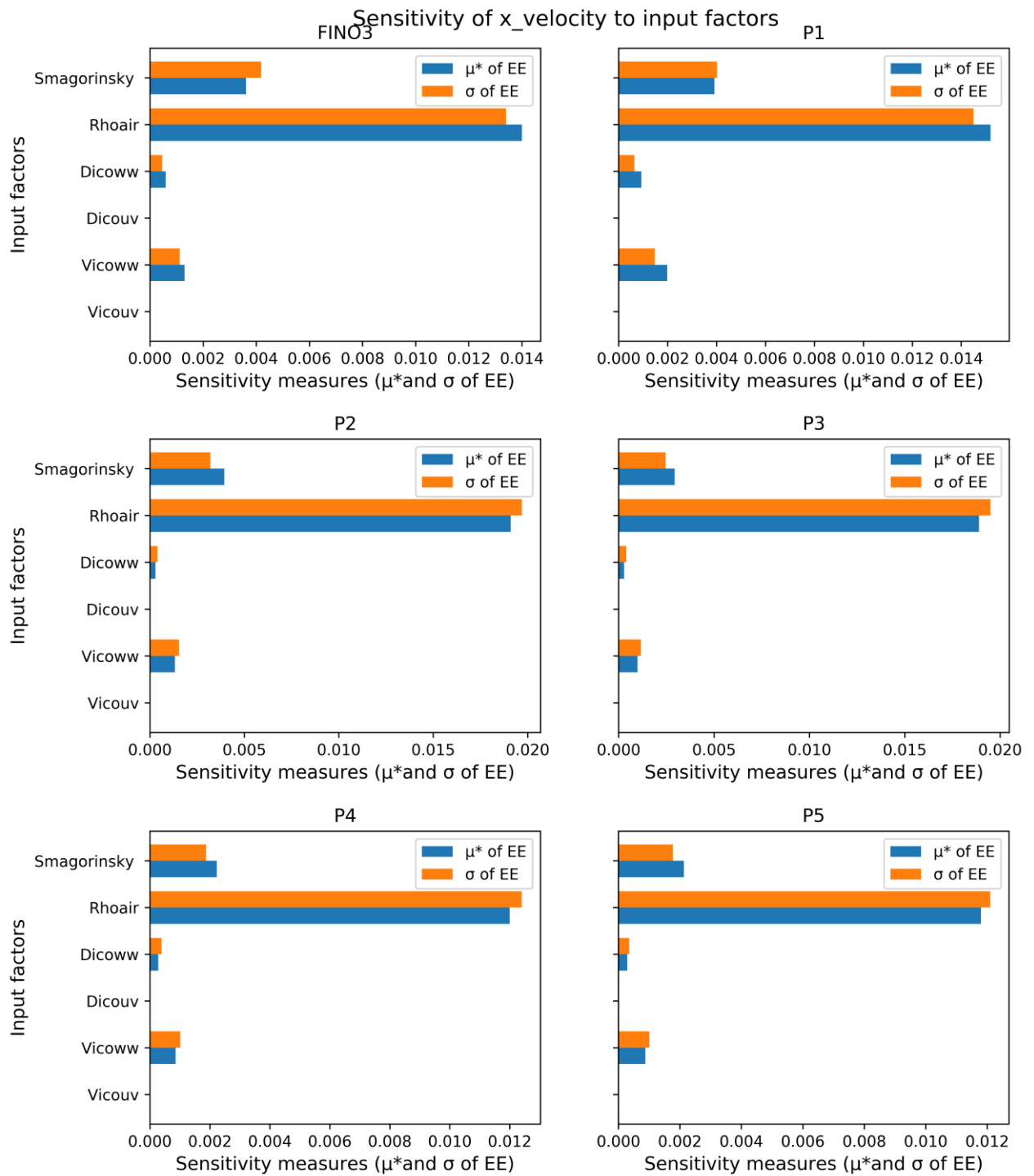


Figure 7.2.6 Variation of sensitivity of current velocity (x-velocity component) to input parameters based on the selected location, calculated by Morris method using 12 trajectories ($r = 12$)

The above results show that the spatial variation of the sensitivity of x-velocity to input factors is negligible for these six locations.

Table 7.2.4 Ranking of Significance of input parameters on current velocity_(x-component) based on location

Parameter	Ranking of input parameter at Location					
	FINO 3	P1	P2	P3	P4	P5
Vicouv	6	6	6	6	6	6
Vicoww	3	3	3	3	3	3
Dicouv	5	5	5	5	5	5
Dicoww	4	4	4	4	4	4
Rhoair	1	1	1	1	1	1
Smagorinsky	2	2	2	2	2	2

Similar to the sensitivity of the x-velocity component, the sensitivity of the y-velocity component to the selected input parameters also has not changed based on the location for the selected area of FINO3.

7.2.2.2. Current velocity - y component

The sensitivity measures obtained from the Morris analysis are shown in Table 7.2.5 for the location FINO3.

Table 7.2.5 Sensitivity measures of current velocity (y-component) to the input parameters calculated using Morris method (for r = 10, 12 and 20) at location FINO3

Parameter	r = 10				r = 12				r = 20			
	μ (m/s)	μ^* (m/s)	σ (m/s)	Rank	μ (m/s)	μ^* (m/s)	σ (m/s)	Rank	μ (m/s)	μ^* (m/s)	σ (m/s)	Rank
Vicouv	0.00E+00	0.00E+00	0.00E+00	6	0.00E+00	0.00E+00	0.00E+00	6	0.00E+00	0.00E+00	0.00E+00	6
Vicoww	8.85E-05	8.81E-04	1.12E-03	3	1.52E-05	6.28E-04	7.67E-04	3	5.27E-05	7.06E-04	8.99E-04	3
Dicouv	0.00E+00	0.00E+00	0.00E+00	5	0.00E+00	0.00E+00	0.00E+00	5	0.00E+00	0.00E+00	0.00E+00	5
Dicoww	3.41E-05	3.31E-04	4.16E-04	4	4.85E-06	2.82E-04	3.68E-04	4	3.75E-05	3.39E-04	4.53E-04	4
Rhoair	4.08E-03	1.12E-02	9.53E-03	1	1.11E-03	1.15E-02	1.20E-02	1	1.17E-03	1.15E-02	1.19E-02	1
Smagorinsky	4.42E-04	3.65E-03	3.78E-03	2	6.67E-04	3.31E-03	2.75E-03	2	3.39E-04	3.40E-03	3.50E-03	2

The tables and graphs for sensitivity measures of the y-velocity component of currents for the other locations are attached to Annex III.

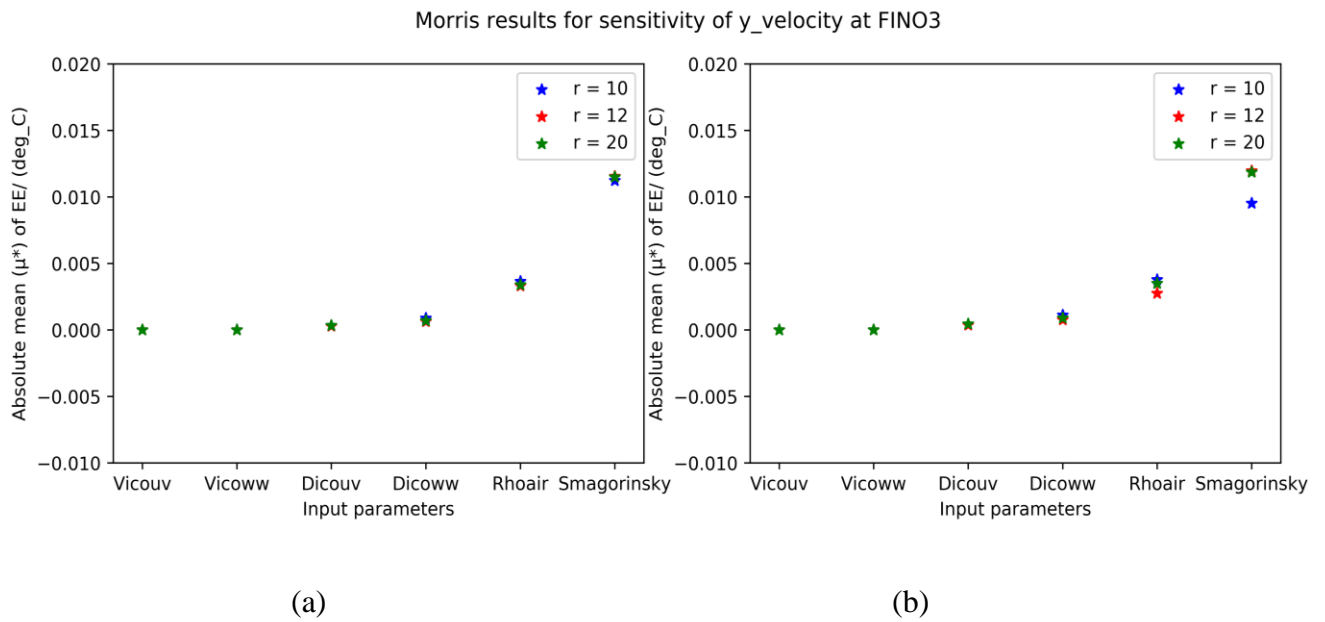


Figure 7.2.7 Sensitivity of y-velocity to each input parameter at FINO3 (a) Absolute mean(μ^*) of EE for input parameters for the three trials ($r=10, 12$ and 20), (b) Standard deviation (σ) of EE for input parameters for the three trials ($r=10, 12$ and 20)

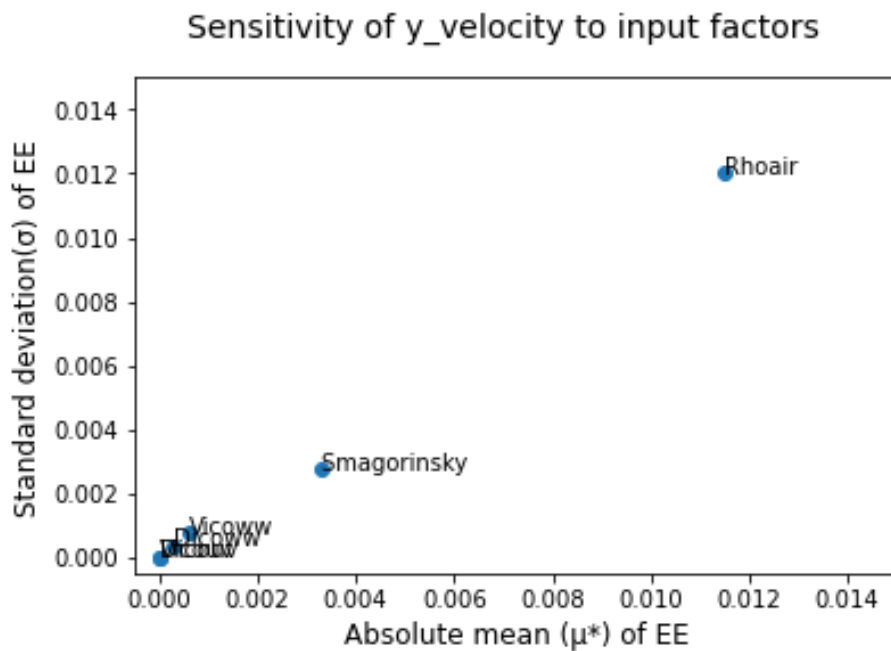


Figure 7.2.8 Morris results for the sensitivity of y-velocity at FINO3; ($r=12$) Scatterplot for y-velocity sensitivity - Variation of standard deviation with absolute mean

The sensitivity measures for the y-velocity component at each location are given in Figure 7.2.9.

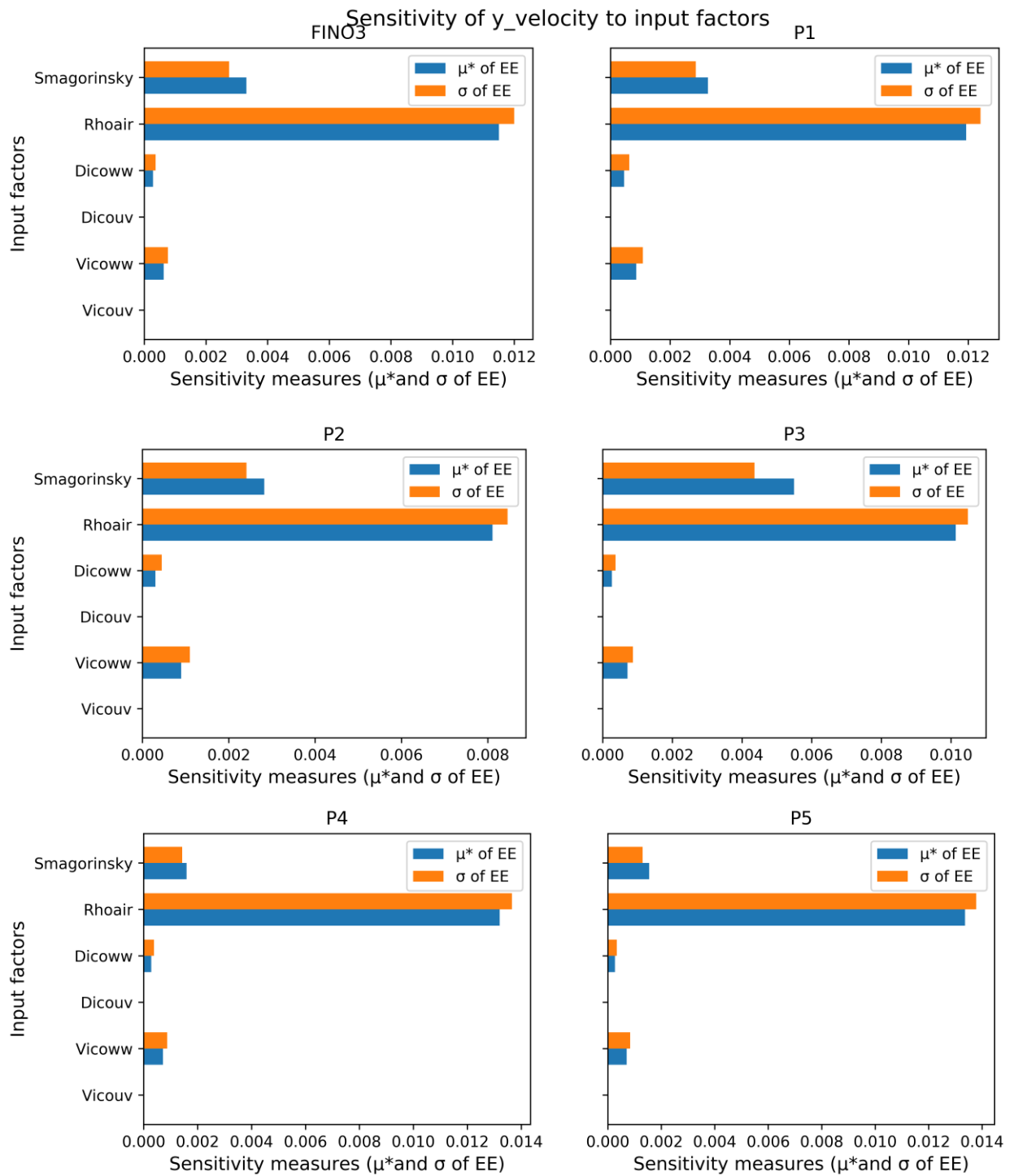


Figure 7.2.9 Variation of sensitivity of current velocity (y-velocity component) to input parameters based on the selected location, calculated by Morris method using 12 trajectories ($r = 12$)

Similar to the sensitivity measures of the x-velocity component, current velocities in y-direction do not exhibit a significant change based on the analysis location.

Table 7.2.6 Ranking of Significance of input parameters on current velocity (y-component) based on location

Parameter	Ranking of input parameter at Location					
	FINO 3	P1	P2	P3	P4	P5
Vicouv	6	6	6	6	6	6
Vicoww	3	3	3	3	3	3
Dicouv	5	5	5	5	5	5
Dicoww	4	4	4	4	4	4
Rhoair	1	1	1	1	1	1
Smagorinsky	2	2	2	2	2	2

7.2.2.3. Current velocity - z component

Table 7.2.7: Sensitivity measures of current velocity (z-component) to the input parameters calculated using Morris method (for r = 10, 12 and 20) at location FINO3

Parameter	r = 10				r = 12				r = 20			
	μ (m/s)	μ^* (m/s)	σ (m/s)	Ra nk	μ (m/s)	μ^* (m/s)	σ (m/s)	Ra nk	μ (m/s)	μ^* (m/s)	σ (m/s)	Ra nk
Vicouv	0.00 E+00	0.00E +00	0.00E +00	6	0.00E +00	0.00E+ 00	0.00E+ 00	6	0.00E +00	0.00E+ 00	0.00E +00	6
Vicoww	2.60 E-10	1.65E -06	1.97E -06	2	2.51E -09	1.33E- 06	1.68E- 06	2	2.15E -09	1.49E- 06	1.86E -06	2
Dicouv	0.00 E+00	0.00E +00	0.00E +00	5	0.00E +00	0.00E+ 00	0.00E+ 00	5	0.00E +00	0.00E+ 00	0.00E +00	5
Dicoww	3.09 E-09	4.31E -07	6.33E -07	4	1.96E -09	3.88E- 07	5.74E- 07	4	1.72E -09	4.34E- 07	6.51E -07	4
Rhoair	1.27 E-07	3.99E -06	3.67E -06	1	5.27E -08	4.04E- 06	4.41E- 06	1	1.89E -08	4.03E- 06	4.39E -06	1
Smagorinsky	6.62 E-09	1.29E -06	1.52E -06	3	5.83E -08	1.17E- 06	1.28E- 06	3	1.13E -08	1.22E- 06	1.45E -06	3

The observed values for all the sensitivity measures (mean, absolute mean, and standard deviation of EE) were comparably lower than the sensitivity measures of the other two velocity components. These nominal values can be expected because of the minimal range of the original current velocities in the z-direction, which were in the range of 10E-4.

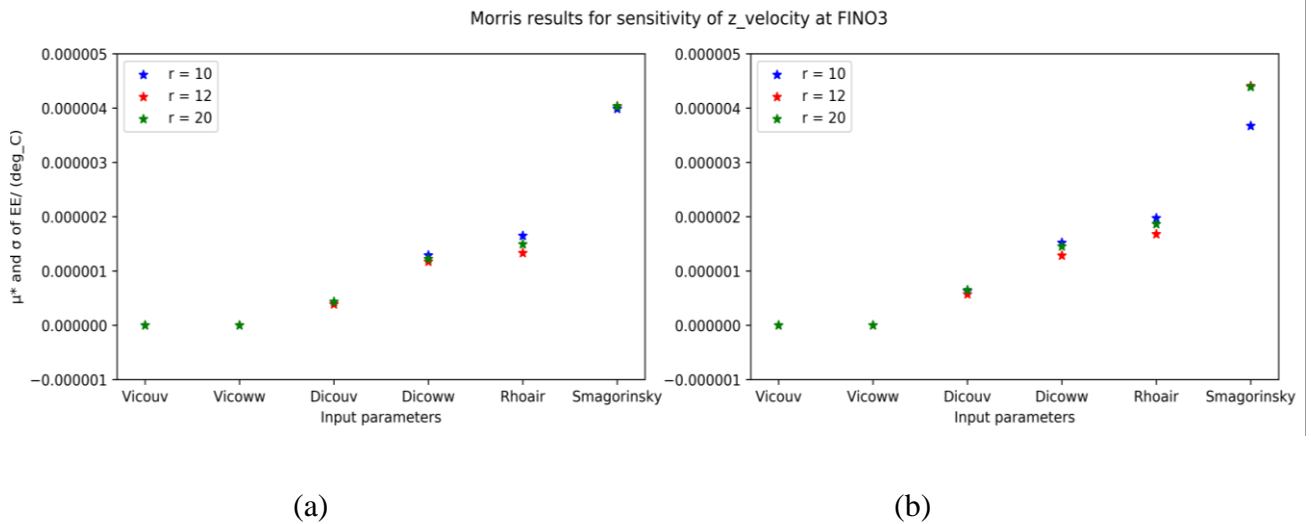


Figure 7.2.10 Sensitivity of z_velocity to each input parameter at FINO3 (a) Absolute mean (μ^*) of EE for input parameters for the three trials ($r=10, 12$ and 20), (b) Standard deviation (σ) of EE for input parameters for the three trials ($r=10, 12$ and 20)

Similar to the previous analyses of x and y velocities, the selected number of trajectories has not significantly changed the calculated sensitivity measures for z-velocity. Therefore, it can be confirmed that using $r=10$ would be sufficient in the analyses.

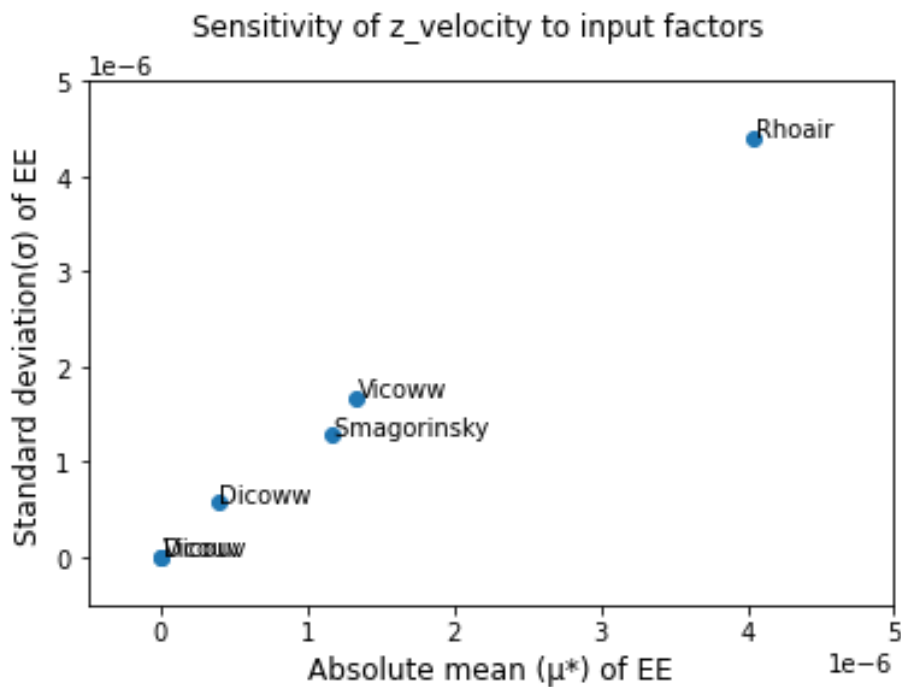


Figure 7.2.11 Morris results for the sensitivity of y-velocity at FINO3; ($r=12$) Scatterplot for y-velocity sensitivity - Variation of standard deviation with absolute mean

All the selected inputs for the analysis of z-velocities lie in the diagonal, indicating that the parameters with higher absolute mean values have higher standard deviations. This denotes

that the parameters, which are identified as significant inputs, have non-linear effects on the output.

The sensitivity measures for the z-velocity component at each location are given in Figure 7.2.12.

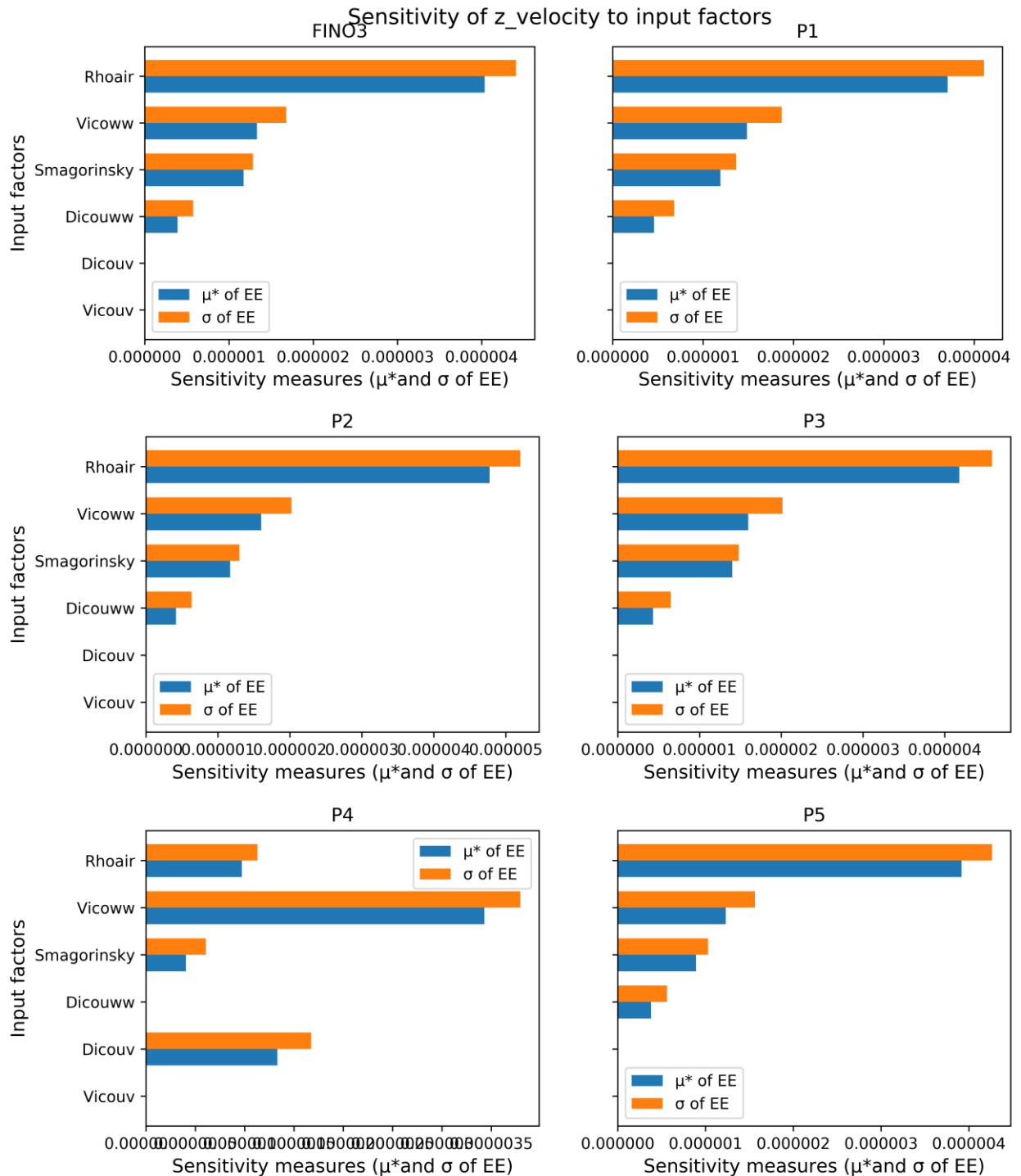


Figure 7.2.12 Variation of sensitivity of current velocity (z-velocity component) to input parameters based on the selected location, calculated by Morris method using 12 trajectories ($r = 12$)

The graphs for Sensitivity measures of the z-velocity component of currents for the other locations are attached to Annex III. The summary of the ranking obtained by the above results is shown in Table 7.2.8.

Table 7.2.8 Ranking of Significance of input parameters on current velocity_(z-component) based on location

Parameter	Ranking of input parameter at Location					
	FINO 3	P1	P2	P3	P4	P5
Vicouv	6	6	6	6	6	6
Vicoww	2	2	2	2	1	2
Dicouv	5	5	5	5	2	5
Dicoww	4	4	4	4	5	4
Rhoair	1	1	1	1	3	1
Smagorinsky	3	3	3	3	4	3

Similar to the sensitivity of the x- and y-velocity components, the z-velocity component also does not change much based on the selected analysis location except for the location P4, where the most significant input parameter was identified as uniform vertical eddy viscosity. Uniform vertical eddy diffusivity stands as the second most significant factor to the z-velocity component at this location. Air density (Rhoair), which was identified as the most significant parameter at the other five locations, was identified to be the third important factor for calculating the z-velocity of the model at P4. Through all these results for the six locations, the four most important input factors, which will be affecting the modeled current velocity in the z-direction, were selected as air density (Rhoair), Smagorinsky factor, Vicoww, and Dicoww.

7.3. Application of Variance-based Sobol' method

As mentioned before, the Sobol' method can calculate the individual and combined effects of each input variances on the output variance. The high computation cost of the variance-based method hinders applying this method to the complex numerical model. Therefore, to reduce the computation effort, it was decided to apply this method for the most significant input parameters screened by the Morris method.

The following input parameters were selected, which were screened from the Morris method, to have a more comprehensive analysis of the sensitivities of output variables to the input parameters. Table 7.3.1 includes these selected input parameters for each output variable.

Table 7.3.1 Input parameters selected by the Morris screening method for the variance-based analysis

Output variable	Selected input parameters
Temperature	Dalton, Smagorinsky, Stanton
Current velocity (x-velocity component)	Rhoair, Smagorinsky, Vicoww, Dicoww
Current velocity (y-velocity component)	Rhoair, Smagorinsky, Vicoww, Dicoww
Current velocity (z-velocity component)	Rhoair, Smagorinsky, Vicoww, Dicoww

7.3.1. Temperature Sensitivity

The Variance decomposition for the temperature with respect to the selected input parameters is given in this section. Here, S_i represents the first order indices, and S_{Ti} represents the total order indices. The spin-up time for the model to be stable was considered as two days, considering the stability of the results. Similar to the previous method, the Sobol' indices were also calculated for different timesteps to have a complete picture of sensitivity measures. However, considering the time taken for the analysis for a considerable number of timesteps (1489 for one month), selecting a range of timesteps for calculations was decided. The average of the indices was taken for the period of 20 timesteps from 13-01-2005: 13:00 to 13-01-2005: 23:00 ($t = 890$ to $t = 910$).

The sensitivity indices obtained for the extracted results for temperature is given in Table 7.3.2.

Table 7.3.2 Sensitivity indices for the temperature to the input parameters calculated using the Sobol' method at FINO 3

Parameter	S_i	S_{Ti}	$S_{Ti} - S_i$	Rank (based on S_i)	Rank (based on S_{Ti})
Smagorinsky	0.1511	0.1639	0.0128	2	2
Dalton	0.8338	0.8469	0.0132	1	1
Stanton	0.0040	0.0048	0.0007	3	3

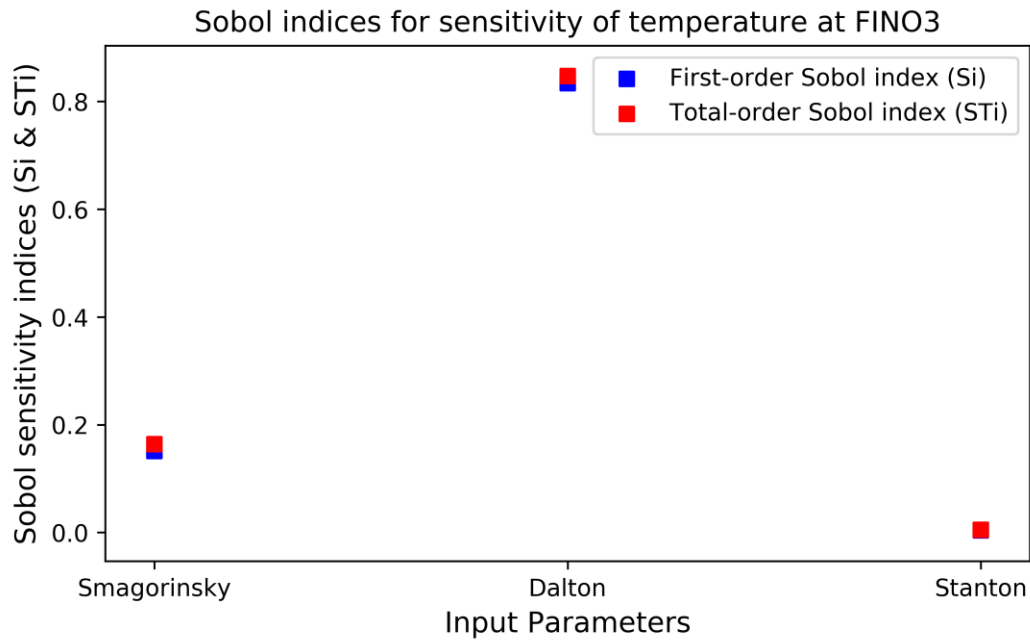


Figure 7.3.1 First-order and total-order Sobol' indices for the location FINO3

The first-order sensitivity index is a quantitative measure of the individual impact of a particular input on the output. According to the resulting values for S_i for the selected three parameters, it was observed that the ranking of the inputs shows a similar order as in the Morris results. 83.4% of the output temperature variability is caused due to the variability of the Dalton coefficient alone. The second most sensitive parameter was observed as the Smagorinsky factor, which accounted for 15.1% of the output variability. The Stanton coefficient contributes to 0.4% of the variance of calculated temperature. All the first-order indices add up to about 0.98. This indicates that the model output variability is caused mainly by the first-order effects, and the second and third-order sensitivities are relatively small. Thus, when considered these three input parameters, the Dalton coefficient, and the Smagorinsky factor account for about 98% of the sensitivity of output temperature of the model.

Total order Sobol' indices are a measure for determining the different types of effects, including the linear, non-linear, additive, and interactions of any order, including first, second, and higher orders (Campolongo & Saltelli, 1997). According to (Saltelli A et al., 2008), inputs are called interacting when the output is associated with two or more input combinations. The first-order index gives information on how one single input parameter's variability creates the output variability. The difference between the total order index and the first-order index ($S_{Ti} - S_i$) indicates the output variabilities generated as a combined effect of a particular input with other input parameters.

According to the above results, the Dalton coefficient has a ($S_{Ti} - S_i$) value of 0.0132, indicating that the factor interacts with the other two parameters and contributes 1.3% of the output temperature variability due to these interactions. Therefore, a high portion of the output variance is created due to two input parameters, including the coefficient of evaporative heat flux (Dalton) and the Smagorinsky coefficient used in calculating the sub-grid scale horizontal

viscosity. Consequently, these observations are comparable with the results obtained through Morris analysis when looking at the ranking order.

Sobol' indices calculated for temperature sensitivity for the other five locations are attached to Annex III. Further, Figure 7.3.3 represents the variation of the first-order and total-order Sobol' indices for the temperature sensitivity depending on the analysis location.

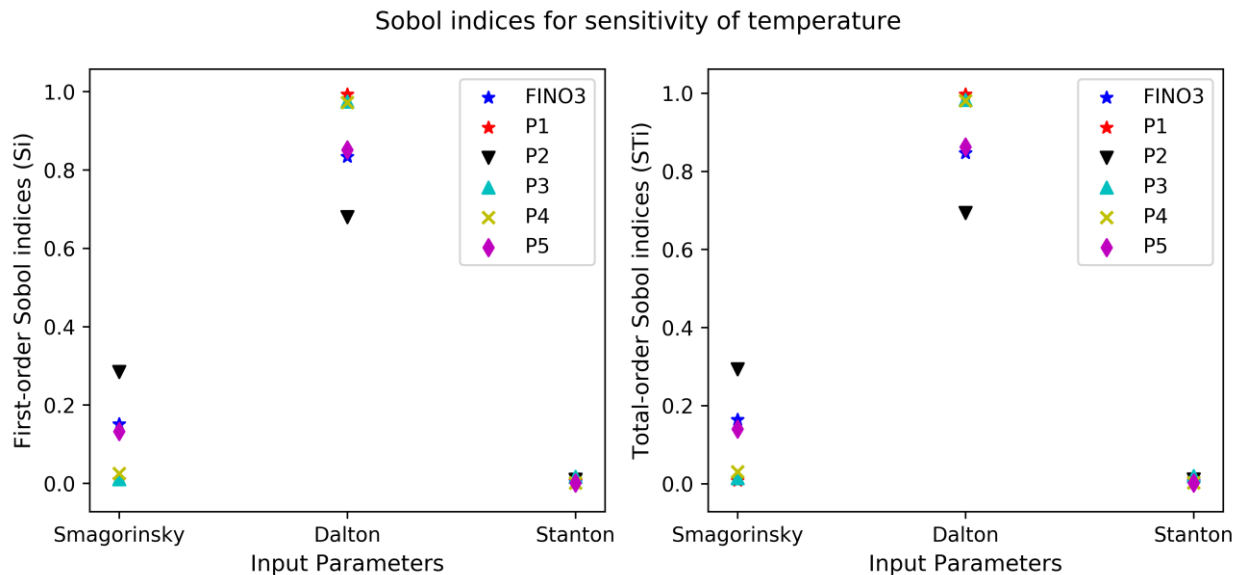


Figure 7.3.3 First-order and total-order Sobol' indices for the temperature at the selected six locations

From the above figure, it is evident that the sensitivity indices of each input parameter show only a slight variation depending on the analysis location. Therefore, using the results for FINO3 is sufficient to conclude the significance of the input parameters selected in the Sobol' analysis of temperature.

7.3.2. Sensitivity of Current velocity

Similar to the analysis done in the Morris method, the spin-up period was considered two days for the model results. As explained in the previous section, considering the analysis time, selecting 20-time steps to calculate the Sobol' indices were decided. After observing the temporal variation of the results for the velocity components of currents, a period between timesteps from 13-01-2005: 13:00 to 13-01-2005: 23:00 (t = 890 to t = 910) was selected for taking the average indices of the input factors for current velocities.

7.3.3. Sensitivity of Current velocity (x-component)

The variance decomposition for the current velocity in the x-direction concerning the selected input parameters is given in this section. The calculated indices for each input parameter are tabulated in Table 7.3.3 and plotted in Figure 7.3.3 for the location FINO3.

Table 7.3.3 Sensitivity indices for x-velocity to the input parameters using the Sobol' method at FINO 3

Parameter	S_i	S_{Ti}	$S_{Ti} - S_i$	Rank (based on S_i)	Rank (based on S_{Ti})
Dicoww	0.0011	0.0153	0.0142	4	4
Vicoww	0.0680	0.0962	0.0282	3	3
Smagorinsky	0.1160	0.1572	0.0411	2	2
Rhoair	0.7709	0.7790	0.0081	1	1

According to the results of the variance-based analysis on x-velocity, it is observable that the most significant parameter for x-velocity calculation out of the selected four parameters is air density (Rhoair) which contributes to 77% of the total variability of the output x-velocity. Smagorinsky factor accounts for 11.6%, and uniform vertical eddy viscosity contributes to 6.8% of the total variance of the output. However, the parameter Rhoair has a smaller value for the difference between the total-order and first-order index ($S_{Ti} - S_i$). This little value indicates that the air density does not have considerable interaction effects on the output x-velocity. Despite that, the other three factors, Smagorinsky and Vicoww, have considerable interaction effects (Smagorinsky factor contributes to 4.1% , Vicoww to 2.8% , and Dicoww to 1.4% of output variance) that create the output variabilities. Thus, we can assume that the three factors, Smagorinsky, Dicoww, and Vicoww interact with each other and contribute to the output variability.

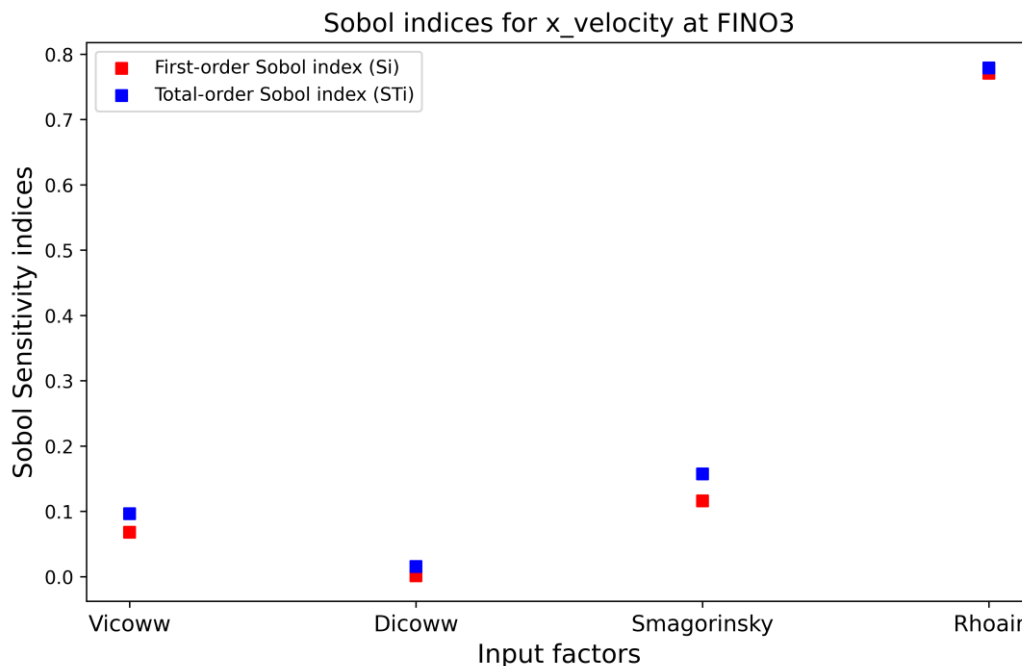


Figure 7.3.2 First-order and total-order Sobol' indices for x-velocity for location FINO3

The calculated values of Sobol' indices for the other five locations are available in Annex III of this report. Figure 7.3.5 represents the variation of the first-order and total-order Sobol' indices for the sensitivity of x-velocity depending on the analysis location.

Sobol indices for sensitivity of x_velocity

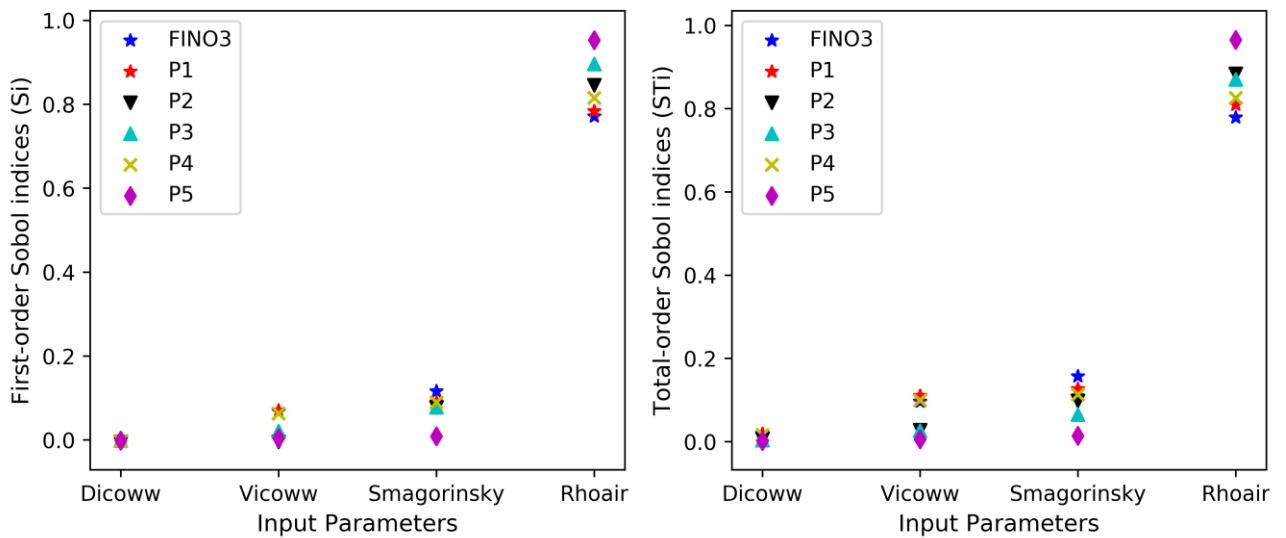


Figure 7.3.5 First-order and total-order Sobol’ indices for x-velocity at the selected six locations

According to the results shown in Figure 7.3.5, it is apparent that there is no significant difference in the importance of input parameters depending on the spatial location. However, at location P5, both the first order and total-order index have values more than 0.95, indicating that the x-velocity depends mainly on air density (Rhoair) and the less affected by the other four parameters.

7.3.4. Sensitivity of Current velocity (y-velocity)

The variance decomposition for the current velocity in the y-direction with respect to the selected input parameters is given in this section.

Table 7.3.4 Sensitivity indices for y-velocity to the input parameters calculated using the Sobol’ method at FINO 3

Parameter	S_i	S_{Ti}	$S_{Ti} - S_i$	Rank (based on S_i)	Rank (based on S_{Ti})
Dicoww	0.0014	0.0056	0.0042	4	4
Vicoww	0.0029	0.0149	0.0120	3	3
Smagorinsky	0.1793	0.1434	-0.0360	2	2
Rhoair	0.8472	0.7939	-0.0533	1	1

Like the x-velocity, the most significant parameter for the y-velocity component was also identified as the air density (Rhoair). The Smagorinsky factor stands as the second most important input parameter. The contributions from uniform vertical eddy viscosity and eddy diffusivity to the variability of y-velocity are insignificant according to the results given by the above results.

In contrast to the results of the x-velocity of currents, here, the interaction effects can be observed for the input parameter Rhoair. For the simulated y-velocity, the interaction effects are mainly observed from Rhoair, Smagorinsky, and Vicoww.

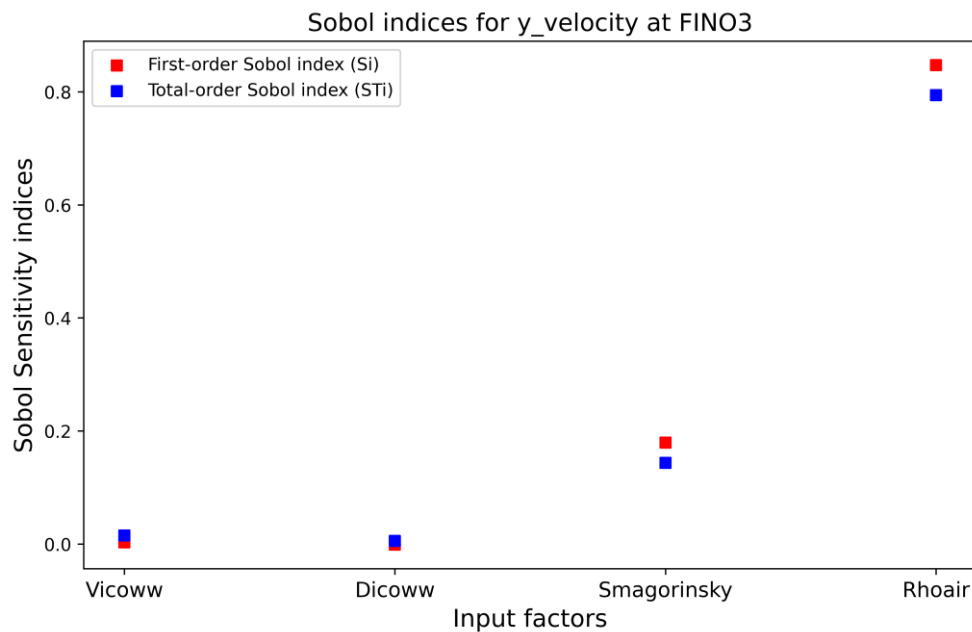


Figure 7.3.6 First-order and total-order Sobol' indices for y-velocity for location FINO3

The first order and total order Sobol' indices calculated for the sensitivity of y-velocity for the selected six locations are presented in Figure 7.3.7. According to the two plots, it is visible that there is no significant difference in the importance of input parameters depending on the spatial location. However, at P1 and P4, the y-velocity depends mainly on the parameter, Rhoair, and the less affected by the other three parameters.

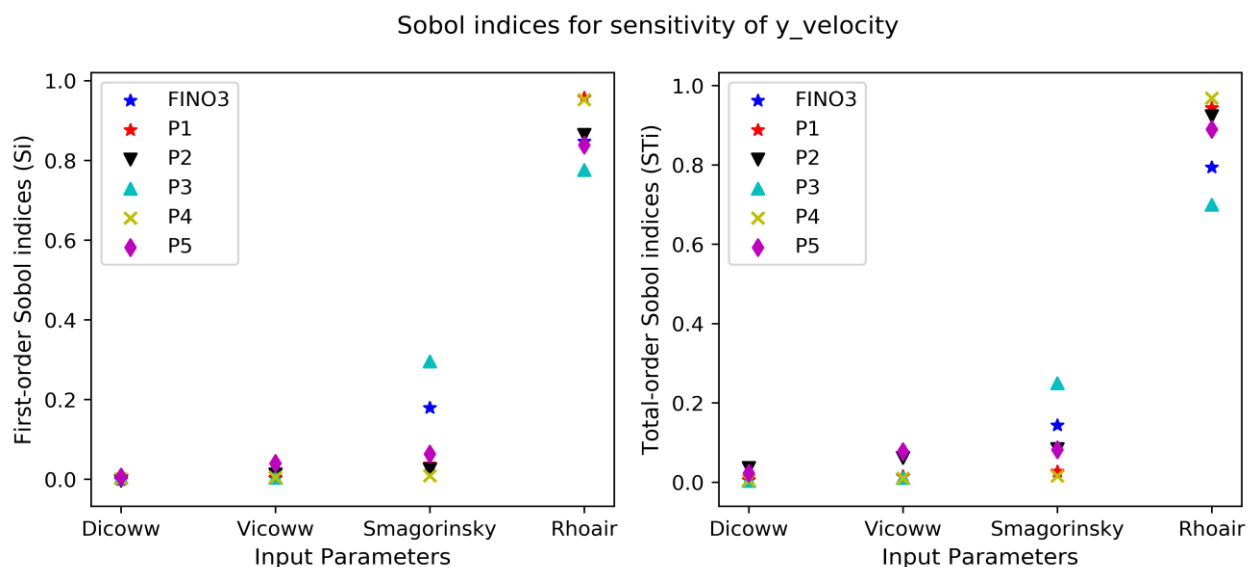


Figure 7.3.7 First-order and total-order Sobol' indices for y-velocity at the selected six locations

7.3.5. Sensitivity of Current velocity (z-velocity)

The variance decomposition for the current velocity in the z-direction for the selected input parameters is shown below.

Table 7.3.5 Sensitivity indices for z-velocity to the input parameters calculated using the Sobol' method at FINO 3

Parameter	S_i	S_{Ti}	$S_{Ti} - S_i$	Rank (based on S_i)	Rank (based on S_{Ti})
Dicoww	0.0040	0.1238	0.1199	4	4
Smagorinsky	0.0376	0.2729	0.2353	3	3
Vicoww	0.1463	0.3751	0.2288	2	2
Rhoair	0.5795	0.8155	0.2360	1	1

The results obtained for the z-velocity of currents shows a different pattern of sensitivity than the other two velocity components. Although the most significant factor was still identified to be the Rhoair, the 2nd most important factor was uniform viscosity in vertical direction (Vicoww). According to the above results, the Smagorinsky factor is less significant in modeling the vertical velocity. As described in section 5.2, Smagorinsky factor is used for calculating the horizontal turbulence of the model. Therefore we can assume that the vertical velocity is not much affected by the model's horizontal turbulence.

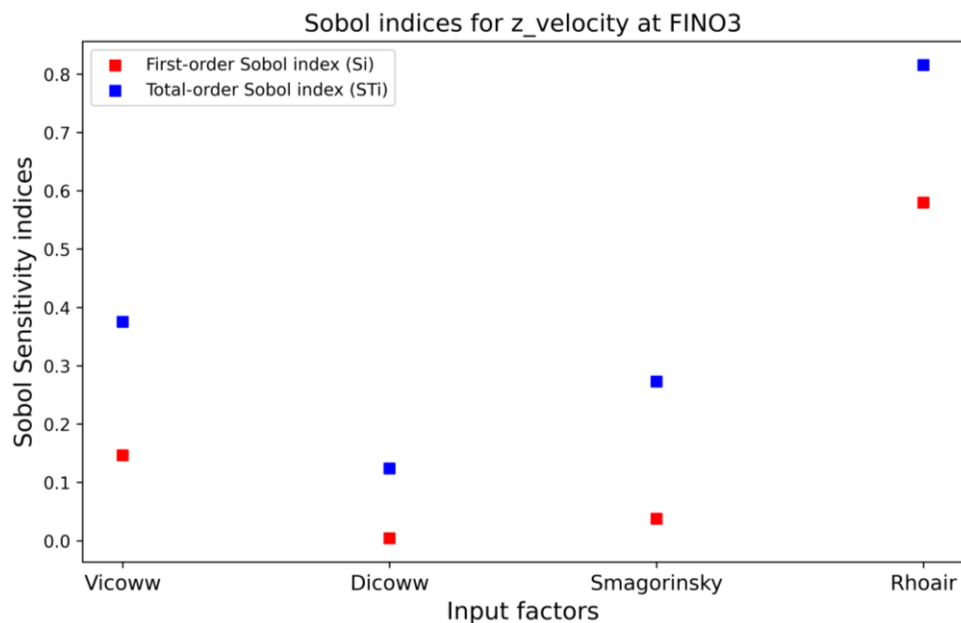


Figure 7.3.8 First-order and total-order Sobol' indices for z-velocity for location FINO3

The first order and total order Sobol' indices calculated for the sensitivity of the z-velocity component for the selected six locations are presented in Figure 7.3.9. According to the two plots, it is visible that there is no significant difference in the importance of input parameters depending on the spatial location. However, the results obtained here for the location P4 are in contrast to the ranking given by the Morris method.

Sobol indices for sensitivity of z_velocity

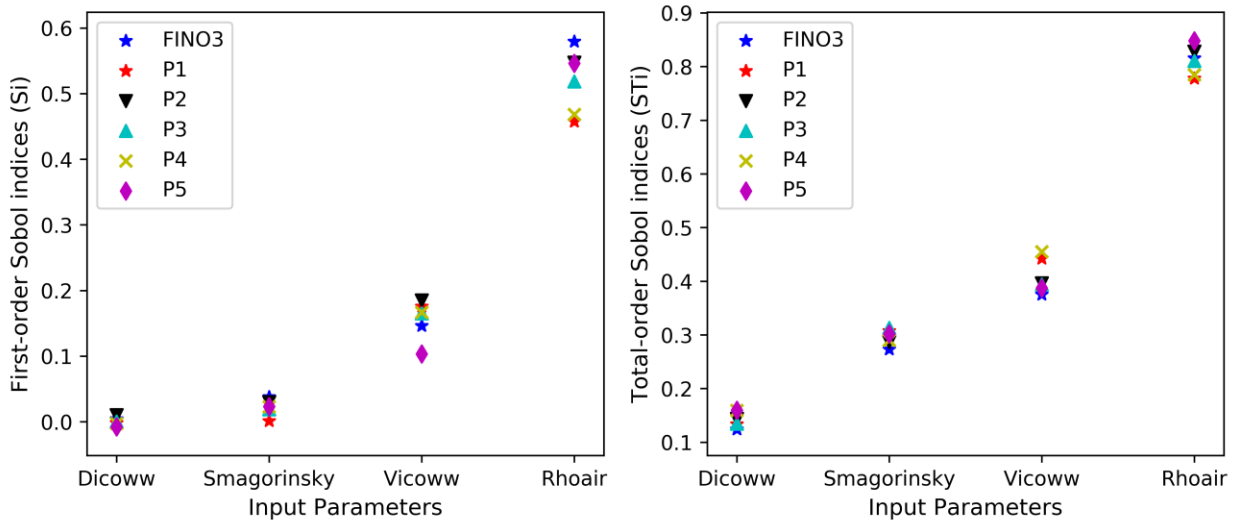


Figure 7.3.9 First-order and total-order Sobol' indices for z-velocity at the selected six locations

7.4. Comparison of the results of Morris and Sobol' methods

In this section, the sensitivity results obtained through the two methods are compared based on the values and definitions of each sensitivity indices. This comparison given here was made for the results of the analysis done at the FINO3 location.

7.4.1. Temperature

Table 7.4.1 shows the results obtained from the two methods for temperature sensitivity to the input factors at the location of FINO3. The correlation between sensitivity measures was estimated by calculating correlation coefficients for indices of the two methods.

Table 7.4.1 Comparison of sensitivity indices for the temperature to the input parameters calculated using the Morris and Sobol' methods at FINO3

Parameter	Morris method results ($r=12$)		Sobol' method results ($N=100$)			Rank (based on Morris method)	Rank (based on Sobol' method)
	μ^*	σ	S_i	S_{Ti}	$S_{Ti} - S_i$		
Smagorinsky	0.0560	0.0433	0.1511	0.1639	0.0128	2	2
Dalton	0.2039	0.2003	0.8338	0.8469	0.0132	1	1
Stanton	0.0271	0.0288	0.0040	0.0048	0.0007	3	3
Vicouv	0.0000	0.0000	-	-	-	7	-
Vicoww	0.0016	0.0021	-	-	-	4	-
Dicouv	0.0000	0.0000	-	-	-	6	-
Dicoww	0.0006	0.0008	-	-	-	5	-

As discussed in Chapter 2, (Campolongo & Saltelli, 1997) have compared the correlation of the sensitivity indices of Morris and Sobol' methods in a study carried out for analyzing the sensitivities of an environmental model. The above research suggested that the Morris absolute mean (μ^*) is correlated with the total order index (S_{Ti}) calculated by the Sobol' method, and the Morris standard deviation (σ) is correlated with the measure ($S_{Ti} - S_i$). However, according to the definitions of these sensitivity measures, it is apparent that the absolute mean of EE can be used as an estimate of how a single input affects the output. The standard deviation of EE catches interactions as well as the non-linear and additive effects. Therefore, a perfect correlation cannot be expected between σ and $S_{Ti} - S_i$. This is evident from the values obtained through our results for σ and ($S_{Ti} - S_i$) for the three parameters shown in Figure 7.4.1, where the parameters with larger μ^* values have higher S_{Ti} , and higher values for ($S_{Ti} - S_i$) have comparatively higher σ values. Nevertheless, in the 2nd case, correlation is less between standard deviation σ and ($S_{Ti} - S_i$) for three input factors.

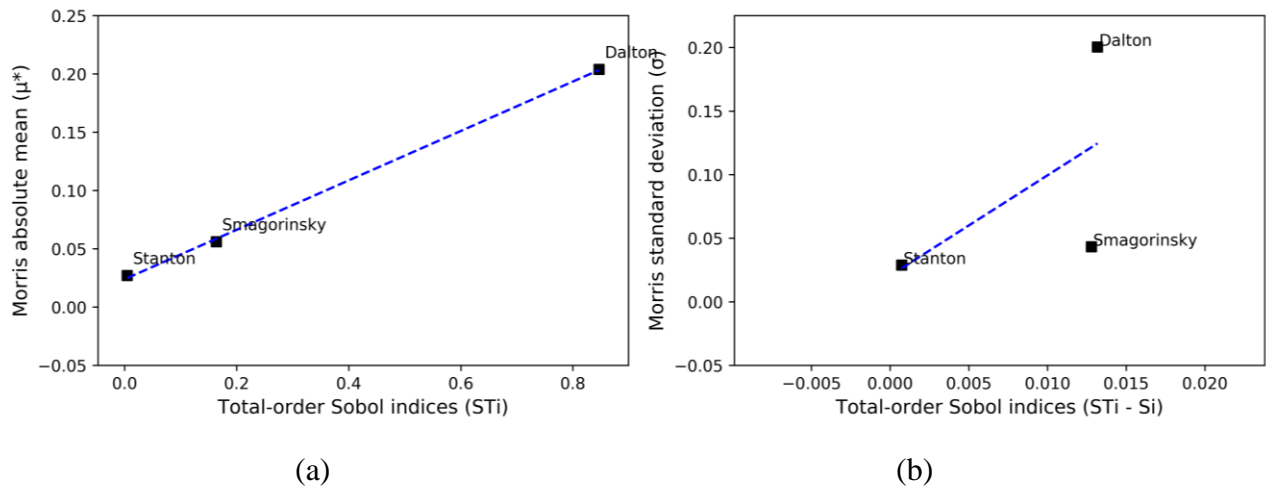


Figure 7.4.1 Correlation of sensitivity measures of Morris method and Sobol' indices (a) Variation of Morris mean with Sobol' S_{Ti} (b) Variation of Morris standard deviation with ($S_{Ti} - S_i$)

The correlation coefficients for the two measures are shown in Table 7.4.3.

Table 7.4.2 Correlation between the sensitivity measures calculated by Morris and Sobol' methods

Sensitivity measures	Correlation coefficient
μ^* and S_{Ti}	0.9997
σ and ($S_{Ti} - S_i$)	0.5866

7.4.2. Current velocity (x-velocity component)

The following table includes the results obtained from the two methods for the sensitivity of x-velocity of currents to the input factors.

Table 7.4.3 Comparison of sensitivity indices for the current velocity (x-velocity component) to the input parameters calculated using the Morris and Sobol' methods at FINO 3

Parameter	Morris method results ($r=12$)		Sobol' method results ($N=100$)			Rank (based on Morris method)	Rank (based on Sobol' method)
	μ^*	σ	S_i	S_{Ti}	$S_{Ti} - S_i$		
Vicouv	0.00	0.00	-	-	-	6	-
Vicoww	8.81E-04	1.12E-03	0.0680	0.0962	0.0282	3	3
Dicouv	0.00	0.00	-	-	-	5	-
Dicoww	3.31E-04	4.16E-04	0.0011	0.0153	0.0142	4	4
Rhoair	1.12E-02	9.53E-03	0.7709	0.7790	0.0081	1	1
Smagorinsky	3.65E-03	3.78E-03	0.1160	0.1572	0.0411	2	2

The input parameter rankings calculated by the two methods were similar for the x-velocity component of currents. Correlation coefficients were calculated between the above sensitivity measures to check the correlation between the sensitivity measures of the two methods. These values of correlation coefficients are given in Table 7.4.3.

Table 7.4.4 Correlation between the sensitivity measures calculated by Morris and Sobol' methods

Sensitivity measures	Correlation coefficient
μ^* and S_{Ti}	0.9871
σ and $(S_{Ti} - S_i)$	-0.3813

Like in the temperature analysis, the μ^* shows a strong positive correlation with S_{Ti} . However, the σ and the difference between two Sobol' indices ($S_{Ti} - S_i$) do not show a good correlation, as observed in the temperature analysis. The reason might be the differences of the two sensitivity measures ($(S_{Ti} - S_i)$ and σ) in capturing the non-linear effects and the interactions. For instance, in Figure 7.4.2. (b), the input factor Rhoair has a higher σ value and comparatively lower value for $(S_{Ti} - S_i)$. Therefore, the factor can have fewer interaction effects while having more non-linear and additive effects, which results in a more significant standard deviation of EE and a small $(S_{Ti} - S_i)$.

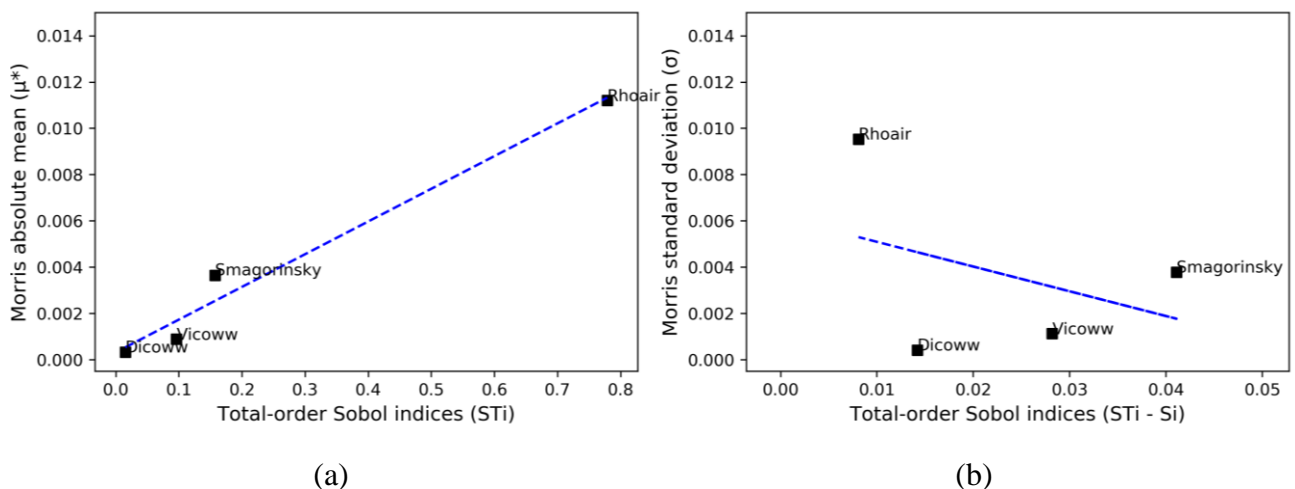


Figure 7.4.2 Correlation of sensitivity measures of Morris method and Sobol' indices (a) Variation of Morris mean (μ^*) with Sobol' S_{Ti} (b) Variation of Morris standard deviation(σ) with $(S_{Ti} - S_i)$

7.4.3. Current velocity (y-velocity component)

The table below summarizes the sensitivity measures calculated for output currents in the y-direction by Morris and Sobol' analysis methods for each input parameters considered in the analysis. Correlation coefficients between measures were calculated to assess the relationship between the sensitivity measures given by two analysis techniques.

Table 7.4.5 Comparison of sensitivity indices for the current velocity (y-velocity component) to the input parameters calculated using the Morris and Sobol' methods at FINO3

Parameter	Morris method results ($r=12$)		Sobol' method results ($N=100$)			Rank (based on Morris method)	Rank (based on Sobol' method)
	μ^*	σ	S_i	S_{Ti}	$S_{Ti} - S_i$		
Vicouv	0.00E+0 0	0.00E+0 0	-	-	-	6	-
Vicoww	6.28E-04	7.67E-04	0.0680	0.0962	0.0282	3	3
Dicouv	0.00E+0 0	0.00E+0 0	-	-	-	5	-
Dicoww	2.82E-04	3.68E-04	0.0011	0.0153	0.0142	4	4
Rhoair	1.15E-02	1.20E-02	0.7709	0.7790	0.0081	1	1
Smagorinsky	3.31E-03	2.75E-03	0.1160	0.1572	0.0411	2	2

The correlation coefficients calculated for the four measures from two methods are shown in Table 7.4.3.

Table 7.4.6 Correlation between the sensitivity measures calculated by Morris and Sobol' methods

Sensitivity measures	Correlation coefficient
μ^* and S_{Ti}	0.9902
σ and $(S_{Ti} - S_i)$	-0.5245

Same as the relationship observed in the results for x-velocity, a clear positive correlation was observed between the absolute mean (μ^*) of EE and the total-order Sobol' index (S_{Ti}). The standard deviation (σ) of EE and the ($S_{Ti} - S_i$) do not clearly correlate. The input factor air density (Rhoair) is highly significant on the y-velocity and comparatively less interaction with the other three input parameters. Smagorinsky factor shows a higher level of interactions that cause the variability of output y-velocity of currents.

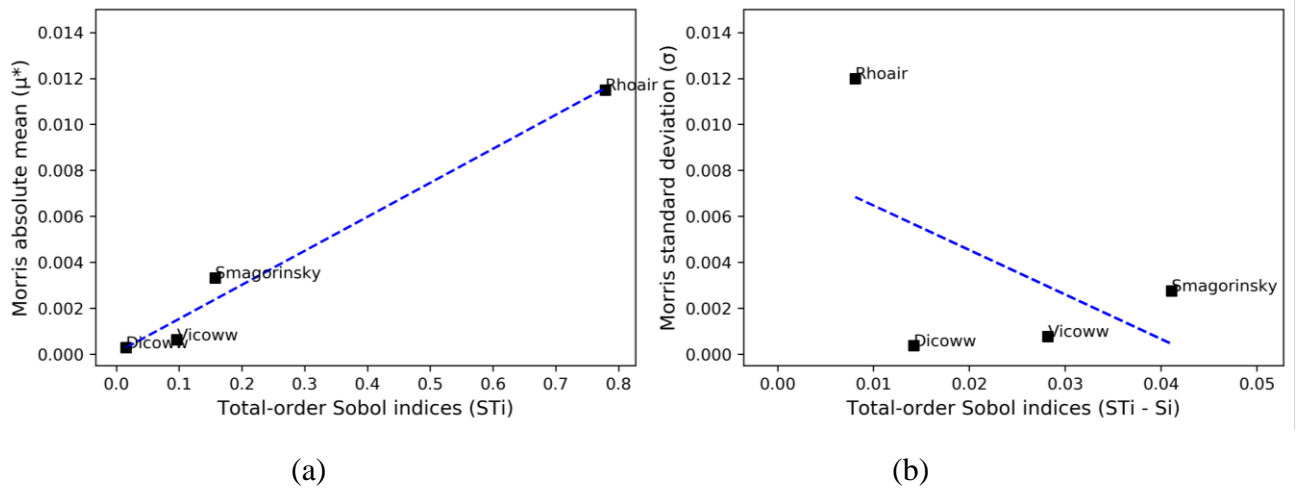


Figure 7.4.3 Correlation of sensitivity measures of Morris method and Sobol' indices (a) Variation of Morris mean with Sobol' S_{Ti} (b) Variation of Morris standard deviation with ($S_{Ti} - S_i$)

7.4.4. Current velocity (Z-velocity component)

This section compares sensitivity measures calculated using the two analysis techniques for output current velocity in the z-direction. Correlation between sensitivity measures has been calculated to estimate the relation between the measures from two methods.

Table 7.4.7 Comparison of sensitivity indices for the current velocity (z-velocity component) to the input parameters calculated using the Morris and Sobol' methods at FINO 3

Parameter	Morris method results ($r=12$)		Sobol' method results ($N=100$)			Rank (based on Morris method)	Rank (based on Sobol' method)
	μ^*	σ	S_i	S_{Ti}	$S_{Ti} - S_i$		
Vicouv	0.00E+0 0	0.00E+0 0	-	-	-	6	-
Vicoww	1.33E-06	1.68E-06	0.1463	0.3751	0.2288	2	2
Dicouv	0.00E+0 0	0.00E+0 0	-	-	-	5	-
Dicoww	3.88E-07	5.74E-07	0.0040	0.1238	0.1199	4	4
Rhoair	4.04E-06	4.41E-06	0.5795	0.8155	0.2360	1	1
Smagorinsky	1.17E-06	1.28E-06	0.0376	0.2729	0.2353	3	3

The correlation coefficients calculated for the two measures are shown in Table 7.4.3.

Table 7.4.8 Correlation between the sensitivity measures calculated by Morris and Sobol' methods

Sensitivity measures	Correlation coefficient
μ^* and S_{Ti}	0.9928
σ and $(S_{Ti} - S_i)$	0.5820

Similar to the relationships observed in x-velocity and y-velocity, the sensitivity measures the absolute mean (μ^*) of EE and the total-order Sobol' index (S_{Ti}) are positively correlated. In contrast to the x and y velocity components, the standard deviation (σ) of EE and the $(S_{Ti} - S_i)$ depict a positive correlation with each other. The input factor air density (Rhoair) is highly significant on the y-velocity and comparatively more minor interaction with the other three input parameters.

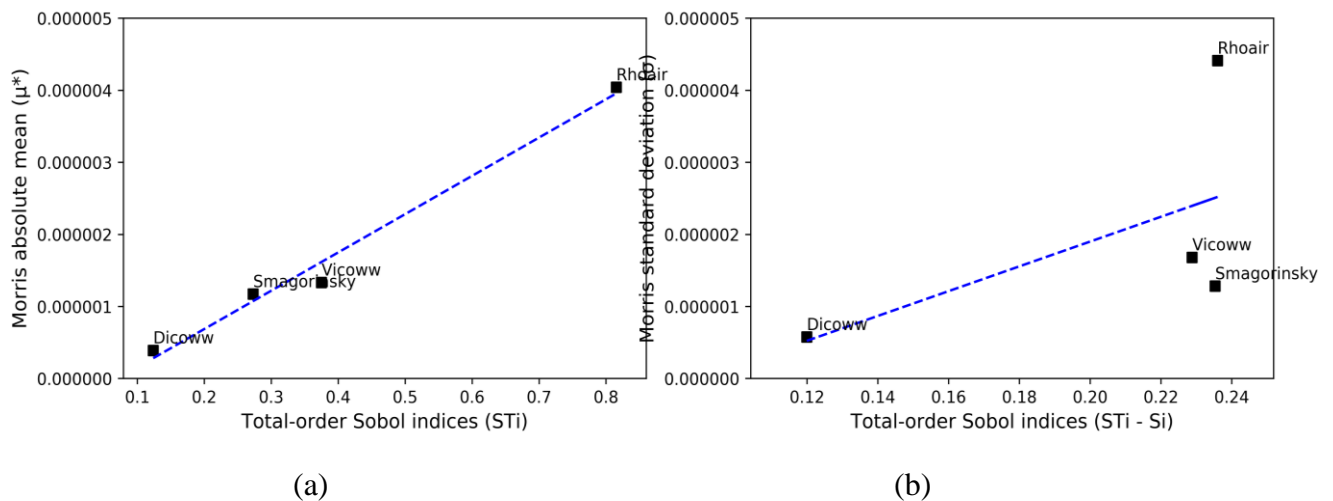


Figure 7.4.4 Correlation of Morris method and Sobol' indices (a) Variation of Morris mean with Sobol' S_{Ti} (b) Variation of Morris standard deviation with $(S_{Ti} - S_i)$

Chapter 8: Summary, Conclusions and Recommendations

8.1. Summary and Conclusions

The main goal of this research was to apply different sensitivity analysis techniques for a hydrodynamic model to determine the most influential parameters and their significance for two selected output variables of the model, which were temperature and current velocity. After considering the model characteristics, complexity, and computational cost, the selection of analysis techniques for achieving this objective was carried out. Morris method, a frequently used local sensitivity analysis technique, was adopted first to screen the input parameters before applying the global sensitivity analysis technique, the variance-based Sobol' method. The Dutch Continental Shelf Model (DCSM) is a hydrodynamic model developed using the D-Flow-FM model suite of the Delft 3D software. The DCSM was used for testing the sensitivities of the above two variables to a selected set of input parameters. In the Morris method, the selected inputs were sampled using the One-At-a-Time sampling, where the samples are generated by changing one parameter at a time for each consecutive sample. In the variance-based method, the quasi-Monte Carlo sampling scheme, defined in section 2.2, was used to generate the input samples for the model.

- Based on the observations, the simulated temperature was most sensitive to the Dalton coefficient for evaporative heat flux from the selected set of the input parameters. The second and third most influential input factors were the Smagorinsky coefficient and the Stanton coefficient for convective heat flux. The results agree with the previous studies ((Twigt, 2006) ; (Baracchini et al., 2020)) on the temperature sensitivity of the 2D and 3D hydrodynamic models. (Twigt, 2006) developed a 3D hydrodynamic model for the South China Sea using the Delft-3D Flow model suite. The above study results demonstrated that these two coefficients (Dalton and Stanton number) significantly affect temperature modeling in the heat flux model. Further, the results obtained in our analysis correspond with the sensitivity results obtained by Baracchini et al. (2020) to apply an automated calibration to a 3D lake hydrodynamic model. The authors have estimated that the Dalton number is more sensitive to the temperature calibration in the model where the Stanton number does not have the same impact as the Dalton coefficient on modeled temperature.
- According to the Morris sensitivity analysis results on current velocities, the most significant factors were the air density (ρ_{air}), the Smagorinsky factor in horizontal turbulence, and the uniform vertical eddy diffusivity and uniform vertical eddy viscosity coefficients. The two factors, uniform horizontal eddy viscosity (ν_{icouv}) and uniform horizontal eddy diffusivity (D_{icouv}) were identified as less influential to the modeled current velocities. However, this contrasts with the previous findings of the sensitivity of currents to uniform background horizontal eddy viscosity ($\nu_{h, back}$) (Deltares, 2009). In a study done based on Delft3D hydrodynamic model validation for a nearshore zone, it has been found that the longshore currents are strongly affected by the uniform background eddy viscosity parameter.

- The global sensitivity analysis gives more comprehensive details on the sensitivities of model outputs. It provides a quantitative measure of sensitivities to determine the significance of the selected input parameters on the output calculations in the hydrodynamic model. The variance-based method is a global SA technique that can be applied to any model irrespective of the model complexity. The results of the variance-based Sobol' method highlights that the variability of the Dalton coefficient contributes to nearly 84% of the simulated temperature variance out of these three most significant input parameters used in this study. The variance of the Smagorinsky factor accounts for around 16% of the output temperature variance, and the Stanton coefficient does not impact much on the temperature compared to the other two factors. The input Rhoair contributes to 78% of the variance of output current velocity in x-direction, while the Smagorinsky factor affects 16%, and Vicoww contributes 9.6%. The sensitivity of y-velocity also shows a similar pattern, where the Rhoair parameter causes 79% of the variability and Smagorinsky causes 14%, while Vicoww contributes 1.5%. When considered the variance of z-velocity, Rhoair has a contribution of 81%, Smagorinsky factor has 37%, and Vicoww has 27%. The interaction effects on outputs were also identified using the Sobol' indices. The rankings obtained for both temperature and currents velocities from the two methods are comparable, where the order of ranking is similar in both methods.
- When comparing the sensitivity measures obtained from the two methods, it was observed that there is a strong correlation between the sensitivity measure, the absolute mean of the EE (μ^*) calculated in the Morris method, and the total-order index (S_{Ti}) calculated in the Sobol' method. The above relationships confirm the results obtained by the previous studies (Campolongo & Saltelli, 1997) on the correlations between the sensitivity measures of these two methods. However, the correlation between the other two indices, (the standard deviation (σ) of the EE and difference of total order and first-order Sobol' indices ($S_{Ti} - S_i$)) does not conform with the experimental results of (Campolongo & Saltelli, 1997), where a perfect correlation could not be observed between the two measures (σ) and ($S_{Ti} - S_i$). However, this can be due to the differences of the two indices in their abilities to capture the effects due to interactions, non-linearities, and additive effects.
- As mentioned in Chapter 1, these sensitivity analysis results will be used to calibrate the Dutch Continental Shelf Model (DCSM) to the project area. Moreover, these model results will be coupled to a water quality model to identify the suitable areas for Blue mussel and Seaweed cultivation in the FINO3 and identify the new sites with favorable conditions for the above aquaculture activities.
- The Python scripts developed for this analysis have the flexibility to use in sensitivity analyses of any other output parameters of the DCSM model and also for any D-Flow FM model. This has to be done by correctly assigning the output variable name and the selected input parameters that are going to be analyzed. Further, these analysis scripts are written in a generic form and can be adjusted easily to be used in the sensitivity analyses for the other numerical models developed using Delft3D, such as water quality models (D-WAQ). Therefore, these Python scripts can be used in the SA of water quality models, which will

be coupled to the existing hydrodynamic model of the North Sea (DCSM) as the next step of the project.

An overview of the results obtained for sensitivity measures at FINO3 location using the Morris method [left] and Sobol' methods [right] are given below. The x-axis of plots created for the Morris method changes the scale as the measures depend on the resulting temperature and current velocity values.

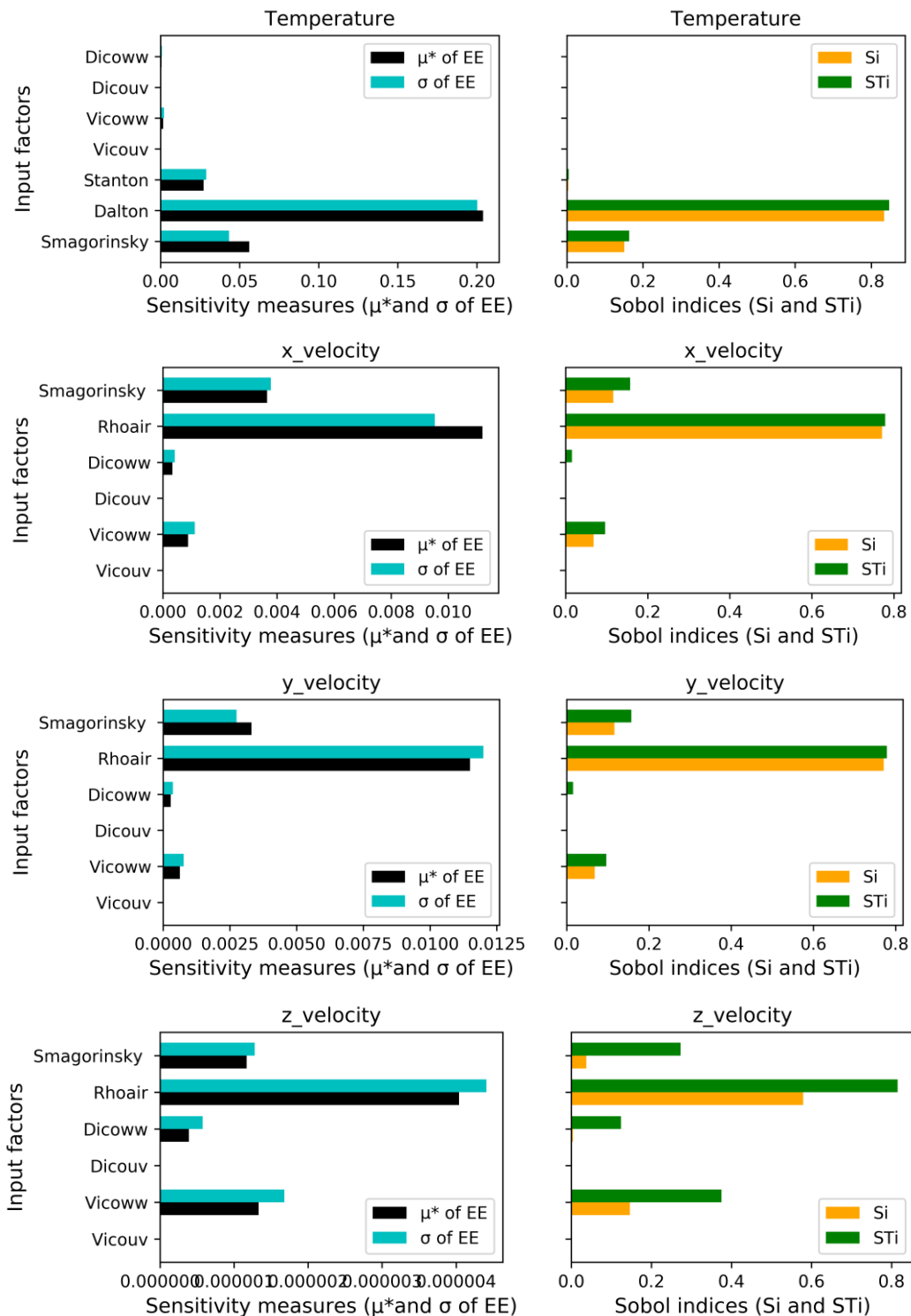


Figure 8.1.1 Overview of results for the sensitivity analysis of Temperature and current velocity

8.2. Limitations and Assumptions of the study

- The high computational demand of the North Sea hydrodynamic model used in this research is one major hindrance to test for a significant number of input parameters. This limitation was addressed by a preliminary screening process based on the literature and expert judgment, assuming the other parameters do not significantly impact the output variables.
- Because of the above limitation of computation demand and the complexity of generating spatially varying inputs using Morris and Sobol' methods, it was decided to focus only on spatially uniform input factors. Selecting only the spatially uniform input parameters is another major limitation of this study. This assumption can result in omitting some of the input parameters that are sensitive to the two outputs.
- The DCSM model is developed with two different grid resolutions (4nm and 0.5nm). The coarse grid is a uniform grid with 4nm, and the 0.5nm grid is a more refined grid where the grid cell size varies based on the distance to the coast. In the 0.5nm grid, coarser cell size is used in open boundaries and deep water, where the resolution is increased up to 0.5nm in shallow waters in nearshore areas. The DCSM is computationally expensive (18 hours of runtime for simulating one year with 4nm grid resolution and 3.5 days for a one-year simulation with 0.5nm resolution). If the 0.5nm grid had been used, the model would have taken an even higher computation time. Therefore, it was decided to use the coarser grid resolution (4nm uniform grid) in this research, assuming the sensitivity results would not change in the model with the finer grid.
- The sensitivity tests were carried out based on results of the hydrodynamic model simulated for one month, which can affect the ability of these results to predict the effect of seasonal variations on the sensitivity of output parameters.
- At the sampling stage, we initially assume possible ranges of parameters. These ranges can affect the sensitivity analysis results. Therefore, these results obtained in this study from Morris and Sobol' methods may change when tested for a different parameter range.

8.3. Recommendation for Future work

- This study on sensitivity analyses for the temperature and current velocities reduces the need to explore parameter space for future calibration and modeling work. As discovered by the results of the two methods, the Dalton coefficient, Smagorinsky factor, and the Stanton coefficient will be significant in simulating the temperature. However, these results are specific to a location and a specific period of the year. Therefore, subsequent work can investigate the spatial and temporal variations of sensitivity of temperature.
- The spatial variation of the two output sensitivities was analyzed only for few selected locations inside and surrounding the FINO3 research platform. However, it is suggested to

analyze the sensitivities to a broader area of the North Sea by selecting different locations covering the whole domain of the grid.

- Our study considers the sensitivity of physical parameters to the simulated temperature and currents. However, the numerical parameters (computation grid size, computation time step, maximum Courant number, smallest allowed timestep, and the other numerical parameters assigned to the model) could also be essential input factors in modeling the outputs in the D-Flow FM model. Therefore, it is recommended to study the sensitivities of these numerical input factors as well.
- On account of the high computation demand, the analysis was carried out only for one month of the year. Thus, it is recommended to analyze the sensitivities of temperature and current velocities for different periods of the year to capture the seasonality of the sensitivity measures.
 - The temperature's highest variability of the measured data is observed in the summer months (June, July, and August). Therefore, the sensitivity of temperature needs to be studied for these periods.

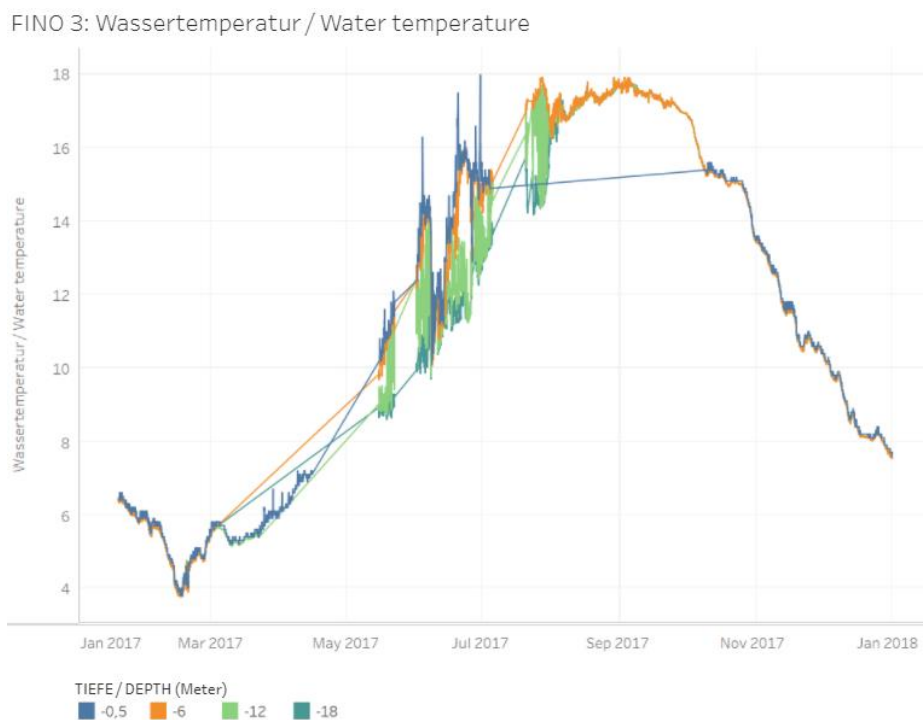


Figure 8.3.1 Measured data for the temperature at FINO3 for the year 2017 (Data source: (BSH, 2021))

- The study uses only two analysis methods, the Elementary Effect method (Morris method) and the Variance-based Sobol' method, because of the high computation demand for the D-Flow FM model for the North Sea. However, in the Variance-based Sobol' analysis, the sample size was selected as 100, which is the minimum recommended sample size mentioned in the literature. Therefore, the method can be used for increased sample sizes in future work to verify the results obtained in this research.

- According to the Sobol' method results, there are differences in the degree of contribution of input parameter variances to the output variance based on the location. Therefore, studying these spatial variations of global sensitivity should be another important aspect for future research on sensitivity analysis.
- Even though the global sensitivity analysis techniques provide extensive details of the sensitivity of input parameters to a specific output, these methods demand a substantial computational cost in terms of the number of model runs. Therefore, research on extensions to the local methods or search for new techniques with lower computation demand is a critical aspect of sensitivity analysis.

References

- Andres, T. H. (1997). Sampling methods and sensitivity analysis for large parameter sets. *Journal of Statistical Computation and Simulation*, 57(1–4), 77–110. <https://doi.org/10.1080/00949659708811804>
- Archer, G. E. B., Saltelli, A., & Sobol', I. M. (1997). Sensitivity measures, anova-like techniques and the use of bootstrap. *Journal of Statistical Computation and Simulation*, 58(2), 99–120. <https://doi.org/10.1080/00949659708811825>
- Baracchini, T., Hummel, S., Verlaan, M., Cimatoribus, A., Wüest, A., & Bouffard, D. (2020). An automated calibration framework and open source tools for 3D lake hydrodynamic models. *Environmental Modelling and Software*, 134. <https://doi.org/10.1016/j.envsoft.2020.104787>
- Bellos, V., Papageorgaki, I., Kourtis, I., Vangelis, H., Kalogiros, I., & Tsakiris, G. (2020). Reconstruction of a flash flood event using a 2D hydrodynamic model under spatial and temporal variability of storm. *Natural Hazards*, 101(3), 711–726. <https://doi.org/10.1007/s11069-020-03891-3>
- Bikker, P., Blaauw, R., Brandenburg, W., van den Burg, S., Dijkstra, J. W., van Duren, L., van Hal, J., Harmsen, P., Huijgen, W., Jak, R., Kamermans, P., van Leeuwen, J., van Krimpen, M., Lindeboom, R., Prins, H., van der Putten, S., Schouten, J.-J., Stuiver, M., van der Werf, A., ... Wald, J. (2016). *North-Sea-Weed-Chain Sustainable seaweed from the North Sea; an exploration of the value chain* Editor: Floris Groenendijk.
- BSH - In the service of maritime navigation and the seas. (2021). Retrieved June 27, 2021, from https://www.bsh.de/EN/Home/home_node.html;jsessionid=E54A1B70BAA7AF785BD76ED2976816D3.live11314
- Caflisch, R. E. (1998). *Monte Carlo and quasi-Monte Carlo methods*.
- Campolongo, F., Cariboni, J., & Saltelli, A. (2007). An effective screening design for sensitivity analysis of large models. *Environmental Modelling and Software*, 22(10), 1509–1518. <https://doi.org/10.1016/j.envsoft.2006.10.004>
- Campolongo, F., & Saltelli, A. (1997). Sensitivity analysis of an environmental model: an application of different analysis methods. In *Reliability Engineering and System Safety* (Vol. 57).
- Chen, S., Garambois, P. A., Finaud-Guyot, P., Dellinger, G., Mosé, R., Terfous, A., & Ghenaim, A. (2018). Variance based sensitivity analysis of 1D and 2D hydraulic models: An experimental urban flood case. *Environmental Modelling and Software*, 109, 167–181. <https://doi.org/10.1016/j.envsoft.2018.08.008>
- Cosenza, A., Mannina, G., Vanrolleghem, P. A., & Neumann, M. B. (2013). Global sensitivity analysis in wastewater applications: A comprehensive comparison of different methods. *Environmental Modelling and Software*, 49, 40–52. <https://doi.org/10.1016/j.envsoft.2013.07.009>

- da Veiga, S. (2015). Global sensitivity analysis with dependence measures. *Journal of Statistical Computation and Simulation*, 85(7), 1283–1305. <https://doi.org/10.1080/00949655.2014.945932>
- Deltares. (2009). *Hydrodynamic validation of Delft3D using data from the SandyDuck97 experiments*.
- Ducrottoy, J.-P., Elliottà, M., & de Jonge, V. N. (2000). *The North Sea. Engineers Edge*. (n.d.). Retrieved May 12, 2021, from <https://www.engineersedge.com/calculators/air-density.htm>
- Forschungs- und Entwicklungszentrum Kiel. (2021). *Blue mussels, seaweed and offshore wind energy in Germany*. Retrieved May 12, 2021, from <https://www.h2020united.eu/pilots/2-uncategorised/40-blue-mussels-seaweed-and-offshore-wind-energy-in-germany>
- Glen, G., & Isaacs, K. (2012). Estimating Sobol' sensitivity indices using correlations. *Environmental Modelling and Software*, 37, 157–166. <https://doi.org/10.1016/j.envsoft.2012.03.014>
- Herman, J., & Usher, W. (2017). *SALib: An open-source Python library for Sensitivity Analysis*. <https://doi.org/10.21105/joss.00097>
- Huang, Y. T., & Liu, L. (2008). A hybrid perturbation and Morris approach for identifying sensitive parameters in surface water quality models. *Journal of Environmental Informatics*, 12(2). <https://doi.org/10.3808/jei.200800133>
- Iooss, B., Saltelli, A., & Addr, A. /. (n.d.). *Title: Introduction: Sensitivity Analysis Name: Introduction: Sensitivity Analysis*.
- Kucherenko, S., Tarantola, S., & Annoni, P. (2012). Estimation of global sensitivity indices for models with dependent variables. *Computer Physics Communications*, 183(4), 937–946. <https://doi.org/10.1016/j.cpc.2011.12.020>
- Lachance-Bernard, M., Daigle, G., Himmelman, J. H., & Fréchette, M. (2010). Biomass-density relationships and self-thinning of blue mussels (*Mytilus* spp.) reared on self-regulated longlines. *Aquaculture*, 308(1–2), 34–43. <https://doi.org/10.1016/j.aquaculture.2010.07.038>
- Landmann, J., Ongsiek, T., Goseberg, N., Heasman, K., Buck, B. H., Paffenholz, J. A., & Hildebrandt, A. (2019). Physical modelling of blue mussel dropper lines for the development of surrogates and hydrodynamic coefficients. *Journal of Marine Science and Engineering*, 7(3). <https://doi.org/10.3390/jmse7030065>
- Legorburu, I., Johnson, K. R., & Kerr, S. A. (2018). Multi-use maritime platforms - North Sea oil and offshore wind: Opportunity and risk. *Ocean and Coastal Management*, 160, 75–85. <https://doi.org/10.1016/j.ocecoaman.2018.03.044>
- Li, G., Rabitz, H., Yelvington, P. E., Oluwole, O. O., Bacon, F., Kolb, C. E., & Schoendorf, J. (2010). Global sensitivity analysis for systems with independent and/or correlated inputs. *Journal of Physical Chemistry A*, 114(19), 6022–6032. <https://doi.org/10.1021/jp9096919>

- Li, Y., Tang, C., Zhu, J., Pan, B., Anim, D. O., Ji, Y., Yu, Z., & Acharya, K. (2015). Parametric uncertainty and sensitivity analysis of hydrodynamic processes for a large shallow freshwater lake. *SCIENCES JOURNAL*, 60(6), 1078–1095. <https://doi.org/10.1080/02626667.2014.948444?needAccess=true>
- Matsson, S., Christie, H., & Fieler, R. (2019). Variation in biomass and biofouling of kelp, *Saccharina latissima*, cultivated in the Arctic, Norway. *Aquaculture*, 506, 445–452. <https://doi.org/10.1016/j.aquaculture.2019.03.068>
- Maulik, R., & San, O. (2016). Dynamic modeling of the horizontal eddy viscosity coefficient for quasigeostrophic ocean circulation problems. *Journal of Ocean Engineering and Science*, 1(4), 300–324. <https://doi.org/10.1016/j.joes.2016.08.002>
- Mizuta, D. D., & Wikfors, G. H. (2019). Depth selection and in situ validation for offshore mussel aquaculture in Northeast United States federal waters. *Journal of Marine Science and Engineering*, 7(9). <https://doi.org/10.3390/jmse7090293>
- Morio, J. (2011). Global and local sensitivity analysis methods for a physical system. *European Journal of Physics*, 32(6), 1577–1583. <https://doi.org/10.1088/0143-0807/32/6/011>
- Morris, M. D. (1991). Factorial Sampling Plans for Preliminary Computational Experiments. In *TECHNOMETRICS* (Vol. 33, Issue 2).
- Nihoul, J. C. J., & Ronday, F. C. (1975). The influence of the “tidal stress” on the residual circulation. *Tellus*, 27(5), 484–490. <https://doi.org/10.3402/tellusa.v27i5.10174>
- Nursidi, Ali, S. A., Anshary, H., & Tahya, A. M. (2017). Environmental parameters and specific growth of *Kappaphycus alvarezii* in Saugi Island, South Sulawesi Province, Indonesia. *Aquaculture, Aquarium, Conservation & Legislation*, 10(4), 698–702. <https://search.proquest.com/scholarly-journals/environmental-parameters-specific-growth/docview/2056425963/se-2?accountid=41859>
- Otto, L. (1983). Currents and Water Balance in the North Sea. In W. Sündermann Jürgen and Lenz (Ed.), *North Sea Dynamics* (pp. 26–43). Springer Berlin Heidelberg.
- Pätsch, J., Burchard, H., Dieterich, C., Gräwe, U., Gröger, M., Mathis, M., Kapitza, H., Bersch, M., Moll, A., Pohlmann, T., Su, J., Ho-Hagemann, H. T. M., Schulz, A., Elizalde, A., & Eden, C. (2017). An evaluation of the North Sea circulation in global and regional models relevant for ecosystem simulations. *Ocean Modelling*, 116, 70–95. <https://doi.org/10.1016/j.ocemod.2017.06.005>
- Pianosi, F., Beven, K., Freer, J., Hall, J. W., Rougier, J., Stephenson, D. B., & Wagener, T. (2016). Sensitivity analysis of environmental models: A systematic review with practical workflow. In *Environmental Modelling and Software* (Vol. 79, pp. 214–232). Elsevier Ltd. <https://doi.org/10.1016/j.envsoft.2016.02.008>
- Ruano, V., Ribes, J., Ferrer, J., & Sin, G. (2011). Application of the Morris method for screening the influential parameters of fuzzy controllers applied to wastewater treatment plants. *Water Science and Technology: A Journal of the International Association on Water Pollution Research*, 63, 2199–2206. <https://doi.org/10.2166/wst.2011.442>
- Saltelli, Andrea, Aleksankina, K., Becker, W., Fennell, P., Ferretti, F., Holst, N., Li, S., & Wu, Q. (2019). Why so many published sensitivity analyses are false: A systematic review of

- sensitivity analysis practices. *Environmental Modelling and Software*, 114, 29–39. <https://doi.org/10.1016/j.envsoft.2019.01.012>
- Saltelli, Andrea, & Annoni, P. (2010). How to avoid a perfunctory sensitivity analysis. *Environmental Modelling and Software*, 25(12), 1508–1517. <https://doi.org/10.1016/j.envsoft.2010.04.012>
- Saltelli, Andrea, & Saisana, M. (2007). Settings and methods for global sensitivity analysis - a short guide. *PAMM*, 7(1), 2140013–2140014. <https://doi.org/10.1002/pamm.200700986>
- Saltelli, Andrea, & Tarantola, S. (2002). On the relative importance of input factors in mathematical models: Safety assessment for nuclear waste disposal. In *Journal of the American Statistical Association* (Vol. 97, Issue 459, pp. 702–709). <https://doi.org/10.1198/016214502388618447>
- Saltelli, A, Ratto, M., Andres, T., Campolongo, F., Cariboni, J., Gatelli, D., Saisana, M., & Tarantola, S. (2008). *Global Sensitivity Analysis. The Primer*. www.wiley.com
- Saltelli A, Ratto M, Andres T, Campolongo F, Cariboni J, Gatelli D, Salsana M, & Tarantola S. (2008). *Global Sensitivity Analysis. The Primer*.
- Saltelli, A, Tarantola, S., & Campolongo, F. (2000). Sensitivity Analysis as an Ingredient of Modeling. In *Statistical Science* (Vol. 15, Issue 4).
- Sarrazin, F., Pianosi, F., & Wagener, T. (2016). Global Sensitivity Analysis of environmental models: Convergence and validation. *Environmental Modelling and Software*, 79, 135–152. <https://doi.org/10.1016/j.envsoft.2016.02.005>
- Shin, M. J., Guillaume, J. H. A., Croke, B. F. W., & Jakeman, A. J. (2013). Addressing ten questions about conceptual rainfall-runoff models with global sensitivity analyses in R. *Journal of Hydrology*, 503, 135–152. <https://doi.org/10.1016/j.jhydrol.2013.08.047>
- Sündermann, J., & Pohlmann, T. (2011). A brief analysis of North Sea physics. In *Oceanologia* (Vol. 53, Issue 3, pp. 663–689). Polish Academy of Sciences. <https://doi.org/10.5697/oc.53-3.663>
- Tarantola, S., Gatelli, D., & Mara, T. A. (2006). Random balance designs for the estimation of first order global sensitivity indices. *Reliability Engineering and System Safety*, 91(6), 717–727. <https://doi.org/10.1016/j.ress.2005.06.003>
- Tarantola, Stefano, Becker, W., & Zeitz, D. (2012). A comparison of two sampling methods for global sensitivity analysis. *Computer Physics Communications*, 183(5), 1061–1072. <https://doi.org/10.1016/J.CPC.2011.12.015>
- Țene, M., Stuparu, D. E., Kurowicka, D., & el Serafy, G. Y. (2018). A copula-based sensitivity analysis method and its application to a North Sea sediment transport model. *Environmental Modelling and Software*, 104, 1–12. <https://doi.org/10.1016/j.envsoft.2018.03.002>
- Twigt, D. J. (2006). *3D temperature modeling for the South China Sea using remote sensing data*.

- Waldeck, P., & Larsson, K. (2013). Effects of winter water temperature on mass loss in Baltic blue mussels: Implications for foraging sea ducks. *Journal of Experimental Marine Biology and Ecology*, *444*, 24–30. <https://doi.org/10.1016/j.jembe.2013.03.007>
- Westerbom, M., Kilpi, M., & Mustonen, O. (2002). Blue mussels, *Mytilus edulis*, at the edge of the range: Population structure, growth and biomass along a salinity gradient in the north-eastern Baltic Sea. *Marine Biology*, *140*(5), 991–999. <https://doi.org/10.1007/s00227-001-0765-6>
- Zijl, F., Laan, S., & Groenenboom, J. (2021). *Development of a 3D model for the NW European Shelf (3D DCSM-FM)*.

Annex I, Annex II

Refer to the digital annexes, Annex I and Annex II

Annex I - Python Scripts for Morris Method

- Script for Creating model setup files with Morris samples
- Script for Sensitivity Analysis using Morris method

Annex II - Python Scripts for Variance-based Sobol' Method

- Script for Creating model setup files with Sobol' samples
- Script for Sensitivity Analysis using Sobol' method

Annex III

Sensitivity Results for Morris method

- Sensitivity of Temperature

Table 8.3.1 Sensitivity of temperature to the input parameters calculated using Morris method (for r = 10, 12, and 20) at locations P1 to P5

Location	Parameter	Trial 1 (r = 10)				Trial 2 (r = 12)				Trial 3 (r = 20)			
		$\mu(^{\circ}\text{C})$	$\mu^{*}(^{\circ}\text{C})$	$\sigma(^{\circ}\text{C})$	Rank	$\mu(^{\circ}\text{C})$	$\mu^{*}(^{\circ}\text{C})$	$\sigma(^{\circ}\text{C})$	Rank	$\mu(^{\circ}\text{C})$	$\mu^{*}(^{\circ}\text{C})$	$\sigma(^{\circ}\text{C})$	Rank
P1	Smagorinsky	-0.0026	0.0163	0.0148	3	-0.004	0.015	0.015	3	-0.0023	0.0173	0.0154	3
	Dalton	-0.0394	0.2149	0.2075	1	-0.069	0.200	0.203	1	-0.0604	0.1986	0.2026	1
	Stanton	-0.0004	0.0287	0.0260	2	0.002	0.027	0.025	2	-0.0016	0.0266	0.0250	2
	Vicouv	0.0000	0.0000	0.0000	7	0.000	0.000	0.000	7	0.0000	0.0000	0.0000	7
	Vicoww	-0.0002	0.0015	0.0012	4	0.000	0.001	0.001	4	0.0001	0.0015	0.0010	4
	Dicouv	0.0000	0.0000	0.0000	6	0.000	0.000	0.000	6	0.0000	0.0000	0.0000	6
	Dicoww	0.0001	0.0009	0.0007	5	0.000	0.001	0.001	5	0.0003	0.0010	0.0008	5
P2	Smagorinsky	-0.0442	0.1047	0.1079	2	-0.071	0.084	0.106	2	-0.0348	0.1061	0.1081	2
	Dalton	-0.0415	0.2337	0.2254	1	-0.076	0.217	0.221	1	-0.0673	0.2157	0.2206	1
	Stanton	-0.0012	0.0359	0.0329	3	-0.002	0.035	0.033	3	-0.0018	0.0349	0.0327	3
	Vicouv	0.0000	0.0000	0.0000	7	0.000	0.000	0.000	7	0.0000	0.0000	0.0000	7
	Vicoww	0.0002	0.0051	0.0044	4	0.000	0.005	0.004	4	0.0000	0.0047	0.0039	4
	Dicouv	0.0000	0.0000	0.0000	6	0.000	0.000	0.000	6	0.0000	0.0000	0.0000	6
	Dicoww	0.0004	0.0014	0.0011	5	0.000	0.001	0.001	5	0.0002	0.0011	0.0008	5
P3	Smagorinsky	-0.0052	0.0166	0.0157	3	-0.071	0.084	0.106	2	-0.0059	0.0176	0.0169	3
	Dalton	-0.0410	0.2242	0.2165	1	-0.076	0.217	0.221	1	-0.0631	0.2071	0.2114	1
	Stanton	-0.0004	0.0314	0.0287	2	-0.002	0.035	0.033	3	-0.0014	0.0295	0.0280	2

	Vicouv	0.000 0	0.000 0	0.000 0	7	0.000	0.000	0.000	7	0.000 0	0.000 0	0.000 0	7
	Vicoww	0.000 0	0.001 2	0.001 0	4	0.000	0.005	0.004	4	0.000 0	0.001 1	0.000 8	4
	Dicouv	0.000 0	0.000 0	0.000 0	6	0.000	0.000	0.000	6	0.000 0	0.000 0	0.000 0	6
	Dicoww	0.000 1	0.000 6	0.000 5	5	0.000	0.001	0.001	5	0.000 1	0.000 5	0.000 5	5
P4	Smagorinsky	- 0.010 4	0.031 9	0.030 7	2	- 0.019 7	0.021 4	0.026 8	2	- 0.010 7	0.031 8	0.031 0	2
	Dalton	- 0.037 5	0.207 1	0.199 9	1	- 0.066 9	0.192 4	0.195 8	1	- 0.058 6	0.191 4	0.195 4	1
	Stanton	- 0.000 7	0.025 3	0.023 0	3	0.002 0	0.024 2	0.022 5	3	- 0.001 8	0.023 6	0.022 1	3
	Vicouv	0.000 0	0.000 0	0.000 0	7	0.000 0	0.000 0	0.000 0	7	0.000 0	0.000 0	0.000 0	7
	Vicoww	0.000 1	0.001 5	0.001 3	4	0.000 1	0.001 2	0.001 0	4	- 0.000 1	0.001 3	0.001 1	4
	Dicouv	0.000 0	0.000 0	0.000 0	6	0.000 0	0.000 0	0.000 0	6	0.000 0	0.000 0	0.000 0	6
	Dicoww	0.000 1	0.000 4	0.000 4	5	0.000 0	0.000 5	0.000 4	5	0.000 1	0.000 4	0.000 4	5
P5	Smagorinsky	- 0.020 6	0.055 1	0.055 6	2	- 0.035 6	0.038 7	0.050 7	2	- 0.017 5	0.053 8	0.054 4	2
	Dalton	- 0.032 5	0.184 0	0.177 5	1	- 0.059 7	0.170 0	0.173 3	1	- 0.052 2	0.169 5	0.173 1	1
	Stanton	- 0.000 8	0.021 9	0.019 9	3	0.000 5	0.021 5	0.020 0	3	- 0.001 3	0.021 1	0.019 7	3
	Vicouv	0.000 0	0.000 0	0.000 0	7	0.000 0	0.000 0	0.000 0	7	0.000 0	0.000 0	0.000 0	7
	Vicoww	0.000 1	0.001 8	0.001 5	4	0.000 0	0.001 5	0.001 3	4	- 0.000 2	0.001 6	0.001 3	4
	Dicouv	0.000 0	0.000 0	0.000 0	6	0.000 0	0.000 0	0.000 0	6	0.000 0	0.000 0	0.000 0	6
	Dicoww	0.000 3	0.000 8	0.000 7	5	0.000 0	0.000 9	0.000 7	5	0.000 3	0.000 8	0.000 7	5

- Sensitivity of Temperature at each location

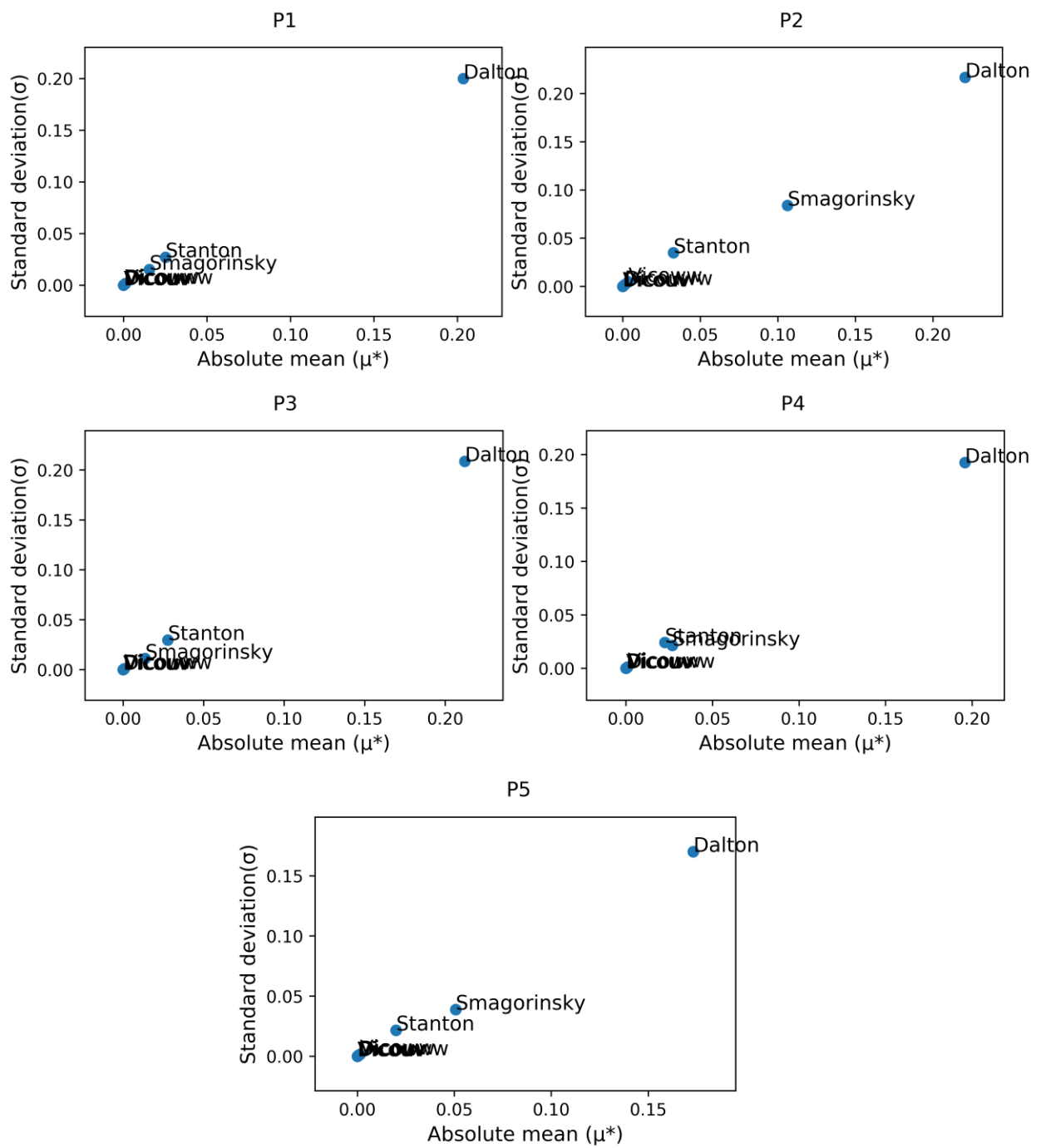


Figure 1. Temperature sensitivity to inputs parameters - Variation of standard deviation with absolute mean of EE

- Sensitivity of Current velocity (x-component)

Table 8.3.6 Sensitivity of x-velocity to the input parameters calculated using Morris method (for r = 10, 12, and 20) at locations P1 to P5

Location	Parameter	Trial 1 (r = 10)				Trial 2 (r = 12)				Trial 3 (r = 20)			
		$\mu(^{\circ}\text{C})$	$\mu^{*}(^{\circ}\text{C})$	$\sigma(^{\circ}\text{C})$	Rank	$\mu(^{\circ}\text{C})$	$\mu^{*}(^{\circ}\text{C})$	$\sigma(^{\circ}\text{C})$	Rank	$\mu(^{\circ}\text{C})$	$\mu^{*}(^{\circ}\text{C})$	$\sigma(^{\circ}\text{C})$	Rank
P1	Vicouv	0.00E+00	0.00E+00	0.00E+00	6	0.00E+00	0.00E+00	0.00E+00	6	0.00E+00	0.00E+00	0.00E+00	6
	Vicoww	-1.08E-04	1.54E-03	1.97E-03	3	-4.06E-04	1.98E-03	1.48E-03	3	-3.99E-06	1.95E-03	1.35E-03	3
	Dicouv	0.00E+00	0.00E+00	0.00E+00	5	0.00E+00	0.00E+00	0.00E+00	5	0.00E+00	0.00E+00	0.00E+00	5
	Dicoww	3.72E-05	6.00E-04	8.05E-04	4	-1.16E-04	9.25E-04	6.49E-04	4	1.03E-04	8.14E-04	5.46E-04	4
	Rhoair	3.14E-03	1.39E-02	1.19E-02	1	1.17E-03	1.52E-02	1.45E-02	1	-1.24E-04	1.49E-02	1.43E-02	1
	Smagorskiy	5.04E-04	3.74E-03	4.02E-03	2	8.87E-04	3.92E-03	4.02E-03	2	7.70E-04	4.17E-03	3.79E-03	2
P2	Vicouv	0.00E+00	0.00E+00	0.00E+00	6	0.00E+00	0.00E+00	0.00E+00	6	0.00E+00	0.00E+00	0.00E+00	6
	Vicoww	-1.21E-06	1.55E-03	1.74E-03	3	-6.60E-05	1.32E-03	1.54E-03	3	-2.30E-05	1.43E-03	1.66E-03	3
	Dicouv	0.00E+00	0.00E+00	0.00E+00	5	0.00E+00	0.00E+00	0.00E+00	5	0.00E+00	0.00E+00	0.00E+00	5
	Dicoww	1.47E-05	2.88E-04	3.72E-04	4	1.61E-05	2.91E-04	4.01E-04	4	8.90E-06	2.75E-04	3.86E-04	4
	Rhoair	9.34E-03	1.90E-02	1.60E-02	1	2.58E-03	1.91E-02	1.97E-02	1	-1.37E-05	1.91E-02	1.97E-02	1
	Smagorskiy	5.50E-04	4.20E-03	4.25E-03	2	9.12E-04	3.93E-03	3.20E-03	2	4.32E-04	4.08E-03	4.12E-03	2
P3	Vicouv	0.00E+00	0.00E+00	0.00E+00	6	0.00E+00	0.00E+00	0.00E+00	6	0.00E+00	0.00E+00	0.00E+00	6
	Vicoww	-1.32E-04	1.18E-03	1.34E-03	3	-1.78E-04	9.95E-04	1.17E-03	3	5.34E-05	1.09E-03	1.28E-03	3
	Dicouv	0.00E+00	0.00E+00	0.00E+00	5	0.00E+00	0.00E+00	0.00E+00	5	0.00E+00	0.00E+00	0.00E+00	5
	Dicoww	5.13E-05	2.64E-04	3.50E-04	4	2.98E-05	2.87E-04	4.03E-04	4	4.70E-05	2.64E-04	3.77E-04	4
	Rhoair	8.95E-03	1.86E-02	1.57E-02	1	2.62E-03	1.89E-02	1.95E-02	1	-6.20E-05	1.89E-02	1.95E-02	1
	Smagorskiy	-3.46E-05	3.25E-03	3.39E-03	2	2.17E-04	2.94E-03	2.47E-03	2	1.83E-04	3.02E-03	3.14E-03	2
P4	Vicouv	0.00E+00	0.00E+00	0.00E+00	6	0.00E+00	0.00E+00	0.00E+00	6	0.00E+00	0.00E+00	0.00E+00	6
	Vicoww	-4.77E-05	1.02E-03	1.19E-03	3	-7.29E-05	8.57E-04	1.01E-03	3	1.65E-05	9.07E-04	1.07E-03	3

	Dicouv	0.00E +00	0.00E +00	0.00E +00	5	0.00E +00	0.00E +00	0.00E +00	5	0.00E +00	0.00E +00	0.00E +00	5
	Dicoww	5.16E -06	2.67E -04	3.48E -04	4	- 1.83E -06	2.78E -04	3.88E -04	4	- 1.85E -05	2.60E -04	3.50E -04	4
	Rhoair	1.98E -03	1.18E -02	1.00E -02	1	4.73E -04	1.20E -02	1.24E -02	1	- 7.33E -06	1.20E -02	1.23E -02	1
	Smagor insky	6.85E -05	2.60E -03	2.77E -03	2	5.96E -05	2.23E -03	1.87E -03	2	- 2.45E -05	2.45E -03	2.57E -03	2
P5	Vicouv	0.00E +00	0.00E +00	0.00E +00	6	0.00E +00	0.00E +00	0.00E +00	6	0.00E +00	0.00E +00	0.00E +00	6
	Vicoww	- 3.82E -05	1.04E -03	1.16E -03	3	- 7.35E -05	8.73E -04	1.01E -03	3	2.47E -05	9.60E -04	1.10E -03	3
	Dicouv	0.00E +00	0.00E +00	0.00E +00	5	0.00E +00	0.00E +00	0.00E +00	5	0.00E +00	0.00E +00	0.00E +00	5
	Dicoww	- 2.96E -06	2.97E -04	3.52E -04	4	- 1.24E -05	2.84E -04	3.54E -04	4	6.12E -06	2.98E -04	3.63E -04	4
	Rhoair	3.01E -03	1.16E -02	9.77E -03	1	1.01E -03	1.18E -02	1.21E -02	1	- 8.64E -05	1.17E -02	1.21E -02	1
	Smagor insky	2.39E -04	2.25E -03	2.32E -03	2	2.86E -04	2.13E -03	1.77E -03	2	1.67E -04	2.27E -03	2.33E -03	2

- Sensitivity of Current velocity (x-component) at each location

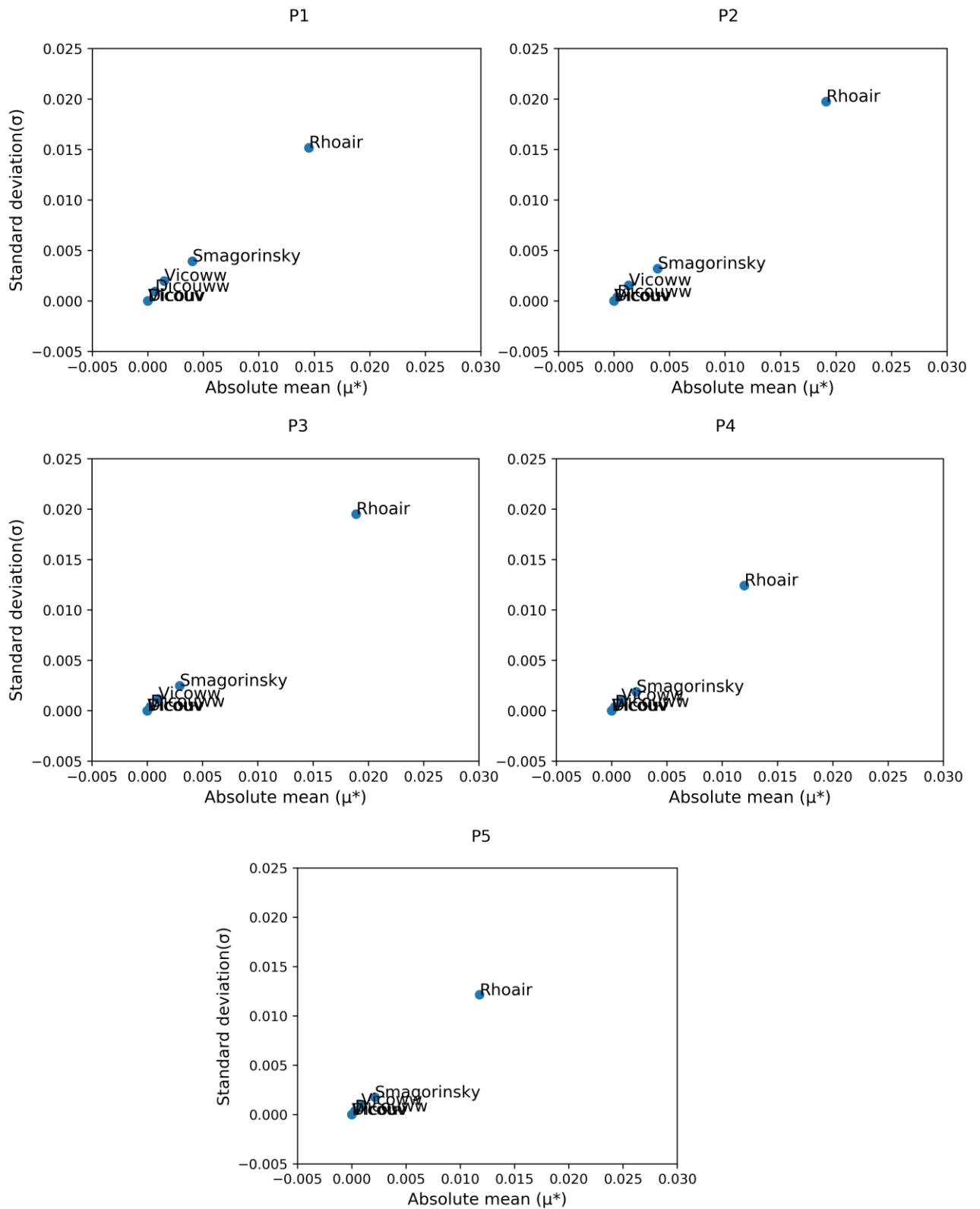


Figure 2. Sensitivity of x-velocity to inputs parameters - Variation of standard deviation with absolute mean of EE

- Sensitivity of Current velocity (y-component)

Table 8.3.6 Sensitivity of y-velocity to the input parameters calculated using Morris method (for r = 10, 12, and 20) at locations P1 to P5

Location	Parameter	Trial 1 (r = 10)				Trial 2 (r = 12)				Trial 3 (r = 20)			
		$\mu(^{\circ}\text{C})$	$\mu^{*}(^{\circ}\text{C})$	$\sigma(^{\circ}\text{C})$	Rank	$\mu(^{\circ}\text{C})$	$\mu^{*}(^{\circ}\text{C})$	$\sigma(^{\circ}\text{C})$	Rank	$\mu(^{\circ}\text{C})$	$\mu^{*}(^{\circ}\text{C})$	$\sigma(^{\circ}\text{C})$	Rank
P1	Vicouv	0.00E+00	0.00E+00	0.00E+00	6	0.00E+00	0.00E+00	0.00E+00	6	0.00E+00	0.00E+00	0.00E+00	6
	Vicoww	0.00E+00	0.00E+00	0.00E+00	5	0.00E+00	0.00E+00	0.00E+00	5	0.00E+00	0.00E+00	0.00E+00	5
	Dicouv	-2.13E-05	4.13E-04	5.34E-04	4	5.88E-05	4.59E-04	6.30E-04	4	-5.82E-05	4.24E-04	6.01E-04	4
	Dicoww	7.42E-05	9.40E-04	1.15E-03	3	2.13E-04	8.64E-04	1.09E-03	3	-3.63E-05	8.53E-04	1.11E-03	3
	Rhoair	-3.55E-04	3.56E-03	3.81E-03	2	-1.02E-03	3.27E-03	2.86E-03	2	-6.37E-04	3.50E-03	3.64E-03	2
	Smagorinsky	3.76E-03	1.16E-02	9.97E-03	1	9.58E-04	1.19E-02	1.24E-02	1	-3.07E-05	1.17E-02	1.22E-02	1
P2	Vicouv	0.00E+00	0.00E+00	0.00E+00	6	0.00E+00	0.00E+00	0.00E+00	6	0.00E+00	0.00E+00	0.00E+00	6
	Vicoww	0.00E+00	0.00E+00	0.00E+00	5	0.00E+00	0.00E+00	0.00E+00	5	0.00E+00	0.00E+00	0.00E+00	5
	Dicouv	9.12E-06	3.17E-04	4.43E-04	4	5.93E-06	3.00E-04	4.49E-04	4	3.90E-05	2.95E-04	4.32E-04	4
	Dicoww	1.21E-04	1.07E-03	1.26E-03	3	1.10E-04	8.96E-04	1.10E-03	3	-7.32E-05	9.71E-04	1.18E-03	3
	Rhoair	-8.20E-04	3.15E-03	3.33E-03	2	-1.66E-03	2.82E-03	2.41E-03	2	-7.68E-04	3.01E-03	3.16E-03	2
	Smagorinsky	3.03E-03	8.17E-03	7.01E-03	1	8.66E-04	8.11E-03	8.46E-03	1	-2.51E-05	8.13E-03	8.44E-03	1
P3	Vicouv	0.00E+00	0.00E+00	0.00E+00	6	0.00E+00	0.00E+00	0.00E+00	6	0.00E+00	0.00E+00	0.00E+00	6
	Vicoww	0.00E+00	0.00E+00	0.00E+00	5	0.00E+00	0.00E+00	0.00E+00	5	0.00E+00	0.00E+00	0.00E+00	5
	Dicouv	-5.37E-06	2.48E-04	3.43E-04	4	1.72E-05	2.64E-04	3.72E-04	4	-6.10E-06	2.61E-04	3.79E-04	4
	Dicoww	5.52E-05	8.30E-04	9.71E-04	3	4.34E-05	7.15E-04	8.71E-04	3	-3.32E-05	7.64E-04	9.31E-04	3
	Rhoair	-1.01E-03	5.84E-03	5.90E-03	2	-1.58E-03	5.49E-03	4.36E-03	2	-7.73E-04	5.81E-03	5.84E-03	2
	Smagorinsky	3.30E-03	9.85E-03	8.36E-03	1	8.92E-04	1.01E-02	1.05E-02	1	-2.56E-05	1.01E-02	1.05E-02	1
P4	Vicouv	0.00E+00	0.00E+00	0.00E+00	6	0.00E+00	0.00E+00	0.00E+00	6	0.00E+00	0.00E+00	0.00E+00	6

	Vicoww	0.00E +00	0.00E +00	0.00E +00	5	0.00E +00	0.00E +00	0.00E +00	5	0.00E +00	0.00E +00	0.00E +00	5
	Dicouv	- 1.79E -05	2.79E -04	3.51E -04	4	- 7.50E -06	2.81E -04	3.82E -04	4	- 8.07E -06	2.87E -04	3.80E -04	4
	Dicoww	3.62E -05	8.18E -04	9.61E -04	3	1.64E -05	7.13E -04	8.70E -04	3	- 1.99E -05	7.33E -04	8.92E -04	3
	Rhoair	1.53E -04	1.78E -03	1.93E -03	2	2.75E -04	1.59E -03	1.43E -03	2	- 1.57E -04	1.65E -03	1.76E -03	2
	Smagor insky	5.05E -03	1.29E -02	1.09E -02	1	1.51E -03	1.32E -02	1.37E -02	1	- 4.55E -05	1.32E -02	1.36E -02	1
P5	Vicouv	0.00E +00	0.00E +00	0.00E +00	6	0.00E +00	0.00E +00	0.00E +00	6	0.00E +00	0.00E +00	0.00E +00	6
	Vicoww	0.00E +00	0.00E +00	0.00E +00	5	0.00E +00	0.00E +00	0.00E +00	5	0.00E +00	0.00E +00	0.00E +00	5
	Dicouv	6.31E -06	2.89E -04	3.57E -04	4	- 6.77E -06	2.66E -04	3.38E -04	4	4.34E -06	2.90E -04	3.65E -04	4
	Dicoww	8.61E -06	8.42E -04	9.65E -04	3	8.26E -07	7.04E -04	8.38E -04	3	1.42E -06	7.73E -04	9.14E -04	3
	Rhoair	- 6.05E -05	1.76E -03	1.86E -03	2	- 1.13E -04	1.55E -03	1.30E -03	2	- 1.99E -05	1.64E -03	1.72E -03	2
	Smagor insky	5.41E -03	1.31E -02	1.11E -02	1	1.54E -03	1.34E -02	1.38E -02	1	- 2.70E -05	1.33E -02	1.37E -02	1

- Sensitivity of Current velocity (y-component) at each location

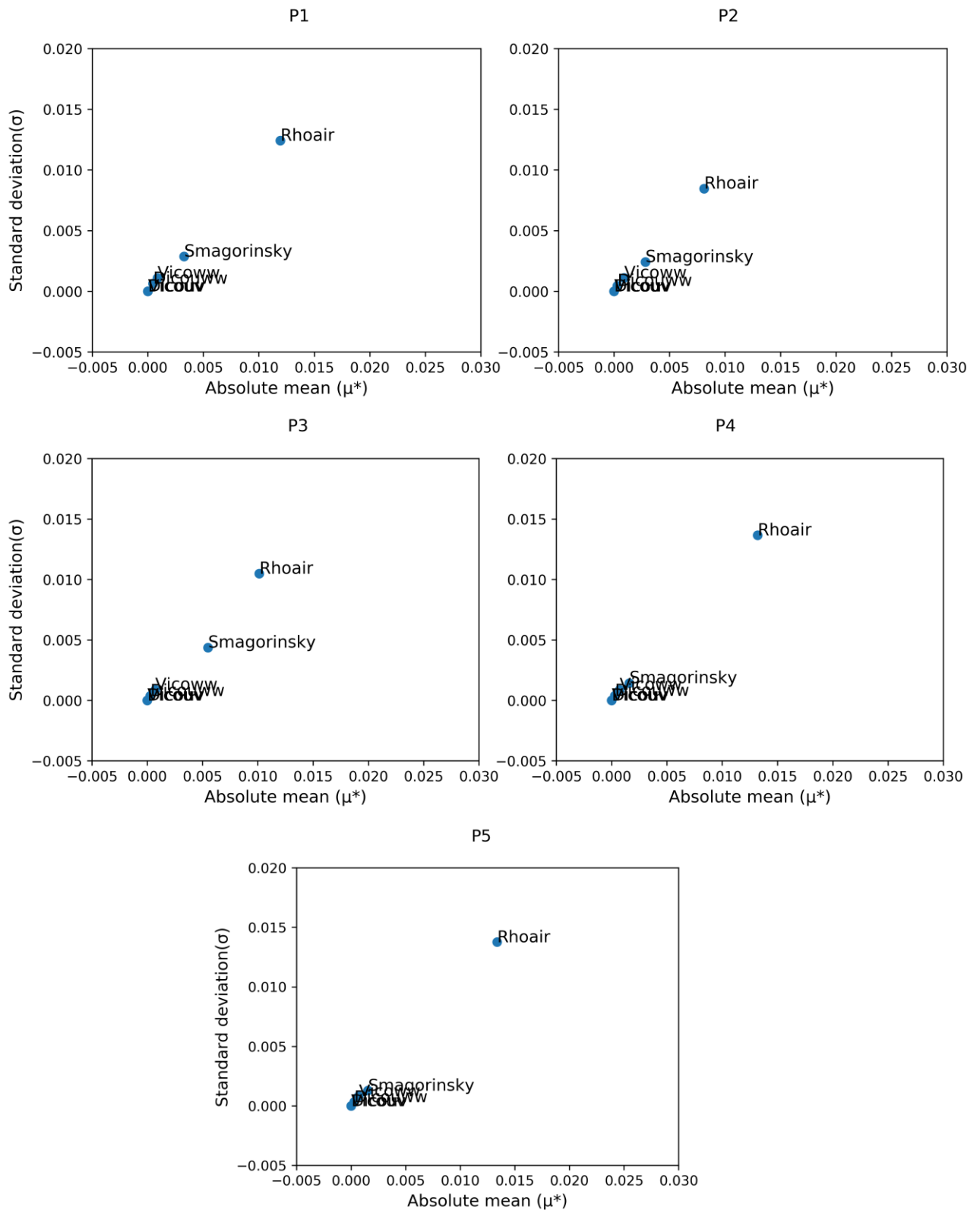


Figure 3. Sensitivity of y-velocity to inputs parameters - Variation of standard deviation with absolute mean of EE

- Sensitivity of Current velocity (z-component)

Table 8.3.6 Sensitivity of z-velocity to the input parameters calculated using Morris method (for r = 10, 12, and 20) at locations P1 to P5

Location	Parameter	Trial 1 (r = 10)				Trial 2 (r = 12)				Trial 3 (r = 20)			
		$\mu(^{\circ}\text{C})$	$\mu^{*}(^{\circ}\text{C})$	$\sigma(^{\circ}\text{C})$	Rank	$\mu(^{\circ}\text{C})$	$\mu^{*}(^{\circ}\text{C})$	$\sigma(^{\circ}\text{C})$	Rank	$\mu(^{\circ}\text{C})$	$\mu^{*}(^{\circ}\text{C})$	$\sigma(^{\circ}\text{C})$	Rank
P1	Vicouv	0.00E+00	0.00E+00	0.00E+00	6	0.00E+00	0.00E+00	0.00E+00	6	0.00E+00	0.00E+00	0.00E+00	6
	Vicoww	0.00E+00	0.00E+00	0.00E+00	5	0.00E+00	0.00E+00	0.00E+00	5	0.00E+00	0.00E+00	0.00E+00	5
	Dicouv	-4.51E-09	4.93E-07	7.17E-07	4	-9.18E-09	4.58E-07	6.80E-07	4	1.33E-08	4.90E-07	7.30E-07	4
	Dicoww	-4.59E-08	1.33E-06	1.60E-06	3	1.17E-07	1.19E-06	1.37E-06	3	2.98E-08	1.23E-06	1.50E-06	3
	Rhoair	-7.34E-09	1.80E-06	2.15E-06	2	1.29E-08	1.49E-06	1.87E-06	2	8.48E-09	1.63E-06	2.02E-06	2
	Smagorinsky	-3.75E-08	3.62E-06	3.41E-06	1	-1.78E-08	3.71E-06	4.11E-06	1	3.24E-08	3.66E-06	4.03E-06	1
P2	Vicouv	0.00E+00	0.00E+00	0.00E+00	6	0.00E+00	0.00E+00	0.00E+00	6	0.00E+00	0.00E+00	0.00E+00	6
	Vicoww	0.00E+00	0.00E+00	0.00E+00	5	0.00E+00	0.00E+00	0.00E+00	5	0.00E+00	0.00E+00	0.00E+00	5
	Dicouv	2.68E-09	4.64E-07	7.06E-07	4	2.55E-09	4.16E-07	6.34E-07	4	1.93E-09	4.77E-07	7.39E-07	4
	Dicoww	1.23E-07	1.31E-06	1.57E-06	3	2.12E-07	1.17E-06	1.30E-06	3	9.41E-08	1.23E-06	1.50E-06	3
	Rhoair	-2.30E-09	2.00E-06	2.38E-06	2	1.21E-09	1.60E-06	2.02E-06	2	-4.09E-10	1.79E-06	2.23E-06	2
	Smagorinsky	-2.22E-08	4.70E-06	4.31E-06	1	-8.72E-09	4.77E-06	5.20E-06	1	5.92E-10	4.74E-06	5.14E-06	1
P3	Vicouv	0.00E+00	0.00E+00	0.00E+00	6	0.00E+00	0.00E+00	0.00E+00	6	0.00E+00	0.00E+00	0.00E+00	6
	Vicoww	0.00E+00	0.00E+00	0.00E+00	5	0.00E+00	0.00E+00	0.00E+00	5	0.00E+00	0.00E+00	0.00E+00	5
	Dicouv	7.19E-09	4.74E-07	7.06E-07	4	1.58E-11	4.32E-07	6.49E-07	4	3.30E-09	4.85E-07	7.35E-07	4
	Dicoww	1.31E-07	1.52E-06	1.77E-06	3	2.54E-07	1.40E-06	1.48E-06	3	1.05E-07	1.45E-06	1.69E-06	3
	Rhoair	-8.72E-10	1.99E-06	2.37E-06	2	2.24E-09	1.60E-06	2.02E-06	2	2.09E-10	1.78E-06	2.22E-06	2
	Smagorinsky	-3.46E-08	4.08E-06	3.79E-06	1	-2.97E-08	4.18E-06	4.58E-06	1	1.17E-08	4.15E-06	4.54E-06	1
P4	Vicouv	0.00E+00	0.00E+00	0.00E+00	6	0.00E+00	0.00E+00	0.00E+00	6	0.00E+00	0.00E+00	0.00E+00	6
	Vicoww	0.00E+00	0.00E+00	0.00E+00	5	0.00E+00	0.00E+00	0.00E+00	5	0.00E+00	0.00E+00	0.00E+00	5

	Dicouv	- 3.98E -09	4.42E -07	6.43E -07	4	- 3.97E -10	4.05E -07	6.06E -07	4	- 2.02E -09	4.50E -07	6.71E -07	4
	Dicoww	- 2.69E -08	1.11E -06	1.36E -06	3	- 3.41E -08	9.72E -07	1.13E -06	3	- 1.15E -08	1.00E -06	1.23E -06	3
	Rhoair	- 6.23E -09	1.63E -06	1.95E -06	2	3.55E -09	1.33E -06	1.68E -06	2	1.48E -09	1.48E -06	1.84E -06	2
	Smagor insky	1.05E -07	3.37E -06	3.15E -06	1	2.73E -08	3.43E -06	3.80E -06	1	- 7.52E -09	3.42E -06	3.77E -06	1
P5	Vicouv	0.00E +00	0.00E +00	0.00E +00	6	0.00E +00	0.00E +00	0.00E +00	6	0.00E +00	0.00E +00	0.00E +00	6
	Vicoww	0.00E +00	0.00E +00	0.00E +00	5	0.00E +00	0.00E +00	0.00E +00	5	0.00E +00	0.00E +00	0.00E +00	5
	Dicouv	6.36E -09	4.34E -07	6.33E -07	4	- 2.70E -09	3.80E -07	5.62E -07	4	5.14E -09	4.32E -07	6.40E -07	4
	Dicoww	1.71E -08	1.00E -06	1.22E -06	3	4.49E -08	8.92E -07	1.03E -06	3	1.95E -08	9.34E -07	1.15E -06	3
	Rhoair	- 5.08E -09	1.52E -06	1.82E -06	2	- 5.30E -09	1.23E -06	1.56E -06	2	4.29E -09	1.37E -06	1.71E -06	2
	Smagor insky	2.74E -08	3.86E -06	3.54E -06	1	- 2.21E -09	3.92E -06	4.26E -06	1	5.92E -09	3.89E -06	4.23E -06	1

- Sensitivity of Current velocity (z-component) at each location

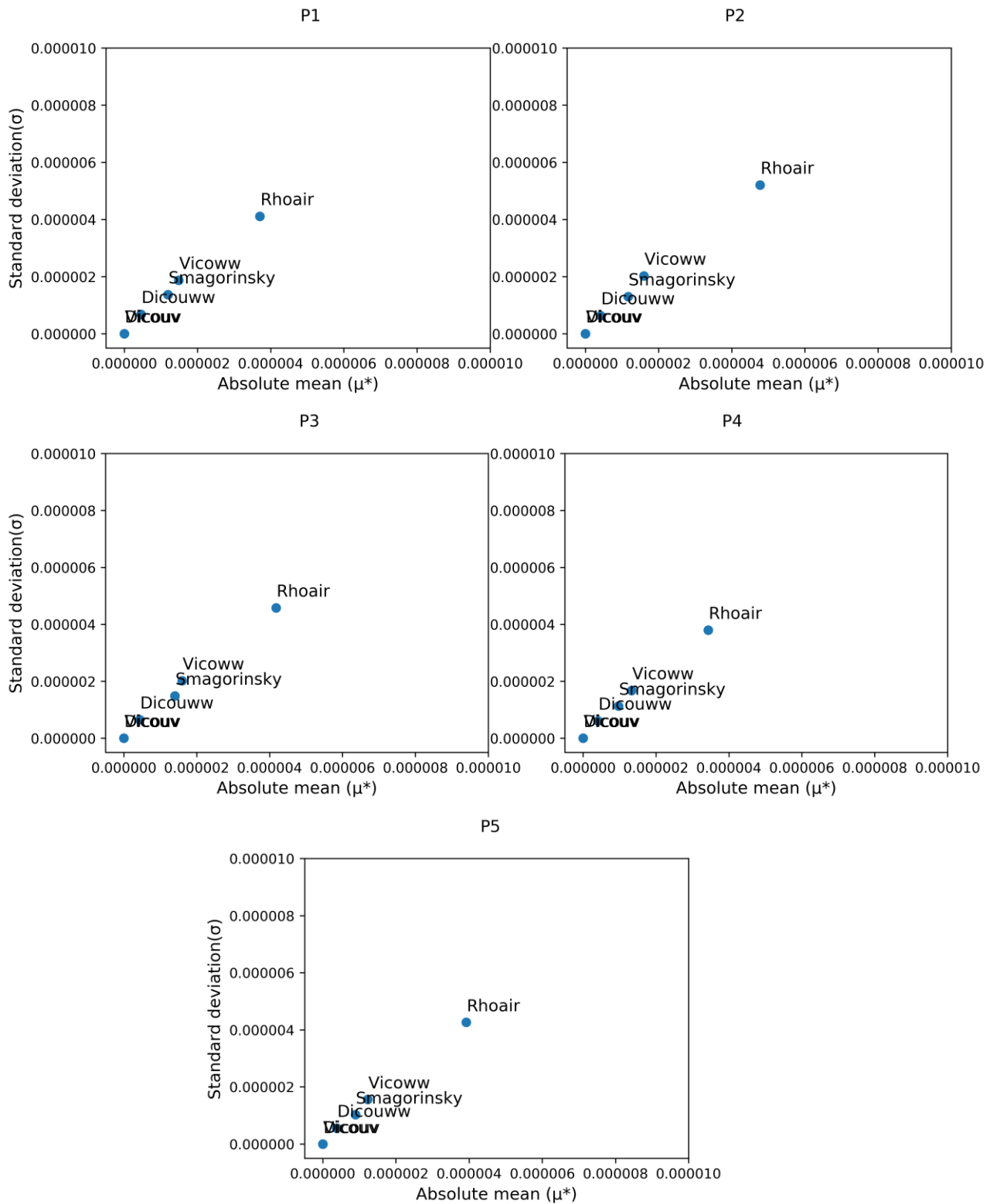


Figure 4. Sensitivity of z-velocity to inputs parameters - Variation of standard deviation with absolute mean of EE

Sensitivity Results for Sobol' method

- Sensitivity of Temperature

Table 7.1: Sensitivity indices for the input parameters using the Sobol' method at P1

Location	Parameter	Si	STi	STi - Si	Rank (based on Si)	Rank (based on STi)
P1	Smagorinsky	0.0065	0.0111	0.0046	2	2
	Dalton	0.9930	0.9969	0.0039	1	1
	Stanton	0.0080	0.0077	-0.0002	3	3
P2	Smagorinsky	0.2843	0.2928	0.0085	2	2
	Dalton	0.6798	0.6935	0.0137	1	1
	Stanton	0.0095	0.0112	0.0017	3	3
P3	Smagorinsky	0.0166	0.0197	0.0030	2	2
	Dalton	0.9746	0.9831	0.0085	1	1
	Stanton	0.0107	0.0141	0.0034	3	3
P4	Smagorinsky	0.0250	0.0303	0.0053	2	2
	Dalton	0.9722	0.9805	0.0083	1	1
	Stanton	0.0004	0.0020	0.0016	3	3
P5	Smagorinsky	0.1325	0.1400	0.0075	2	2
	Dalton	0.8513	0.8625	0.0112	1	1
	Stanton	0.0008	0.0017	0.0009	3	3

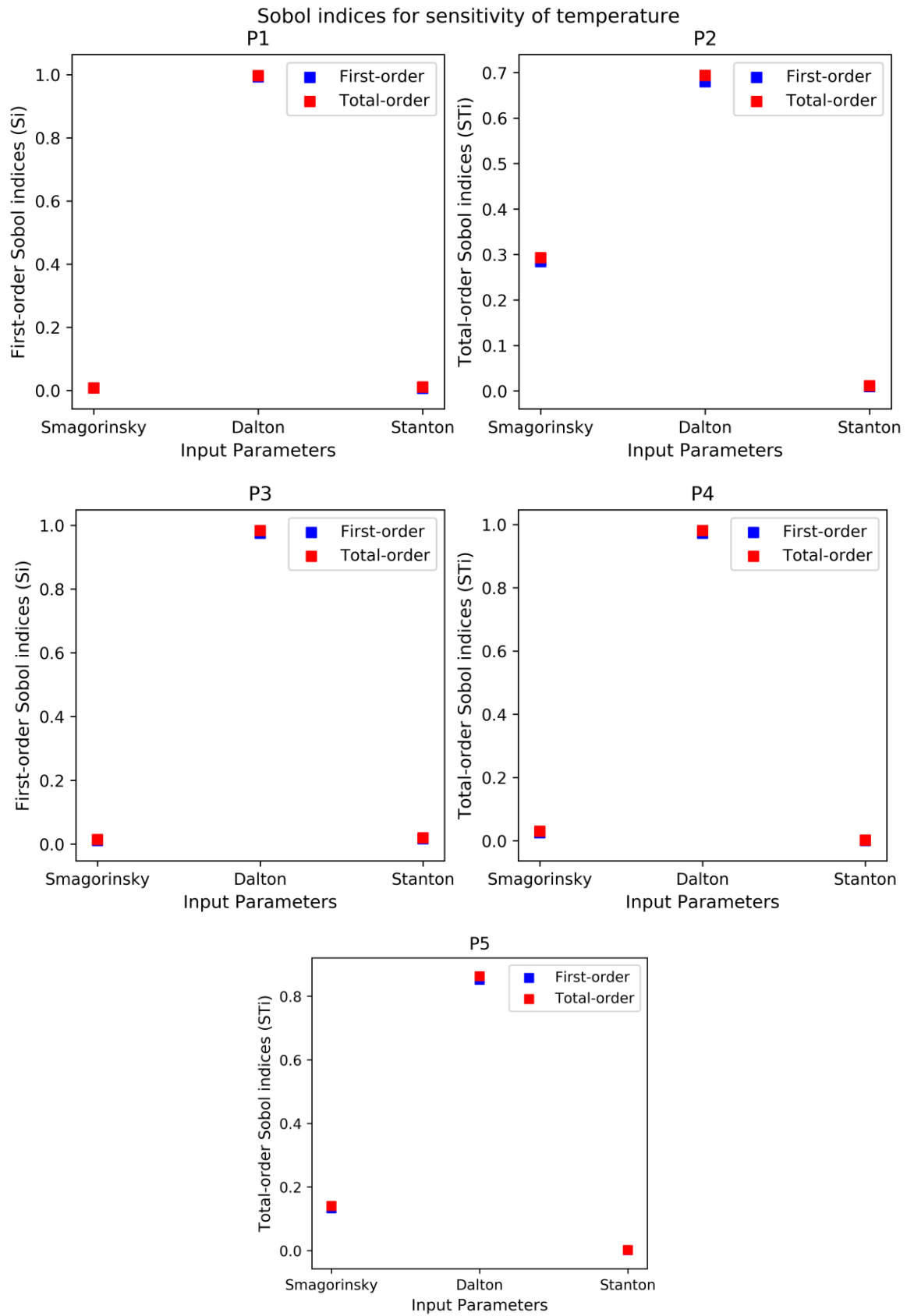


Figure 5. First-order and total-order Sobol' indices for temperature sensitivity for the locations P1 - P5

- Sensitivity of Current velocity (x-velocity)

Table 8.3.5 Sensitivity indices for the input parameters using the Sobol' method at P1

Location	Parameter	S_i	S_{Ti}	$S_{Ti} - S_i$	Rank (based on S_i)	Rank (based on S_{Ti})
P1	Vicoww	0.070311	0.110262	0.039951	3	3
	Dicoww	0.001257	0.018852	0.017595	4	4
	Smagorinsky	0.089342	0.126808	0.037466	2	2
	Rhoair	0.783627	0.809291	0.025664	1	1
P2	Vicoww	0.004653	0.027509	0.022856	3	3
	Dicoww	0.004419	0.006785	0.002366	4	4
	Smagorinsky	0.07744	0.098212	0.020772	2	2
	Rhoair	0.845391	0.883469	0.038078	1	1
P3	Vicoww	0.020822	0.026074	0.005252	3	3
	Dicoww	0.000987	0.003844	0.002857	4	4
	Smagorinsky	0.078166	0.065255	-0.01291	2	2
	Rhoair	0.89563	0.86999	-0.02564	1	1
P4	Vicoww	0.063245	0.09936	0.036116	3	3
	Dicoww	0.002845	0.015908	0.013063	4	4
	Smagorinsky	0.089329	0.113482	0.024154	2	2
	Rhoair	0.815189	0.826005	0.010816	1	1
P5	Vicoww	0.003649	0.005416	0.001767	3	3
	Dicoww	0.001591	0.001874	0.000283	4	4
	Smagorinsky	0.008724	0.013893	0.00517	2	2
	Rhoair	0.952876	0.965265	0.012389	1	1

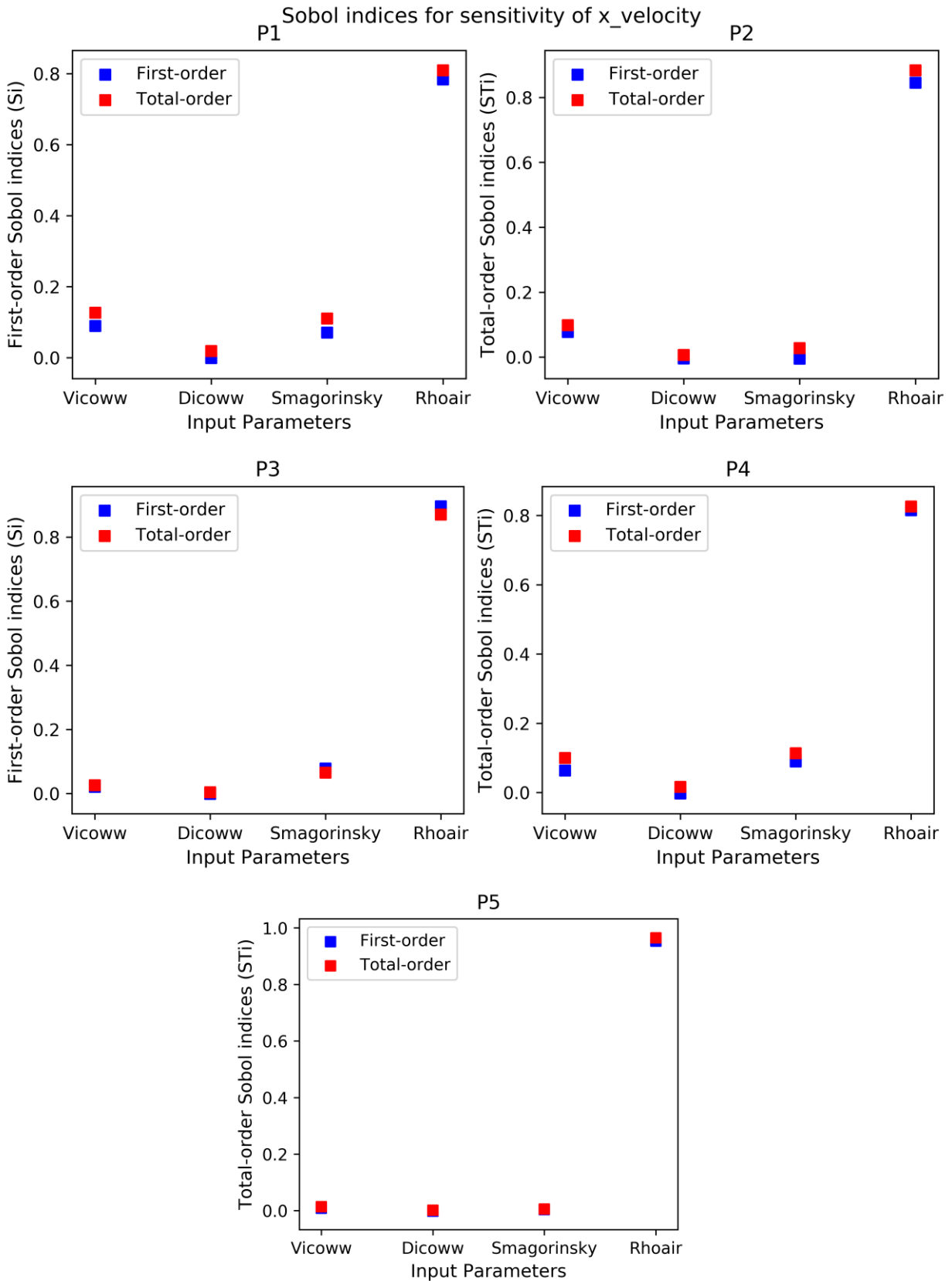


Figure 6. First-order and total-order Sobol' indices for sensitivity of x-velocity for the locations P1 - P5

- Sensitivity of Current velocity (y-velocity)

Table 8.3.5 Sensitivity indices for the input parameters using the Sobol' method

Location	Parameter	S_i	S_{Ti}	$S_{Ti} - S_i$	Rank (based on S_i)	Rank (based on S_{Ti})
P1	Vicoww	0.004146	0.014732	0.010586	3	3
	Dicoww	0.001693	0.005891	0.004198	4	4
	Smagorinsky	0.037669	0.027215	-0.01045	2	2
	Rhoair	0.957388	0.943714	-0.01367	1	1
P2	Vicoww	0.012119	0.061433	0.049313	3	3
	Dicoww	0.003469	0.036086	0.032617	4	4
	Smagorinsky	0.024599	0.083941	0.059342	2	2
	Rhoair	0.8642	0.923199	0.058999	1	1
P3	Vicoww	0.003899	0.010477	0.006577	3	3
	Dicoww	0.00441	0.003643	-0.00077	4	4
	Smagorinsky	0.295872	0.249905	-0.04597	2	2
	Rhoair	0.775831	0.699632	-0.0762	1	1
P4	Vicoww	0.004155	0.009951	0.005796	3	3
	Dicoww	0.001195	0.004476	0.003281	4	4
	Smagorinsky	0.008544	0.015432	0.006889	2	2
	Rhoair	0.952195	0.968154	0.015958	1	1
P5	Vicoww	0.039546	0.077271	0.037725	3	3
	Dicoww	0.005532	0.022576	0.017044	4	4
	Smagorinsky	0.06352	0.082215	0.018695	2	2
	Rhoair	0.838076	0.889717	0.051641	1	1

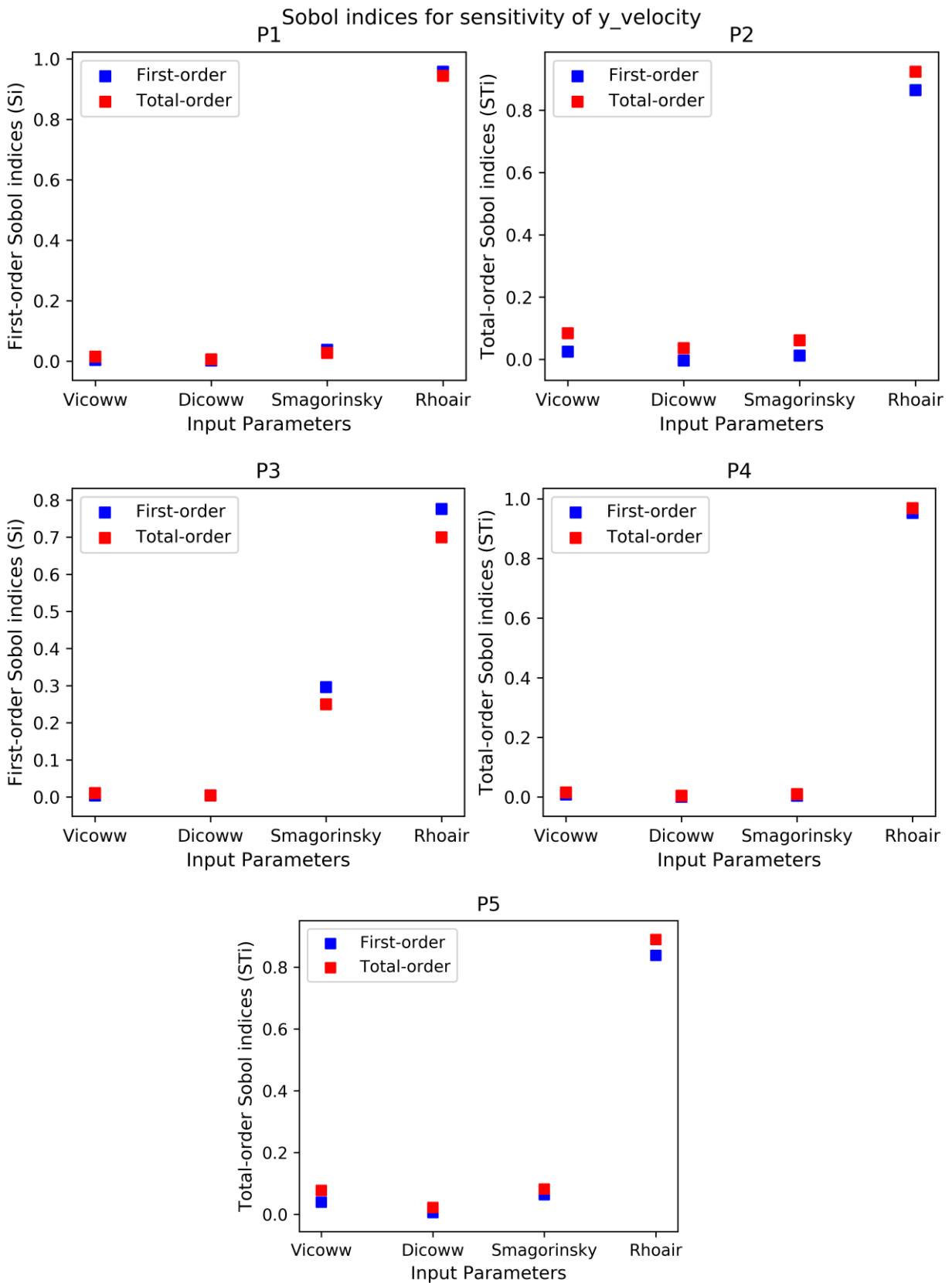


Figure 6. First-order and total-order Sobol' indices for sensitivity of y-velocity for the locations P1 - P5

- Sensitivity of Current velocity (z-velocity)

Table 8.3.5 Sensitivity indices for the input parameters using the Sobol' method

Location	Parameter	S_i	S_{Ti}	$S_{Ti} - S_i$	Rank (based on S_i)	Rank (based on S_{Ti})
P1	Vicoww	0.1756	0.4423	0.2667	2	2
	Dicoww	0.0019	0.1338	0.1320	3	3
	Smagorinsky	0.0012	0.3072	0.3060	4	4
	Rhoair	0.4574	0.7776	0.3202	1	1
P2	Vicoww	0.1850	0.3963	0.2113	2	2
	Dicoww	0.0099	0.1436	0.1336	4	4
	Smagorinsky	0.0297	0.2868	0.2572	3	3
	Rhoair	0.5472	0.8279	0.2807	1	1
P3	Vicoww	0.1652	0.3940	0.2288	2	2
	Dicoww	0.0004	0.1344	0.1341	4	4
	Smagorinsky	0.0191	0.3134	0.2943	3	3
	Rhoair	0.5186	0.8104	0.2918	1	1
P4	Vicoww	0.1666	0.4548	0.2882	2	2
	Dicoww	0.0027	0.1589	0.1563	4	4
	Smagorinsky	0.0228	0.2898	0.2670	3	3
	Rhoair	0.4684	0.7844	0.3160	1	1
P5	Vicoww	0.1033	0.3871	0.2838	2	2
	Dicoww	0.0079	0.1598	0.1519	4	4
	Smagorinsky	0.0232	0.3020	0.2787	3	3
	Rhoair	0.5461	0.8480	0.3018	1	1

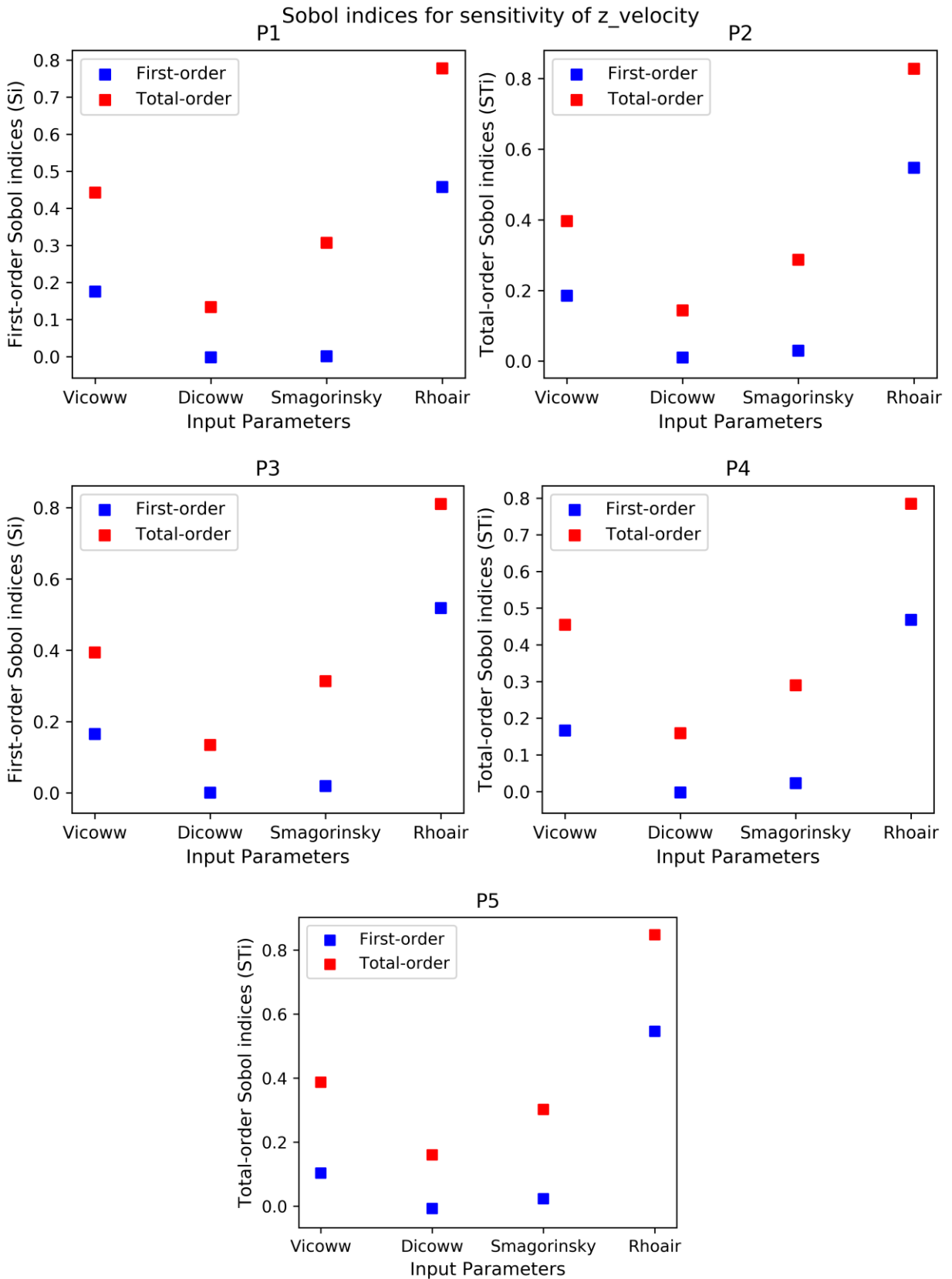


Figure 6. First-order and total-order Sobol' indices for sensitivity of z-velocity for the locations P1 - P5

Annex IV

The computation grid of the DCSM

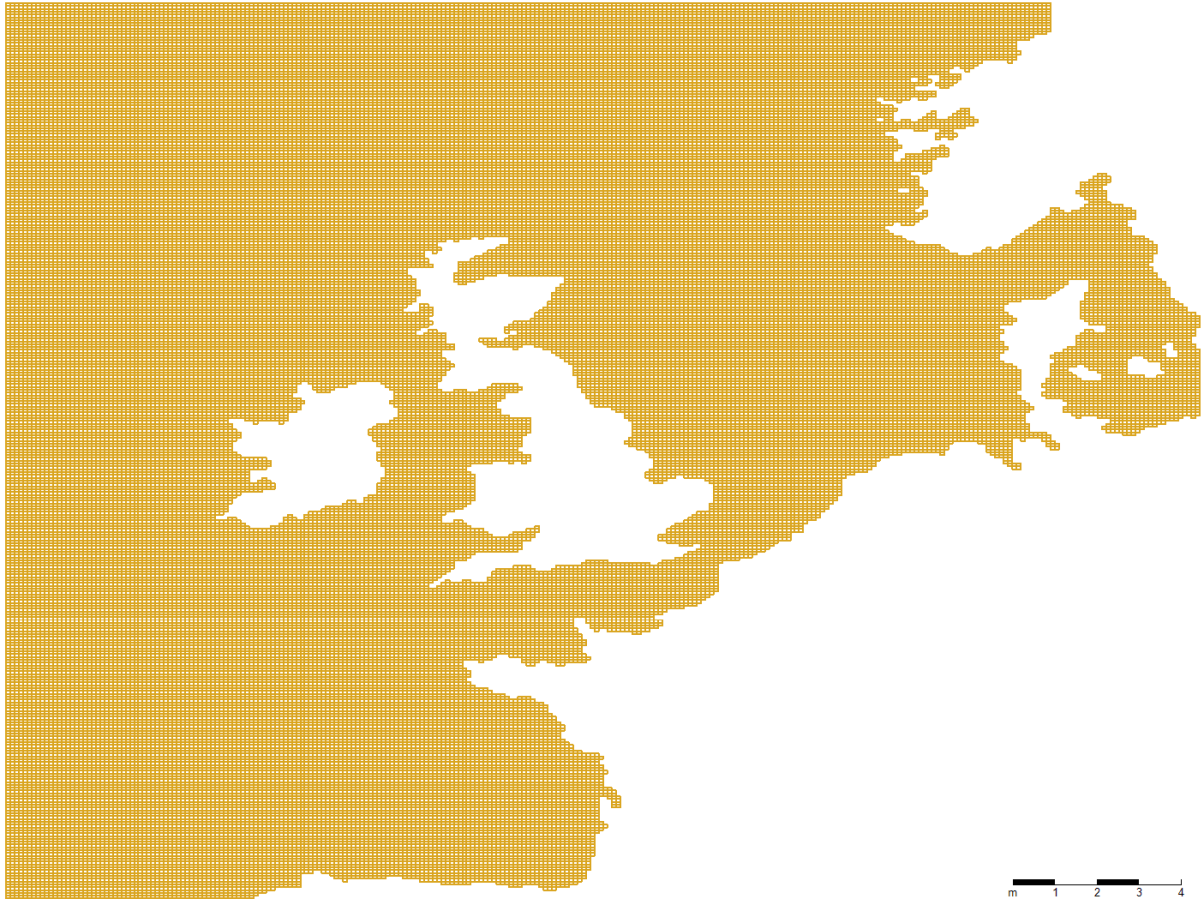


Figure 7. Computation grid of the DCSM

